DETERMINING STRUCTURAL AND STRATIGRAPHIC CONTROLS ON NATURAL GAS PRODUCTION OF THE UPPER DEVONIAN GORDON SANDSTONE, CATSKILL DELTA COMPLEX, SOUTHERN WEST VIRGINIA

By
Jonathan R. Noles

July, 2017

Director of Thesis: Donald W. Neal

Major Department: Geological Sciences

Understanding the controls on natural gas production from the Upper Devonian Gordon sandstone may help petroleum geologists and reservoir engineers better develop and implement a plan for reservoir restimulation to recover addition petroleum resources in southern West Virginia. To test whether the controls are structural, stratigraphic or a combination, downhole geophysical data were obtained from the West Virginia Geologic and Economic Survey. A variety of parameters were used as proxies to determine physical characteristics of the rocks in question: gamma ray, bulk density, and density porosity. Gamma-ray was used as a proxy for lithology to correlate the Gordon sandstone from northern West Virginia into southern West Virginia, to determine thickness and lithology variation within the Gordon interval, thickness and distribution of the Gordon interval that is ≥50% sand, create cross sections, structure contour maps, and isopach maps. Bulk density was used to calculate the log porosity fraction of the material, and later converted to log porosity percent. Using petrophysical data from Ameri et al. (2001) predicted permeability values were calculated for the Gordon sandstone.

Cross-sections illustrate that the Gordon interval is correlative across West Virginia; however, the individual sand bodies that comprise the Gordon are lenticular in shape and non-

continuous. Gordon sediments are thickest in the northeast along the Catskill delta complex and thin to the west and southwest in a basinward direction. This is also true for Gordon sediments comprised of >50% sand. However, in the south, there is a NNE-SSW linear trend of thicker more sand-rich sediments than that of adjacent Gordon sediments. The primary tract is located along strike of a slight structural high, that is comprised of a thicker sandy Gordon interval that exhibits higher porosity values (12% - 15%), and permeability values (5mD – 20mD) than adjacent Gordon sediments (6% - 9%; 0.7mD – 3mD respectively).

Traditionally in northern West Virginia the Gordon sandstone is defined as marginal marine at the point of maximum regressions in late Devonian time. Analysis of the maps produced for this study indicate that Gordon sediments in southern West Virginia were likely deposited as continental shelf sheet sands south of the Catskill delta complex.

Determining Structural and Stratigraphic Controls on Natural Gas Production of the Upper Devonian Gordon Sandstone, Catskill Delta Complex, Southern West Virginia

A Thesis

Presented to the faculty of the Department of Geological Sciences

East Carolina University

In Partial Fulfillment of the Requirement for the

Degree Master of Science Geology

By: Jonathan R. Noles

July, 2017

Determining the Structural and Stratigraphic Controls on Natural Gas Production of the Upper Devonian Gordon Sandstone, Catskill Delta Complex, Southern West Virginia

By: Jonathan R. Noles

APPROVED BY:

DIRECTOR OF THESIS: _____

Dr. Donald W. Neal, PhD

COMMITTEE MEMBER: _____

Dr. Eric Horsman, PhD

COMMITTEE MEMBER: _____

Dr. David Mallinson, PhD

COMMITTEE MEMBER: _____

Ms. Katharine L. Avary, MS

CHAIR OF THE DEPARTMENT

OF GEOLOGICAL SCIENCES: _____

Dr. Stephen Culver, PhD

DEAN OF THE

GRADUATE SCHOOL: _____

Dr. Paul J. Gemperline, PhD

ACKNOWLEDGEMENTS

To start, I would to thank my advisor, Dr. Donald W. Neal for his unwavering support, time, patience, and guidance throughout this project. I would also like to thank my committee, Dr. Dave Mallinson, Dr. Eric Horsman, and Ms. Katharine L. Avary for all of their support, assistance and knowledge. Without the assistance of these four people, this project would not be possible.

Also, I would like to thank Dr. Richard Spruill for his insight, interest, and time; John Woods and Jim Watson, for all of their technical support and assistance with a wide variety of tasks over the years; Kim West and Dare Merritt for all their help over the years. A special thank you to East Carolina University and the Department of Geological Sciences for the opportunity to earn a degree of Masters of Science in Geological Sciences. I would also like to thank the countless number of colleagues and friends who have pushed me to be a better student, scientist, and colleague.

I would also like to give thanks to my parents, Jim and Jackie Noles, who have supported me in my decision to further my education and support me. Thank you for teaching me how to never give up, work hard, and strive for greatness no matter the circumstance.

TABLE OF CONTENTS

LIST OF FIGURES

Figure 13: A) Typical gamma-ray response to sediment type, and gamma-ray signature geometries. Modified from Serra and Sulpice (1975) and Muslim (2014). B) Gamma-ray response of the Gordon interval and the three parasequences that compose the Gordon. Abbreviations that correspond to arrows on the gamma-ray log, indicate coarsening upward (CU) and fining upward (FU) sediment trends.

Figure 14: Gamma-log for well 2533 in McDowell County, West Virginia. Gamma-ray response show typical gamma-ray signature for the Gordon sandstone. Displays the total Gordon interval, and the three parasequences that comprise the Gordon. Displays the 0% sand line (shale baseline), 100% sand line, and 50% sand line that were utilized to determine isolith thickness values for each well.

Figure 15: Cross-sections show lateral correlative Gordon sediments across West Virginia, variable thickness values for the Gordon sandstone, and variable occurrence of the Gordon as a function of depth from the datum, Berea Sandstone.

Figure 16: Detailed structure contour map for the top of the Berea sandstone and its correlative conformity in the focal study area, south-central West Virginia.

Figure 17: Detailed structure contour map for the top of the Gordon sandstone in the focal study area, south-central West Virginia.

Figure 18: Detailed structure contour map for the base of the Gordon sandstone in the focal study area, south-central West Virginia.

Figure 19: Isopach map of the total Gordon interval for central West Virginia

Figure 20: Detailed isopach map for the total Gordon interval in the focal study area, south-central West Virginia.

Figure 21: Isolith map of Gordon sediment that is ≥50% sand for central West Virginia.

Figure 22: Detailed isolith map of Gordon sediment that is ≥50% sand in the focal study area, south-central West Virginia.

Figure 23: Detailed map of calculated maximum log porosity for the Gordon Sandstone interval in the focal study area, south-central West Virginia.

Figure 24: Cross-plots of measured porosity and permeability from cores taken at the same interval from the Jacksonburg-Stringtown oil field. A) Whole core porosity-permeability cross plot. Statistics: $R^2=0.835$, $y=0.0072^{0.4237x}$.

Figure 25: Detailed map of maximum predicted permeability (mD) for the Gordon sandstone interval in the focal study area, south-central West Virginia.

Figure 26: Illustrates the similarity between the shelf edge delta front mouth bar deposit gamma-ray signature of the Carvajal and Steel (2009) study and that of the shelf edge interpreted mouth bar deposits of the Gordon sandstone in southern West Virginia. The basal parasequence in both studies exhibit a symmetrical and serrated gamma-ray geometry. The upper parasequence in both studies exhibit a funnel and serrated gamma-ray geometry.

Figure 27: Schematic cross-section from the peripheral forebulge to the Acadian mountains. Red star indicates the location of Gordon deposition along the shelf edge.

Figure 28: Schematic east-west cross-section showing the distribution of Catskill delta complex sandstones in the Upper Devonian. T= transgressive horizon; R= regressive horizon.

Figure 29: Graphic correlation between relative sea level and shoreline position by correlating conodont biostratigraphy zones. Curve A- Relative sea level curve; Curve B- Position of strike-trending sandstones in northern and central West Virginia, produced by Johnson and others (1985).

Figure 30: Detailed isolith map of Gordon parasequence 1 sediment that is ≥50% sand in the focal study area.

Figure 31: Cross-plot of parasequence 1 thickness and parasequence 1 log porosity in the focal study area. Statistics: R^2= 0.393.

Figure 32: Detailed log porosity map for the Gordon sandstone parasequence 1 in the focal study area.

Figure 33: Detailed isolith map of Gordon parasequence 2 sediment that is ≥50% sand in the focal study area.

Figure 34: Cross-plot of parasequence 2 thickness and parasequence 2 log porosity in the focal study area. Statistics: R^2= 0.438.

Figure 35: Detailed log porosity map for the Gordon sandstone parasequence 2 in the focal study area.

Figure 36: Detailed isolith map of Gordon parasequence 3 sediment that is ≥50% sand in the focal study area.

Figure 37: Cross-plot of parasequence 3 thickness and parasequence 3 log porosity in the focal study area. Statistics: R^2= 0.177.

Figure 38: Detailed log porosity map for the Gordon sandstone parasequence 3 in the focal study area.

Figure 39: Carvajal and Steel (2009) mapped isolith thickness of the ≥50% sand fraction in southern Wyoming, US. Blue dash lines from Carvajal and Steel (2009) indicate the shelf edge margin for cycles 1 and 2. Southern West Virginia, US isolith of the Upper Devonian Gordon shelf edge.

Figure 40: Describes the gamma-ray signature for the Logan Co. 1230 well located along the lower slope, basinward of the projected shelf edge. The gamma-ray signature of the Gordon interval is divided in three distinct parasequences, each parasequence exhibits a funnel and serrated geometry.

LIST OF PLATES

INTRODUCTION

The Appalachian Basin (Figure 1) has been a prolific producer of petroleum resources since the early 1900's. The first well drilled with the purpose of producing petroleum was in Titusville, Pennsylvania, in 1859. Since its installment more than 3.5 billion barrels of oil (BBO) and 41 trillion cubic feet (TCF) of natural gas have been produced from over 500,000 wells throughout the Appalachian Basin spanning across 3100 fields (Burns and Claus, 1985; de Witt and Milici, 1989). The basin covers over 536,000 km^2 west of the Appalachian Mountains, is 2,050 km long and 530 km wide (Colton, 1970) (Figure 1). The extensive production of petroleum resources from the Appalachian Basin can largely be attributed to the structural development of the basin and post-depositional deformation that produced a vast quantity of stratigraphic traps or a combination of stratigraphic and structural traps that have been exploited for their petroleum. Large volumes of petroleum resources have been recovered from the Upper Devonian sands, one which is the Gordon sandstone, a Late Devonian sandstone deposited during an episode of maximum regression.

Structural development of the Appalachian Basin persisted through much of the Paleozoic. However, three major orogenic events are largely responsible for its genesis and sustained source of sediment: the Taconic, Acadian, and Alleghenian orogenies. However, only the Taconic and Acadian orogenies influenced structural development preceding the deposition of the Gordon sandstone. During each of the orogenic events, continental lithosphere experienced crustal thickening by suturing island arc systems and microcontinents to Laurentia. This resulted in cratonward lithospheric subsidence forming a foreland basin and uplift of a peripheral bulge, the innermost craton physiographic boundary (Ettensohn, 2005). As the

Appalachian Basin subsided, the ocean transgressed across the craton, forming an epicontinental seaway (Figure 2). In Devonian time, the Appalachian Basin experienced a typical, seven-part, foreland basin sedimentation cyclicity as defined by Ettensohn (1984).

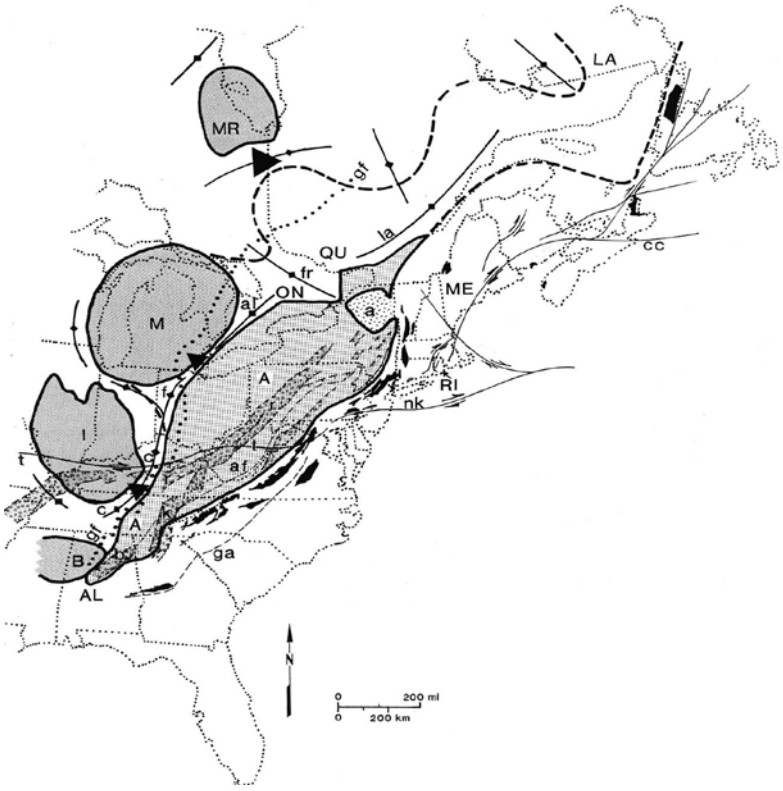

Figure 1: Location of Appalachian foreland basin and nearby structural features in eastern United States and southeastern Canada, where dotted lines represent modern political boundaries. Preserved parts of the Appalachian foreland basin (A) are shown in coarse stipple and other possible parts of the basin to the northeast and northwest are outlined in dark dashes. The Black Warrior Basin (B) and the Illinois (I),Michigan (M), and Moose River (MR) intracratonic basins are shown in light stipple. The basins are separated from each other by cratonic arches (la, Laurentian arch; fr, Frontenac arch; al, Algonquin arch; f, Findlay arch; c, Cincinnati arch).The large dark triangles show the directions and locations of yoking between the Appalachian and adjacent intracratonic basins. Major Iapetan rifts (r, Rome trough; k, Knoxville graben; b, Birmingham graben), defining the former keel of the basin, are shown in a sand-and-gravel pattern bound by tick-marked dashes. Reactivation of some former rifts and cratonic arches at times served to subdivide the larger Appalachian basin into sub-basins. Blackened areas east of the Appalachian Basin represent a chain of Grenvillian, Mesoproterozoic basement inliers or massifs, called the Blue Ridge in the south and central Appalachians, which were parts of the old continental margin that were transported westward during various Appalachian orogenies; the Adirondak massif (a) is an inlier of similar age that was not involved in Appalachian orogenies. The Piedmont or Piedmont Plateau is the area of largely metamorphic and igneous rocks between the Blue Ridge and the Coastal Plain overlap. Other major structural features include the Grenville Front (gf), southern gravity anomaly (ga), the Allegheny Front (af), the 38th Parallel Lineament (t), the Ontario Embayment (o), the Quebec Basin (q), the Narragansett Basin (n), and a series of Carboniferous--Mesozoic strike slip faults (nk, N40-Kelvin fault zone; cc, Cobequid-Chedabucto fault zone) along which smaller sedimentary basins developed. ME, Maine; Qu, Quebec; ON, Ontario; RI, Rhode Island; cpo, Coastal Plain overlap; and AL, Alabama. From Ettensohn (2005).

As the basin subsided, transgression of the Kaskaskia epicontinental seaway (Figure 2) scoured the craton and deposited the newly reworked sediment as a lag deposit. The juvenile shallow sea deposited a thin widespread veneer of marine sediments. As the rate of subsidence outpaced sedimentation deposition of flysch (interbedded shale and carbonate) occurred, followed by tectonic quiescence during which the basin experienced coarse-grained siliciclastic sedimentation from delta progradation. From the sixth to the seventh stage of the foreland basin sedimentation cycle, the basin reached tectonic equilibrium that resulted in basin uplift, erosion, transport and deposition of basin sediments as molasse deposits (Ettensohn, 2005).

West Virginia is located in the central sub-basin of the Appalachian Basin, which developed during the Acadian orogeny in early Devonian time and persisted through late Mississippian time, as the Avalonian terranes (Figure 2) collided against the Virginia Promontory (Figure 3b) (Ettensohn, 2005). A promontory is a physiographic feature that extends away from the craton. During convergence, it experiences increased crustal shorting, deformation, and, therefore, increased crustal thickening. Resulting in increased subsidence in the foreland basin and uplift of the peripheral forebulge parallel to the direction of collision against the promontory further structurally developing the basin during the Acadian orogeny (Dewey and Burke, 1974; Dewey and Kidd, 1974).

The Acadian orogeny is the second of two full orogenic events that formed the Appalachian Basin and occurred in four tectophases (Figure 3a). A tectophase is a subset of an orogeny. In the case of the Acadian orogeny, the tectophases are associated with the oblique convergence of the Avalonian terranes (Figure 2) against the promontories (Figure 3b) located along the eastern margin of Laurentia. Pertinent to the Gordon, is the third tectophase of the Acadian orogeny (Figure 3a) defined by convergence against the Virginia promontory (Figure

3b). During the third tectophase (Figure 3a), the seventh and final stage of the foreland basin sedimentation deposited the Gordon sandstone (Ettensohn, 1985).

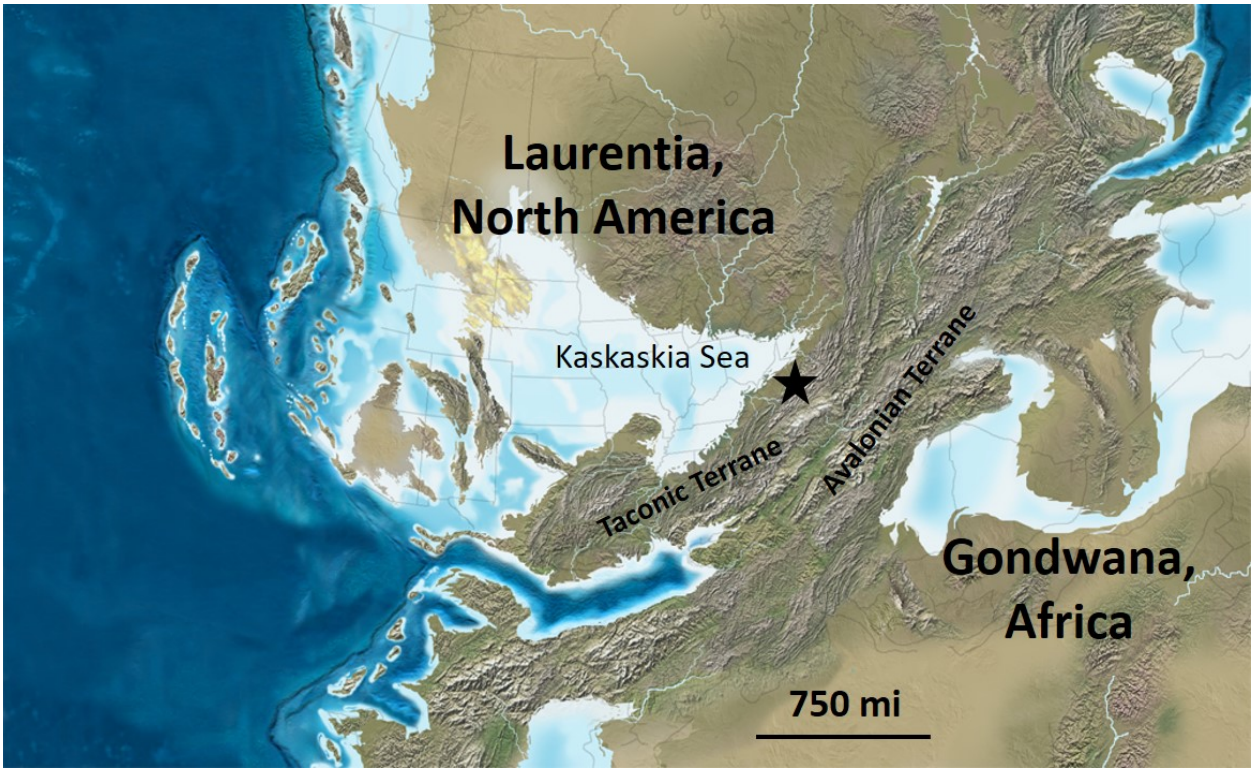

Figure 2: Schematic diagram of the shallow Kaskaskia epicontinental seaway transgressing Laurentia during the Alleghenian Orogeny and the formation of Pangea. Star indicates location of West Virginia. Modified from Colorado Plateau Geosystems, (2016).

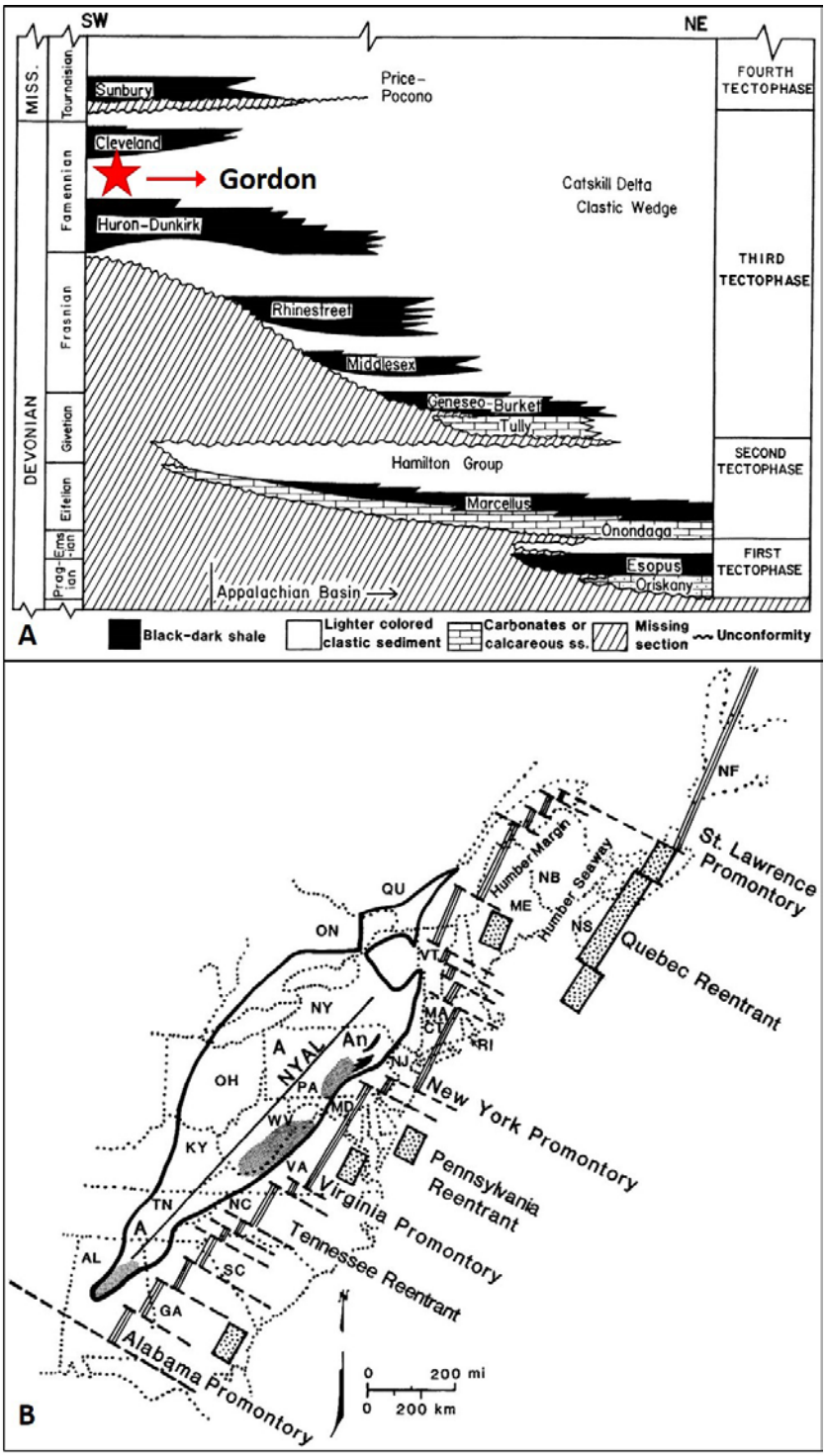

Figure 3: A) Schematic diagram, not to scale, of a cross-section from north-central Ohio to east-central New York showing the tectophases that compose the Acadian orogeny, and the vertical and spatial location of variable lithologies in the Appalachian basin. The red star marks the stratigraphic position of the Gordon sandstone. Modified from Ettensohn (1987, 1994, and 2005). B) Schematic diagram of the four promontories that border the eastern margin of Laurentia: St. Lawrence, New York, Virginia, and Alabama promontories; laid over modern state boundaries. Partially modified from Thomas (1993, 2006) and Hatcher et al. (1989).

The purpose of the study is to determine the controls on natural gas production from the Gordon sandstone in southern West Virginia. No production analysis was conducted due a lack of data, which is resultant of co-mingled well production. This study was originally focused entirely in southern West Virginia; the Gordon is a drillers' term rather than a formal unit name. Therefore, its nomenclature could be regional or locally used so the Gordon in southern West Virginia may not be the same sand body as in northern West Virginia. Clarification for the consistent use of the Gordon nomenclature was essential. To accomplish this, correlation of Gordon sediments from northern West Virginia to southern West Virginia was necessary. Cross-sections indeed show that the nomenclature was used consistently throughout the state of West Virginia (Figure 4). Production from the Gordon occurs along two linear tracts that strike NNE-SSW. The primary, larger, tract is the eastern most tract, while the secondary tract is smaller and occurs to the west (Figure 5).

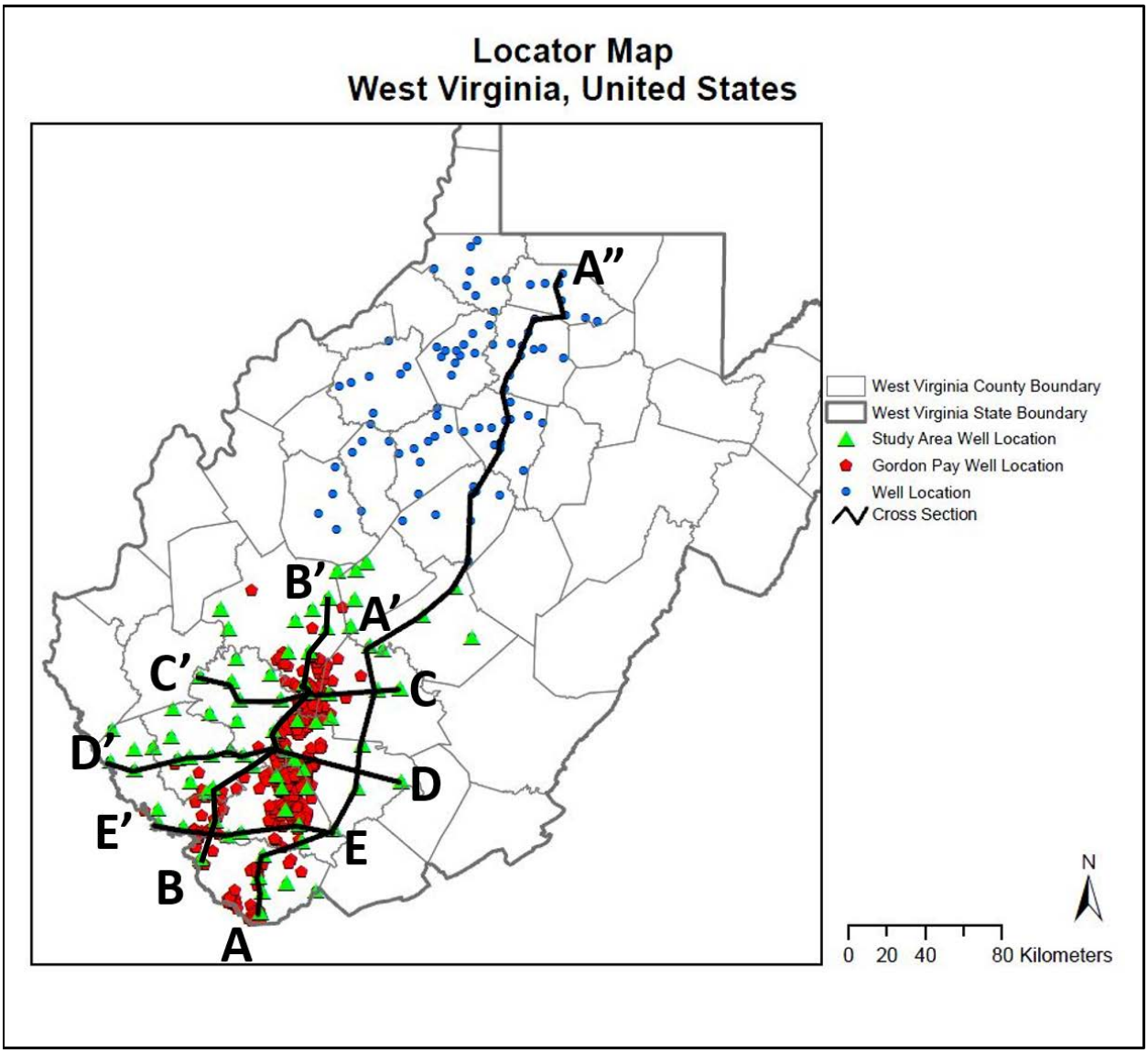

Figure 4: Locator map showing the location of wells from which geophysical data were collected. Blue circles indicate wells used for state-wide correlation and interpolation. Green circles indicate wells within the study area used to generate detailed maps from geophysical data. Red pentagons indicate wells from which petroleum was produced from the Gordon sandstone in southern West Virginia. Thick black lines represent the cross-sections constructed to show correlative Gordon sediments statewide. Well locations are from the West Virginia Geological and Economic Survey (WVGES) oil and gas database.

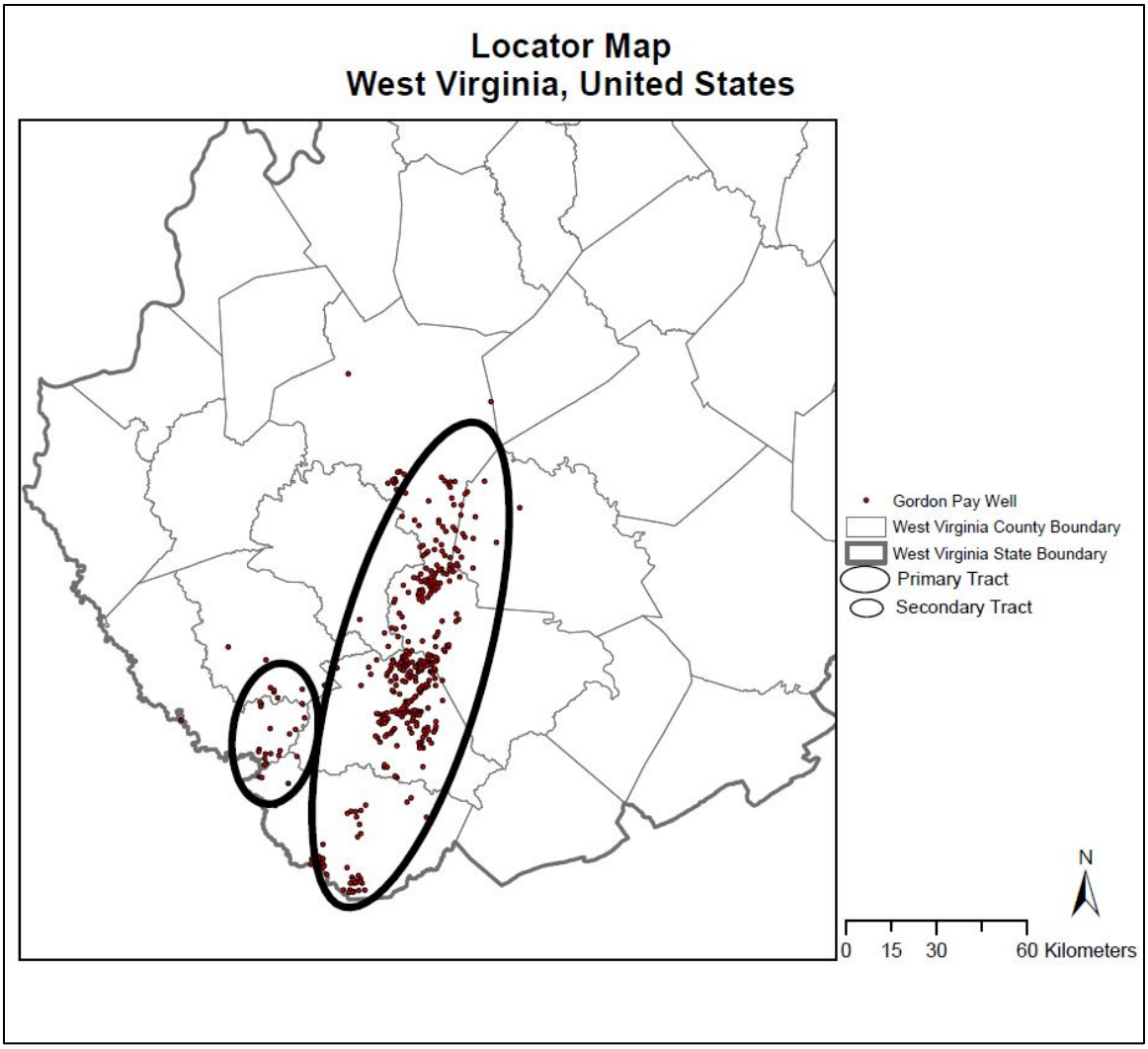

Figure 5: Map shows the location of the two linear tracts from which petroleum was produced from the Gordon sandstone. The larger eastern tract is the primary tract of production, whereas the smaller western tract is the secondary tract of production. Data sourced from WVGES.

FORELAND BASIN SEDIMENTATION CYCLE AND LITHOSPHERIC FLEXURE

The foreland basin sedimentation cycle is an idealized cycle based upon a lithospheric flexure model with little complexity (Figure 6) (Ettensohn, 2005). The sedimentation cycle can develop through an entire orogenic event, or within individual tectophases associated with a complex orogenic event.

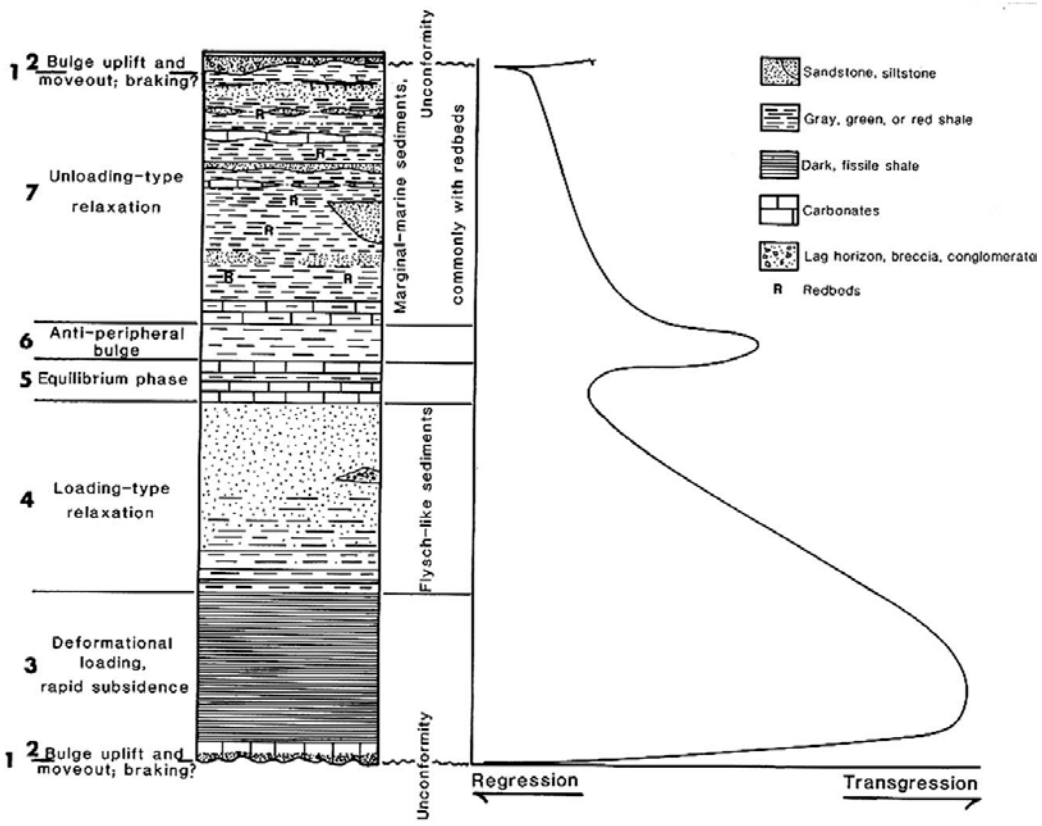

Figure 6: Generalized tectophase sequence, lithology sequence, and shoreline migration associated with foreland basin lithospheric flexure. Lithology thicknesses are generalized, but are to scale relative to one another. Adopted from Ettensohn, 1994.

To understand the cycle of sedimentation within the foreland basin, one must understand how a foreland basin develops and the physiographic features that compose the basin. The onset of tectonic convergence develops thrust faults and crustal thickening of the lithosphere along the craton margin. To compensate for the additional load of crustal material, the adjacent cratonward lithosphere experiences downwarped flexure forming the foreland basin. On the cratonward

margin of the basin, bending of the rigid lithosphere generates a peripheral forebulge (Figure 7) (Ettensohn, 2005). Both the peripheral forebulge and orogen act as paleoslopes and sediment sources to the basin (Beaumont, 1981; Tankard, 1986) (Figure 7). Additional lithospheric loading, in the form of crustal thickening (e.g. sediment deposition in the basin, thrust belts producing mountains, accreting terranes), cause increased subsidence in the basin, uplift of the forebulge, as it shifts in the basinward direction (Figure 7).

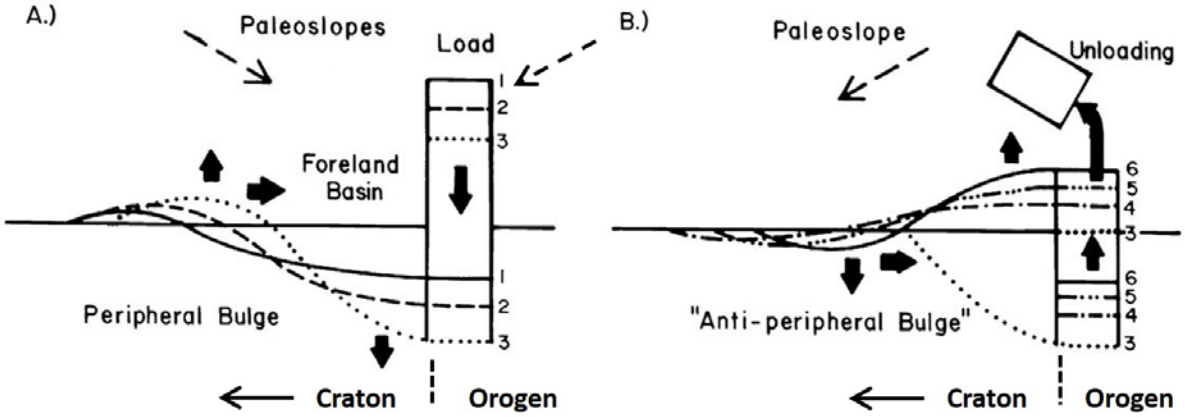

Figure 7: Schematic diagram showing two lithosphere responses to lithospheric loading and unloading. A) "Loading- type" relaxation- thrust migration ceases, results in the downward flexure of the foreland basin to accommodate the increased thickness (e.g. mountains), or load, of the lithosphere. Generating two paleoslopes that results in two directions of sediment transport into the basin (1- Newly formed mountains from crustal thickening, 2- Peripheral bulge). B) "Unloading-type" relaxation- erosion of the crustal load results in an upward lithospheric rebound and sag of the peripheral forebulge. Previously buried basin sediment is uplifted, eroded, and transported as "molasse-type" sediments in one predominate direction (cratonward). Adopted from Ettensohn, 2005 (redrawn from Beaumont et. al., 1988).

Each cycle is composed of seven stages. Individual stages have a characteristic lithospheric flexure response to tectonic loading and unloading, resulting in unique sedimentation in the basin. Each cycle is always bound by unconformities, and generally has a coarsening upward trend through the seven stages (Ettensohn, 2005).

1. *Basal unconformity*

Immediately succeeding the onset of tectonic loading is uplift and basinward migration of the forebulge. A regional unconformity is produced upon uplift and sub-aerial exposure of the

forebulge or elevated basin material. The unconformity is located near the locus of tectonism parallel to the strike of the orogen and perpendicular to the direction of convergence (Dewey and Burke, 1994; Dewey and Kidd, 1994; Ettensohn, 1993, 1994). However, adjacent to the deformed promontories in the foredeep, the unconformity may not develop as the rapidly subsiding basin outpaces the development of an unconformity.

2. *Shallow-water transgressive deposits*

Following the uplift and moveout of the forebulge (Figure 7a) and the development of the basal unconformity, rapid transgression of a shallow epicontinental sea occurs. The transgressive lag deposits are thin due to the rapid rate of basin subsidence. In subtropical areas where precipitation and sediment influx rates into the basin are low, clean to muddy carbonates are typically deposited. In regions where precipitation is high, siliciclastic sedimentation occurs in the basin (Cecil et al., 1991). Other clastic deposits (e.g. sandstone, conglomerates, and breccia) associated with very rapid subsidence and extreme scouring of the sea floor by interaction with wave base erosion develop a transgressive lag deposit and a sharp overlying contact of fine-grained sediment as the basin is drowned (Ettensohn, 2005).

3. *Dark-mud sedimentation*

Jamieson and Beaumont (1988) concluded that early on in an orogeny the isostatic response first order driver is deformational loading (e.g. crustal shortening and load transfer) along a short, but steep, basement ramp that can accommodate approximately 20 km of vertical deformation without developing significant sub-aerial relief, and becoming a sediment source. This results in rapid subsidence of the basin and very little amount of sediment flux into the basin, sediment starvation, meaning the predominant sediment input are organic matter and suspended muds. Rapid basin subsidence outpaces sediment input and results in a anoxic

stratified water column that increases preservation potential of the organic matter in black muds. Deposition of black muds and continued subsidence indicate that tectonism is still active.

4. *Flysch sedimentation*

Black mud sedimentation into the central parts of the basin persists if tectonic convergence is still occurring. As tectonic convergence declines and the crustal load becomes static, the lithosphere relaxes, resulting in basin subsidence as the forebulge is uplifted and shifts toward the basin. At this point in the cycle, significant sub-aerial relief has developed, along with fluvial networks that transport siliciclastic material from the highlands into the deep basin as deltaic deposits. Highly immature siliciclastic sediments such as these are called flysch deposits. Extremely rapid deep basin fill of flysch sediments redistributes the highlands load into the basin causing increased subsidence and uplift of the forebulge, once again, and is referred to as "loading-type relaxation" by Ettensohn (2005).

5. *Thin, regressive, shallow-water deposits*

As basin subsidence rates decrease, the sedimentation rate exceeds that of subsidence. At the same time the sediment flux has decreased significantly as a result of decreased elevation of the sediment source. Basin infilling results in decreased depth of the epicontinental sea, enabling the deposition of shallow marine regressive deposits. If the basin is in an arid sub-tropical environment, carbonates predominate; however, if the basin is in a humid equatorial environment, siliciclastic mud dominates sediment input (Ettensohn, 2005). This stage has been referred to as the "elevation equilibrium phase" by Ettensohn (2005), and is short-lived as the basin rebounds upward as an isostatic response to erosion of the orogenic belt, also known as unroofing.

6. *Thin, transgressive, marine sequence*

The short lived “elevation equilibrium phase” of isostatic rebound generates uplift of the basin and subsidence of the forebulge during the “anti-peripheral bulge phase” (Figure 7b). The removal of the tectonic load, erosion of the orogenic belt, is the 1st order driver. As the forebulge subsides, creating an anti-peripheral bulge (a sag), a shallow marine sea transgresses across the peripheral sag depositing a thin layer of carbonate or shale. The sediment type is dependent on the region’s climate as previously discussed.

7. *Marginal marine and terrestrial clastic wedge*

As the peripheral bulge subsides and the foreland basin is uplifted (Figure 7b), a single paleoslope is developed dipping cratonward. The uplifted foreland basin is composed of carbonates, fine- grained black muds (flysch deposit) which are sub-aerially exposed across low gradients adjacent to the sea, as a wide variety of depositional environments are developed. Associated lithofacies consist of redbeds, paleosols, coals, fluvial deposits, marginal marine deposits, and carbonates. The erosion of the basinal sediments, now acting as highlands, are transported cratonward and are interpreted as delta deposits. The Gordon sandstone was deposited during this stage of the sedimentation cycle in the Catskill delta clastic wedge, as these are the most extensive regressive deposits associated with the cycle (Ameri et. al., 2001; Boswell, 1988, 1992; Ettensohn, 1985, 2005).

ENVIRONMENTAL AND REGIONAL SETTING

Tectonic History

The eastern margin of Laurentia, present day North America, has a lengthy and complex tectonic history that begins with the Grenville orogeny that formed the Laurentia craton basement (Shumaker and Wilson, 1996). Succeeding the Grenville orogenic event, an early to mid-Cambrian rifting event developed a large graben structure that has been identified as the Rome trough (Figure 6), and has experienced reactivation throughout much of the Paleozoic (Hatcher, 1980; Goa, 1986; Shumaker, 1996; Shumaker and Wilson, 1996). Additional structural development of the Appalachian foreland basin persisted through three Paleozoic orogenic events: the Ordovician Taconic orogeny, the Devonian Acadian orogeny, and the Carboniferous Alleghenian orogeny (Hatcher, 1980; Gao, 1994; Shumaker, 1996; Shumaker and Wilson, 1996). The Taconic and Acadian orogenies are the two primary orogenic events that are most pertinent to this study of the Gordon sandstone (e.g. structural development of the Appalachian basin, sediment source, sedimentation cyclicity).

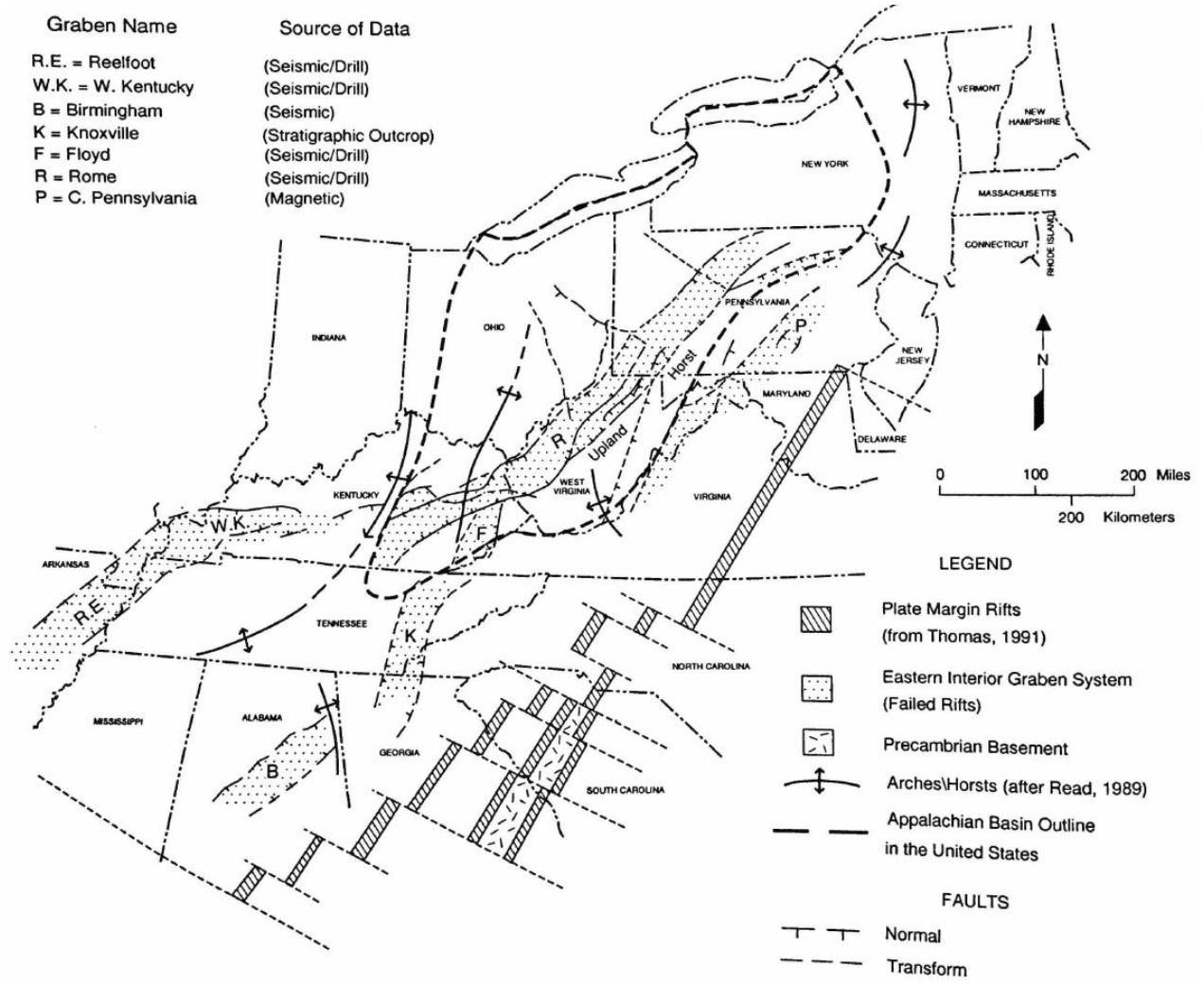

Figure 8: Schematic diagram of eastern Laurentia (North America) graben structures. Stipple pattern represent failed rifts, R= Rome trough. (Shumaker and Wilson, 1996).

Taconic Orogeny

During mid-Ordovician time through early Silurian time, encroachment of the Taconic terrane, also known as the Piedmont terrane, against the eastern margin of Laurentia occurred as the northwestern part of the Iapetus Ocean was closing (Hatcher and Odom, 1980). Subduction and obduction of ocean crust along eastern Laurentia resulted in crustal deformation and crustal thickening as the Iapetus Ocean basin fully closed, causing the accretion and suturing of the Taconic terrane to Laurentia (Figure 9). The thickened crust and tectonic loading of the

lithosphere resulted in lithospheric flexure and subsidence, developing the Appalachian foreland basin (Ettensohn, 1985, 2005). The accretion of the Taconic terrane to Laurentia produced the Taconic orogen. This orogen was the initial highland adjacent to the Appalachian Basin and, therefore the primary source of sediment to the basin following the onset and transgression of the epicontinental seaway (Ettensohn, 2005).

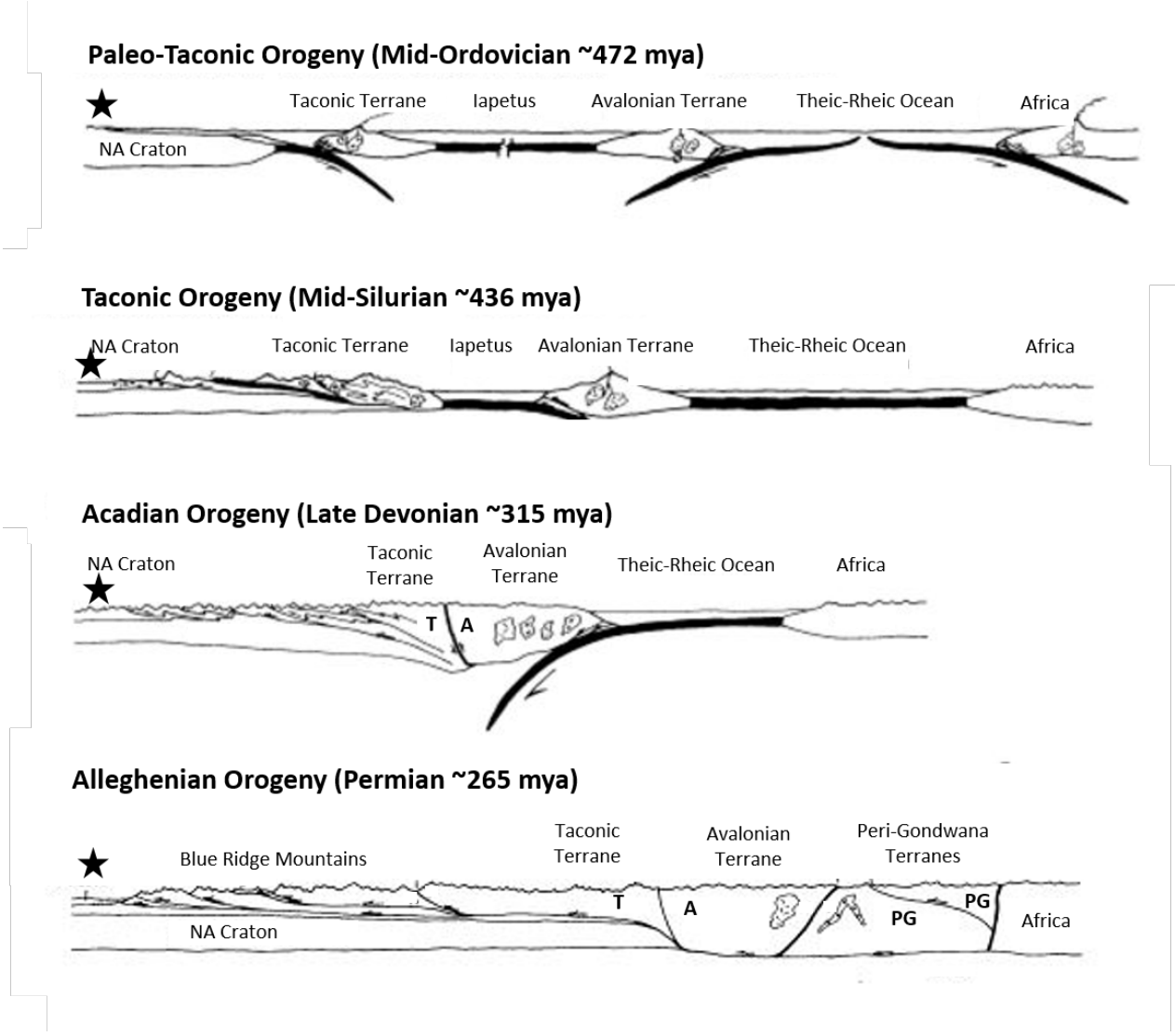

Figure 9: Schematic cross-section from Laurentia, North American craton (NA Craton), to Gondwana (Africa) from the mid-Ordovician through the Late Permian. Black star indicates the approximate location of West Virginia and present day Appalachian Basin. Modified from Hatcher and Odom, 1980.

Acadian Orogeny

Following the Taconic orogeny and a period of quiescence, the southeastern part of the Iapetus Ocean was closing. Early Devonian time marked the collision of the Baltic Shield against northeastern Laurentia and the middle to late Devonian collision of the Avalonian terrane against eastern and southeastern Laurentia (Figure 9). The southern migration of the convergence along the eastern Laurentia is the result of dexteral transpression of the Avalonian terrane and Peri-Gondwana terranes (Figure 9 and 10). Convergence of the Avalonian terrane to Laurentia occurred in four tectophases. Each tectophase has been defined by the convergence of Avalonia into the four promontories along the eastern margin of Laurentia: St. Lawrence, New York, Virginia, and Alabama promontories (Ettensohn, 1985) (Figure 3b). Maps of the regional unconformities along the peripheral forebulge and adjacent basinal black shales reveal a western and southern migration of tectonic convergence, respectively, which enabled the reconstruction of the Taconic and Acadian orogeny's tectonic history, spatially and temporally (Ettensohn, 1985).

Alleghenian Orogeny

Succeeding the Acadian orogeny and a brief period of quiescence, final closure of the Theic-Rheic Ocean ensued (Figure 9). Closure of the Theic-Rheic Ocean resulted in dexteral transpressional shear along the eastern margin of Laurentia (Hatcher, 1999). Locus of tectonism was focused in the central basin of the Appalachian Basin that generated fold-thrust belts and transport of previously deposited Paleozoic orogenic related sediment and strata. (Hatcher, 2005). The timing and locus of tectonism provides evidence that the Alleghenian orogeny is the likely orogenic event that caused the post depositional deformation of the Gordon sandstone.

Paleoclimate and Paleogeography

Paleoclimate and paleogeography are two factors one must consider when thinking of basin sedimentation rates and eustasy as tectonic plates collide with one another and migrate through global climate belts. Global climate zones are influenced by paleoclimate and paleogeography, altering the regional climate, e.g. rain shadow effect associated with an orogenic belt (Ettensohn et al., 2002; Cecil and DuLong, 2003; Cecil et al. 2004).

From early Cambrian time to latest Mississippian time, Laurentia migrated from approximately 40°S to 5°S (Figure 10). During Laurentia's migration, it passed through a low pressure humid to sub-humid environment (Figure 11a) into high pressure arid conditions (Figure 10b) and into a low pressure humid tropical climate (Figure 10c) (Scotese, 2003). Humid to sub-humid climate favored siliciclastic sedimentation in the Appalachian Basin due to increased rainfall, erosion and transport of siliciclastic-rich sediment from the highlands. During arid conditions, the basin and landmass received less rainfall and therefore less erosion and transport of siliciclastic material, allowing the preferential deposition of shallow marine carbonates or evaporites (Scotese, 2003).

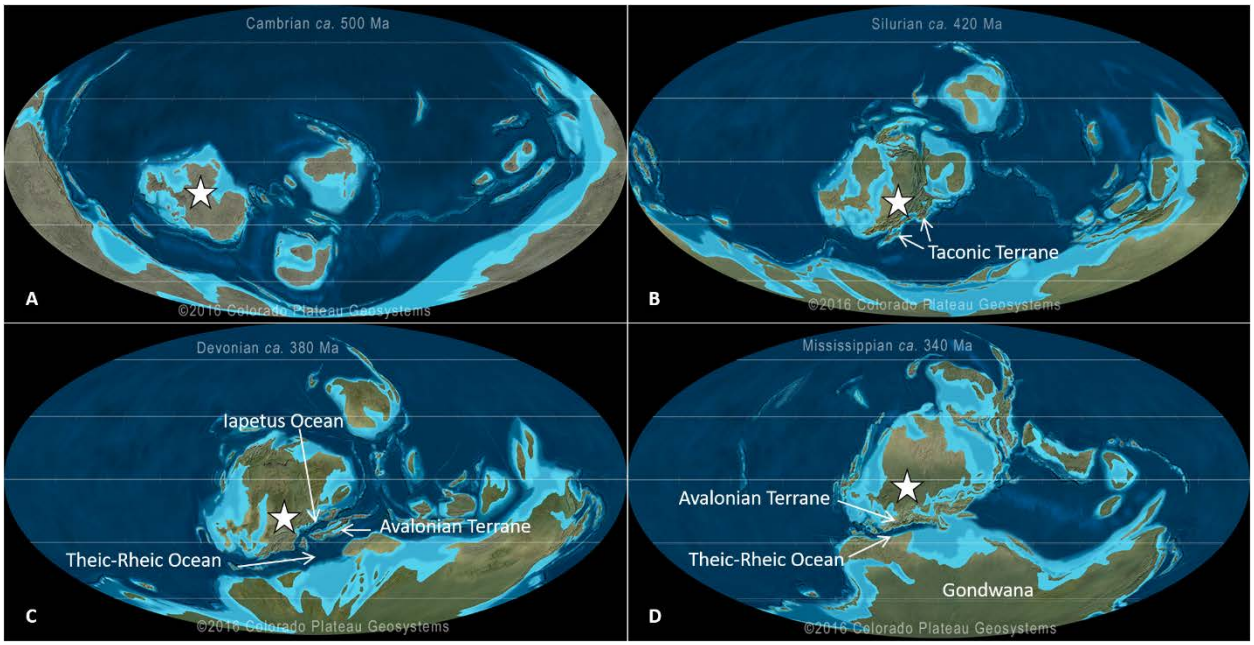

Figure 10: Schematic reconstruction of continents' paleogeographic location and orientation in space and time. A) Mid-Cambrian ~500 Ma. B) Silurian ~420 Ma. C) Devonian ~380 Ma. D) Mid-Mississippian ~340 Ma. The white star marks the location of Laurentia (Scotese, 2003).

Eustasy

Variability of eustasy in the Appalachian Basin has always been difficult to constrain because of the nearly continuous craton marginal convergence throughout the entire Paleozoic (Ettensohn, 2005). The often tectonically active eastern margin of Laurentia, and episodic tectonic quiescence, make traditional global eustasy models nearly irrelevant within the Appalachian basin. This suggests that much of the eustatic variance was controlled by tectonics (Dickenson et al., 1994). Scientists compared recurrence intervals related to global eustatic changes to reveal that 2^{nd} – 4^{th} order sea level cycles (10^7 – 10^5 years) within the basin are likely attributed to tectonics, whereas 5^{th} – 6^{th} order sea level cycles are likely associated with climatic changes and glacial and interglacial periods (Dickenson et al., 1994). Local deviation from either of these cycles suggests that local basement structures were reactivated causing localized

vertical motion of the crust. Most sediment sequences within the Appalachian basin suggest that the dominant factor that influenced local sea-level change was tectonics (Dickenson et al., 1994).

Gordon Sandstone

The Gordon sandstone has been defined as the most regressive deposit of sand during the third tectophase of the Acadian orogeny (Boswell, 1988, 1992). During the third tectophase (383 mya – 359 mya) the Kaskaskian epicontinental seaway experienced intermittent periods of transgression and regression of the shoreline. In the Appalachian Basin during the Late Devonian relative sea level was lowering as a result of tectonic uplift of the foreland basin (Boswell, 1988, 1992; Ettensohn, 1995). Maps of the Devonian Catskill shoreline (Figure 11) and a generalized stratigraphic cross-section of the Upper Devonian Catskill delta clastic wedge (Figure 12) generated from multi-well log studies, provide evidence that the Gordon is the maximum regressive deposit during the Late Devonian (Boswell, 1988, 1992).

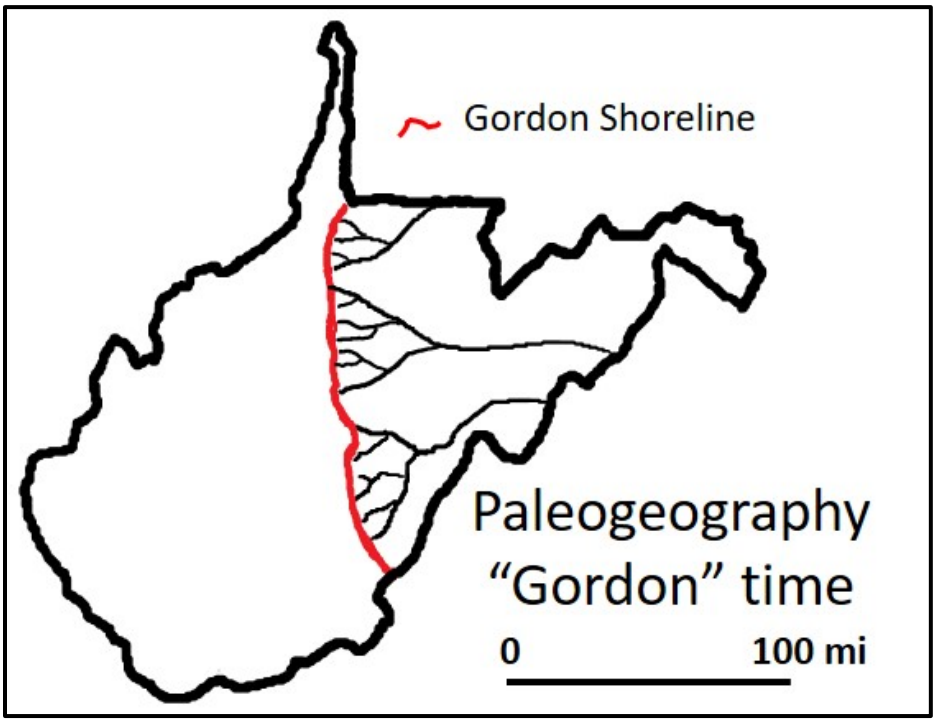

Figure 11: Schematic map of the Upper Devonian Gordon shoreline. Area east of the Gordon shoreline was sub-aerially exposed land. Modified from Boswell, 1992.

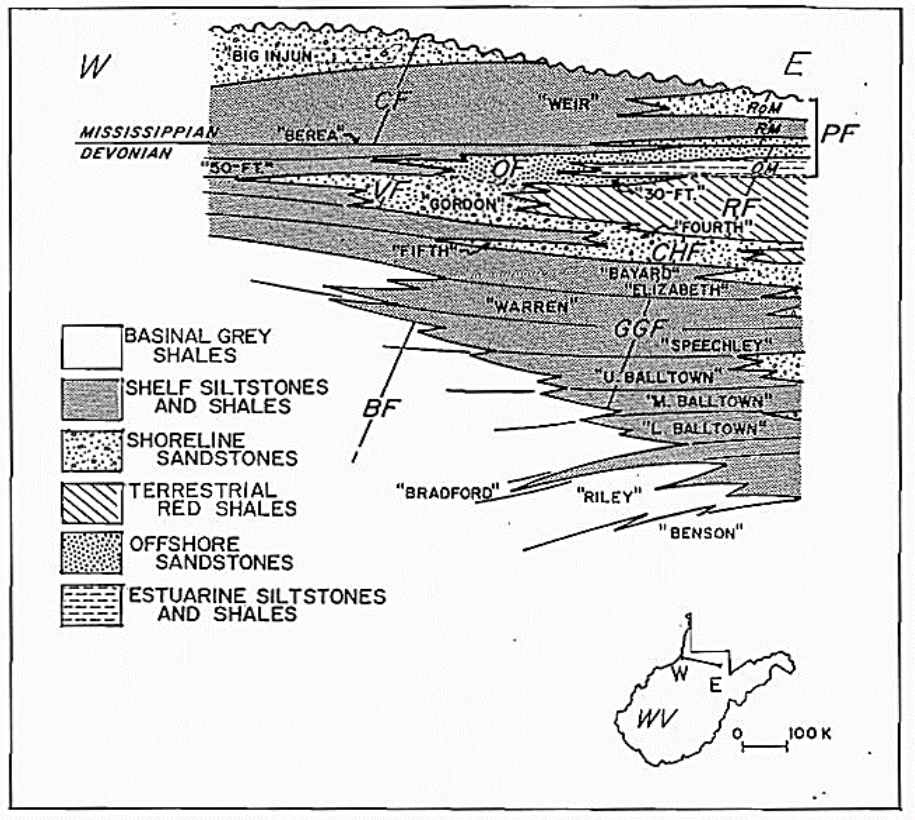

Figure 12: Generalized stratigraphic cross-section of the Upper Devonian Catskill delta clastic wedge in northern West Virginia. Adapted from Boswell, (1992).

The Gordon sandstone has been a prolific producer of petroleum resources in West Virginia. The Gordon sandstone in the Jacksonburg-Stringtown field in northern West Virginia has produced 88,500,000 barrels of oil following a gas injection project in 1931, and a waterflood project in 1990 (Ameri et al., 2001). The Gordon sandstone is the western most regressive sand body associated with the Upper Devonian Catskill delta clastic wedge, and was deposited in the seventh stage of the foreland basin sedimentation cycle (Marginal Marine and Terrestrial Clastic Wedge) (Ameri et. al., 2001; Boswell, 1988, 1992; Ettensohn, 1985, 2005). The Catskill delta clastic wedge is located along a late Devonian shoreline on the western flank of the Appalachian Mountains and the eastern margin of the Appalachian basin in what is present day Pennsylvania and West Virginia. Deposition of Gordon sediments occurred during the third

tectophase of the Acadian orogeny defined by the onset of oblique convergence and accretion of the Avalonian and Carolina terranes against the Virginia promontory located on the eastern margin of Laurentia (Figure 3a, b). The increased crustal deformation of the Virginia promontory resulted in increased subsidence of the Appalachian basin and uplift of the peripheral forebulge. This caused sub-aerial exposure of the lithosphere generating a regional unconformity along the western margin of the Appalachian basin and deposition of basinal black shales in the rapidly subsiding basin. Over time, the basin progressed through the foreland basin sedimentation cycle (Ettensohn, 1985). During the relaxation or tectonic unloading of the seventh, and final stage of the cycle, deposition of Gordon sediments occurred. Traditionally, the Gordon is described as marginal marine, composed of coarse-grained molasse type sediment that has been characterized as highly porous and permeable in a study of the Jacksonburg-Stringtown oil field in northern West Virginia, Ameri et al., (2001). The Gordon sandstone is composed of three parasequences and a variety of lithofacies; shale, heterolithic bioturbated, laminated sandstone, conglomerate sandstone, and featureless sandstone. Ameri et al., (2001) defined the pay zone in the Jacksonburg-Stringtown field as a featureless, fine-grained, well-sorted, lower shoreface sandstone in this location.

The gamma-ray signature of the Gordon consists of three parasequences. Each parasequence is bound by flooding surfaces and shale beds. The gamma-ray response to the individual Gordon parasequences suggest the Gordon is primarily composed of sand (Figure 13). Deposition of the Gordon sand bodies occurred during periods of regression, and the bounding shale beds found during periods of transgression. The gamma-ray signature geometry for the Gordon parasequences can be interpreted as blocky or symmetrical; both geometries exhibit

smooth and serrated response to the parasequence intervals (Figure 13). Each parasequence gamma-ray response exhibits a coarsening and then fining upward trend (Figure 13).

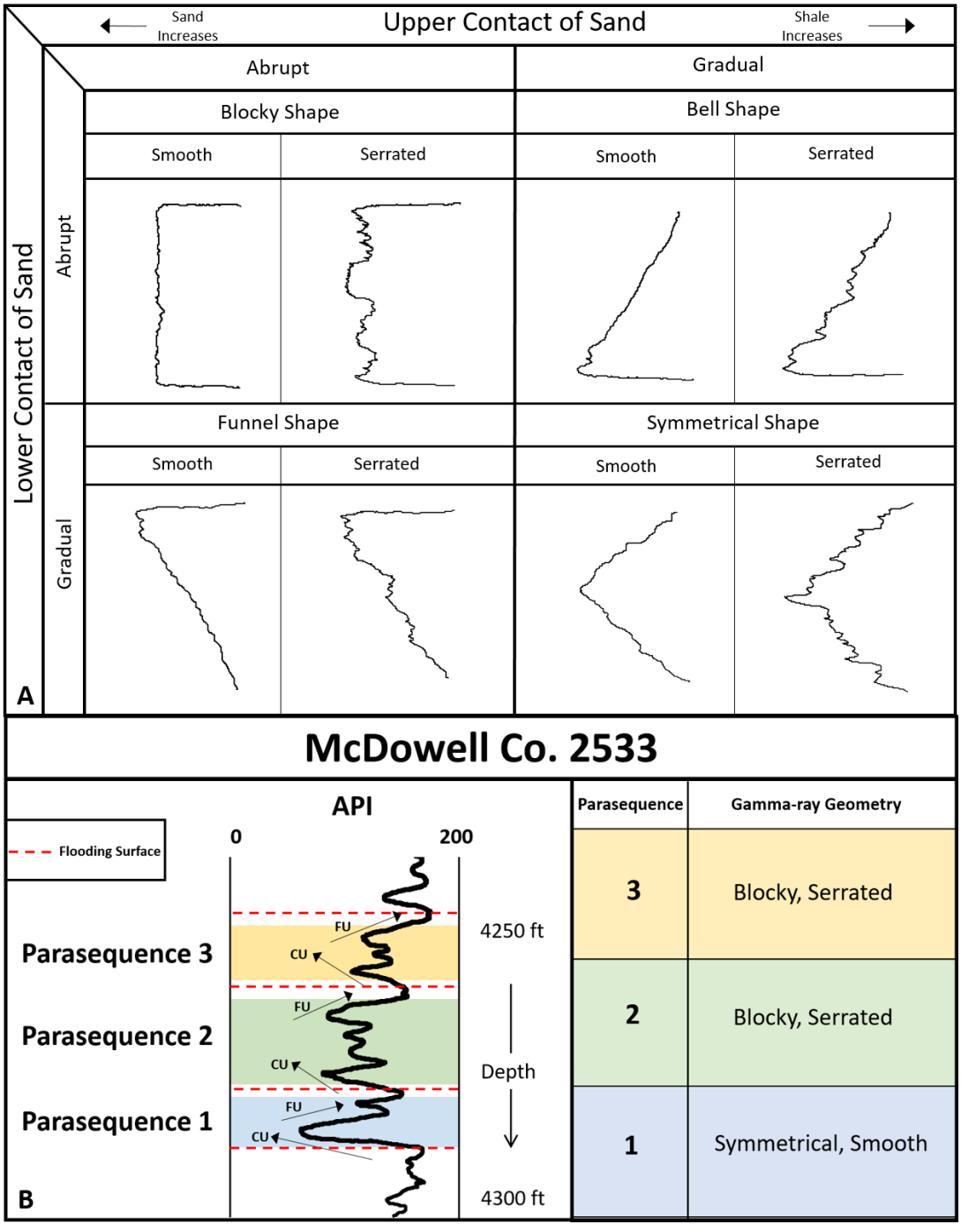

Figure 13: A) Typical gamma-ray response to sediment type, and gamma-ray signature geometries. Modified from Serra and Sulpice, (1975) and Muslim (2014). B) Gamma-ray response of the Gordon interval and the three parasequences that compose the Gordon. Abbreviations that correspond to arrows on the gamma-ray log, indicate coarsening upward (CU) and fining upward (FU) sediment trends.

METHODOLOGY

Data Collection

All data, geophysical and petrophysical, were obtained from the West Virginia Geological and Economic Survey (WVGES) online database.

Geographic Data

For every wireline log, latitude, longitude, county name, elevation, and vertical datum values were recorded from the WVGES online database and each well log header. Latitude and longitude were recorded in decimal degrees. The vertical datum was determined by the point from which the wireline log was measured (e.g. Kelly Bushing, Ground Level) and is recorded as feet above sea level.

Geophysical Data

Geophysical wireline data are public information and were obtained from the WVGES online database. Two wireline parameters, gamma-ray and bulk density, were analyzed across 127 wells and used as proxies to interpret physical rock properties.

Gamma-ray values were used to determine the API value for each well that is equal to 50% sand (Figure 14). The 50% sand technique is that used by Boswell (1988, 1993) for mapping Upper Devonian sands along the Catskill delta clastic wedge (e.g. Gordon sandstone). The gamma-ray log signature was used as a proxy for lithology and to determine the thicknesses for a particular lithology and associated gamma-ray signature. Low API values (left kicking gamma-ray response) generally may be interpreted as sandstone or carbonates, whereas high API values (right kicking gamma-ray response) generally may be interpreted as shale (Figure 14) (Schlumberger, 1989).

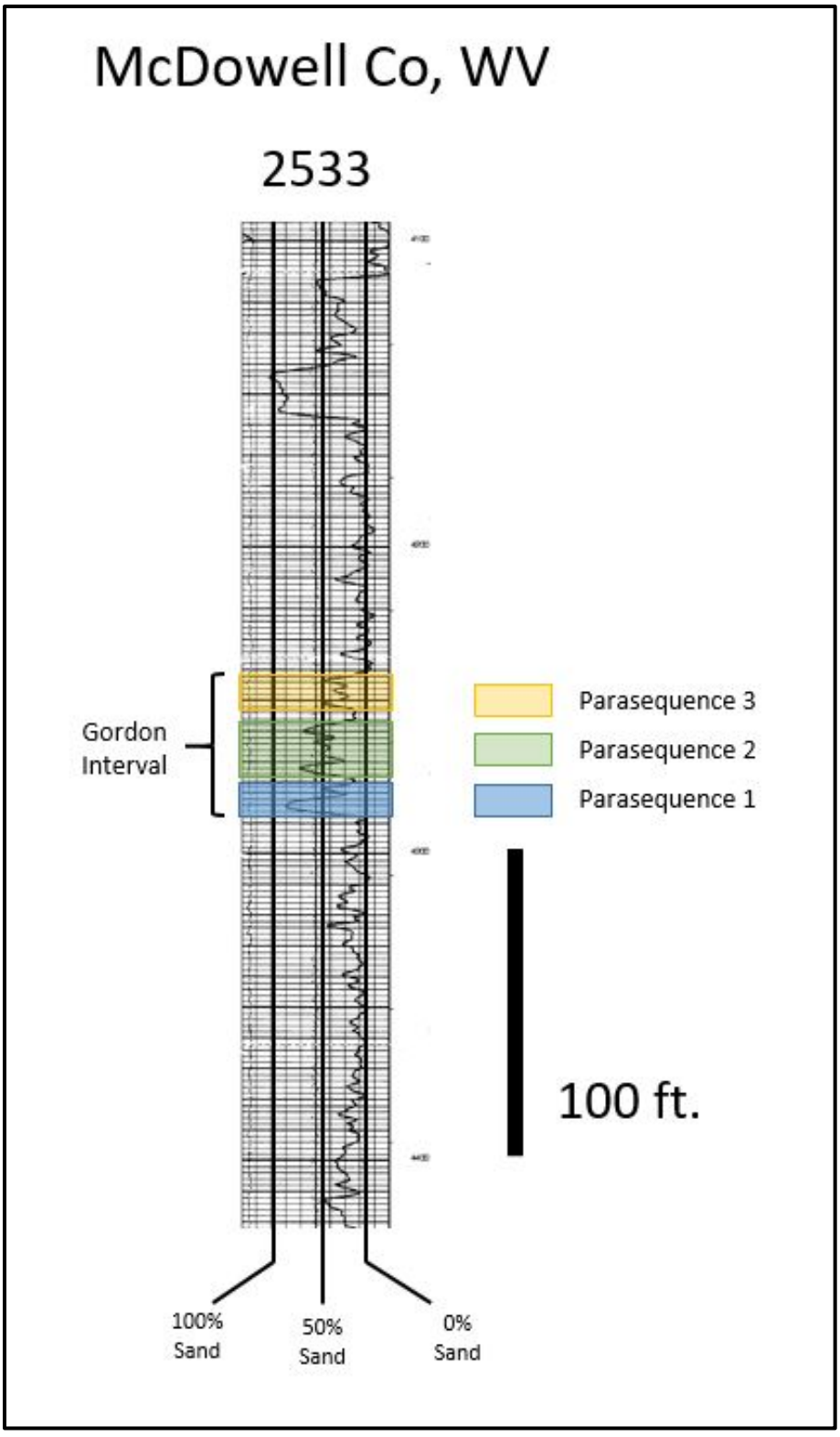

Figure 14: Gamma-log for well 2533 in McDowell County, West Virginia. Gamma-ray response show typical gamma-ray signature for the Gordon sandstone. Gamma-ray log of the total Gordon interval, including the three component parasequences, are shown. Lines used to constrain isolith thickness, are included as 0% sand, 50% sand, and 100% sand.

Cross-Sections

Cross-sections were hung from the top of the Berea Sandstone with the assumption that it represents a planar surface. This assumption is made on the premise that the top of the Berea represents a maximum flooding surface (MFS) (Muslim, 2014) as defined by Catuneanu (2006). The Gordon is a drillers' term and may be defined differently locally and regionally. Assurance for consistent usage of Gordon nomenclature was achieved by producing cross-sections (Plate 1) that show correlative Gordon sediments across West Virginia.

Structure Contours

Elevation values for the structural surfaces of the: top of the Berea Sandstone, top of the Gordon sandstone, and base of the Gordon sandstone; are recorded as a function of depth from the datum or where the wireline was measured (e.g. Kelly Bushing or Ground Level). The structure contour values for each well were calculated by determining the difference between the elevation of the structures surface, recorded from the wireline log, and the datum from which the wireline log was measured. The surfaces were picked by using the gamma-ray log as a proxy for distinguishing lithologies and identifying the signature of the Berea Sandstone and the Gordon sandstone.

Isopach

Thickness values were calculated from wire-line gamma-ray logs for the entire Gordon sandstone interval and rocks that overlie the Gordon to the top of the Berea. Thickness for the total Gordon interval was calculated by determining the difference between the top and base of the Gordon. Isopach values were mapped to show regional trends.

Isolith

Isolith values are thickness values of a particular lithology. To be consistent with Boswell's (1988) study, the 50% sand fraction was calculated and mapped. The 50% sand fraction was determined by taking the average of the well's shale baseline API value (0% sand) and the cleanest sand API value (100% sand) (Figure 14) (Boswell and Jewell, 1988; Boswell et al., 1993).

Well Log Porosity

Minimum bulk density values were used in the Archie equation (Equation 1) (Schlumberger, 1989) to calculate the fraction of the log porosity within a sample, and then converted to log porosity percent for the selected interval (e.g. total Gordon interval, individual parasequences). To calculate log porosity, the density of the fluid (ρ_f) and density of the matrix (ρ_{ma}) are recorded from the well log header, and bulk density of an interval (ρ_b) from the wire-line log.

$$\Phi = \frac{\rho_{ma} - \rho_b}{\rho_{ma} - \rho_f}$$

Φ Log Porosity

ρ_{ma} Matrix Density

ρ_b Formation Density

ρ_f Density of Fluid

Equation 1: Archie equation used to calculate log porosity, expressed as fractional percent, from the bulk density log. Schlumberger (1989).

Petrophysical Data

Seven cores were drilled by Pennzoil, and used by Ameri et al., (2001) to measure the petrophysical properties (core-measured porosity and core-measure permeability of a sample) for the Gordon interval to characterize the reservoir in the Jacksonburg-Stringtown field in northern

West Virginia. All data collection techniques are recorded in Ameri et al., (2001). The core-measured porosity and core-measured permeability data collected in the Ameri et al., (2001) study were plotted against one another and an exponential trend line was calculated.

Modeling and Data Processing

Microsoft Excel

Microsoft Excel®, a spreadsheet program, was used to record and calculate values for mapping and geospatial analysis. The following values were calculated using Excel: structure contour values for the top of the Berea Sandstone and the Gordon's top and bottom, API value that represents 50% sand fraction, isopach values used as a proxy for paleo-topography and the Gordon sandstones' total interval, log porosity, and predicted permeability.

ArcGIS 10.4.1®

ArcGIS 10.4.1® is a geographic information management system that is used to store and manipulated geographic datasets for this study the software was used to store raster geophysical well data. The inverse distance weight (IDW) geostatistical analysis tool was used to interpolate selected values between well locations.

Structure Contour Maps

Structure contour maps were generated using the (IDW) geostatistical analysis tool in ArcGIS 10.4.1® to interpolate spatial variation of the elevation of selected surfaces. These maps enable the interpretation of the surfaces as a function of its depth from sea level.

Isopach Maps

Isopach maps were generated using the IDW geostatistical analysis tool in ArcGIS 10.4.1® to interpolate thickness between wells that have defined thickness values. These maps enable the interpretation of spatial variation sandstone thickness. Interpreting thickness values

relative to their proximity to the source of sediment and energy regimes for a geographic area were used as a proxy to define environments of deposition along the Upper Devonian Catskill delta clastic wedge.

Isolith Maps

Isolith maps were generated using the IDW geostatistical analysis tool in ArcGIS 10.4.1® to interpolate values between wells that have defined thickness values for rocks composed of ≥50% sand. Thickness values were used as a proxy for local or regional energy regimes and depositional environment.

Log Porosity

Log porosity maps were generated using the IDW geostatistical analysis tool in ArcGIS 10.4.1® to interpolate porosity values between wells that have defined calculated log porosity values. Log porosity maps were used to evaluate spatial trends of porosity in Gordon sedimentary rocks in the study area.

Permeability Prediction

Petrophysical and petrological data, consisting of core-measured permeability, and core-measured porosity from Ameri et al., (2001), were plotted against one another. An exponential trendline was fit to the dataset. Two cross-plots were generated; one used the max porosity value and its associated permeability value for each of the seven cores, whereas the second plot utilized all porosity values and their associated permeability values along the entire length of the core for each of the seven cores.

Maximum porosity values were taken from the pay zone that was characterized as lower shoreface by Ameri et. al., (2001). Gordon sediments in south-central West Virginia are interpreted to be continental inner shelf sands to continental shelf edge sands that would experience very

similar energy regimes, and have similar sediment characteristics to lower shoreface environments. Thus, lower shoreface petrophysical data collected by the Ameri et al., (2001) study to be used as a proxy for the continental shelf sheet sands that characterize the Gordon sandstone in south-central West Virginia.

Log porosity values calculated from wire-line bulk density values were input into the equation that defines the exponential curves for each cross-plot, which enabled the calculation of predictive permeability value for the Gordon across the study area in southern West Virginia.

RESULTS

Cross-Sections

Cross-sections show Gordon sediments are correlative across West Virginia and the study area in south-central West Virginia, confirming consistent use of Gordon nomenclature in West Virginia (Plate 1). Transects are hung on the top of the Berea Sandstone which is the latest maximum flooding surface of the fourth tectophase of the Acadian orogeny (Ettensohn, 1995; Muslim, 2014). Cross-sections show vertical variation (depth, thickness) of Gordon sediments along each cross-section, and lateral thinning in a basinward (westward) direction. Along the Catskill delta complex in northern West Virginia, Gordon sediments are thickest and thin in a southern or basinward direction. Cross-sections, A-A'-A'' (Plate 1) is a NNE-SSW oriented transect across West Virginia that illustrates that Gordon sediments are correlative across West Virginia from the Catskill delta complex to the study area. Transect A-A' (Figure 15a) is the southern extension of A-A'-A" (Plate 1) located in the study area, along with B-B' (Figure 15b), and are oriented in a NNE-SSW direction. Transects C-C' (Figure 15c), D-D' (Figure 15d), and E-E' (Figure 15e) are located in the south-central West Virginia study area, and are oriented in an east to west direction.

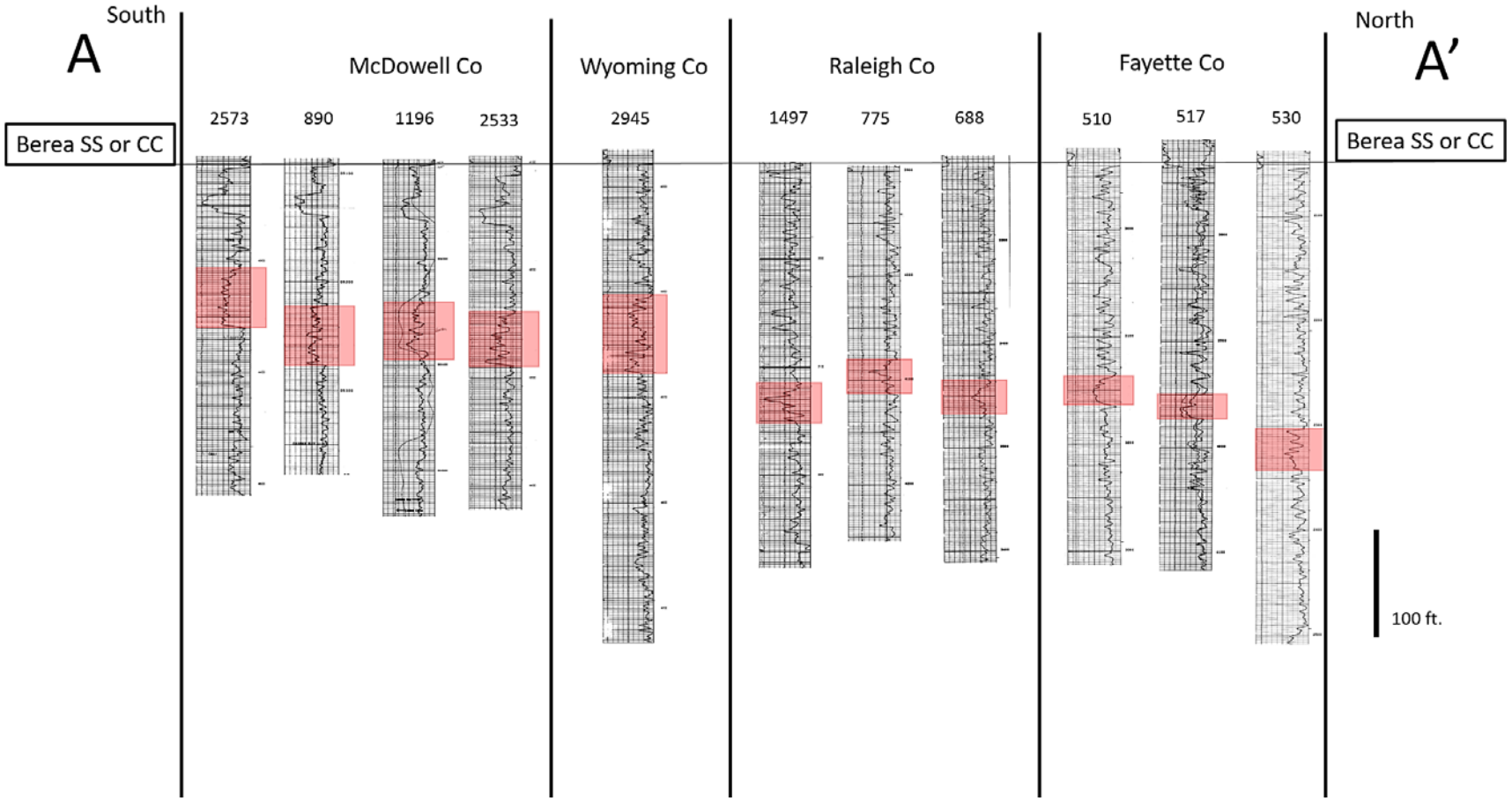

Figure 15: Cross-sections; A, B, C, D, E show the lateral continuity of the Gordon sandstone and correlative sediments across West Virginia. No horizontal scale. Well logs are shown spaced equidistantly. See Figure 4 for location of cross-sections.

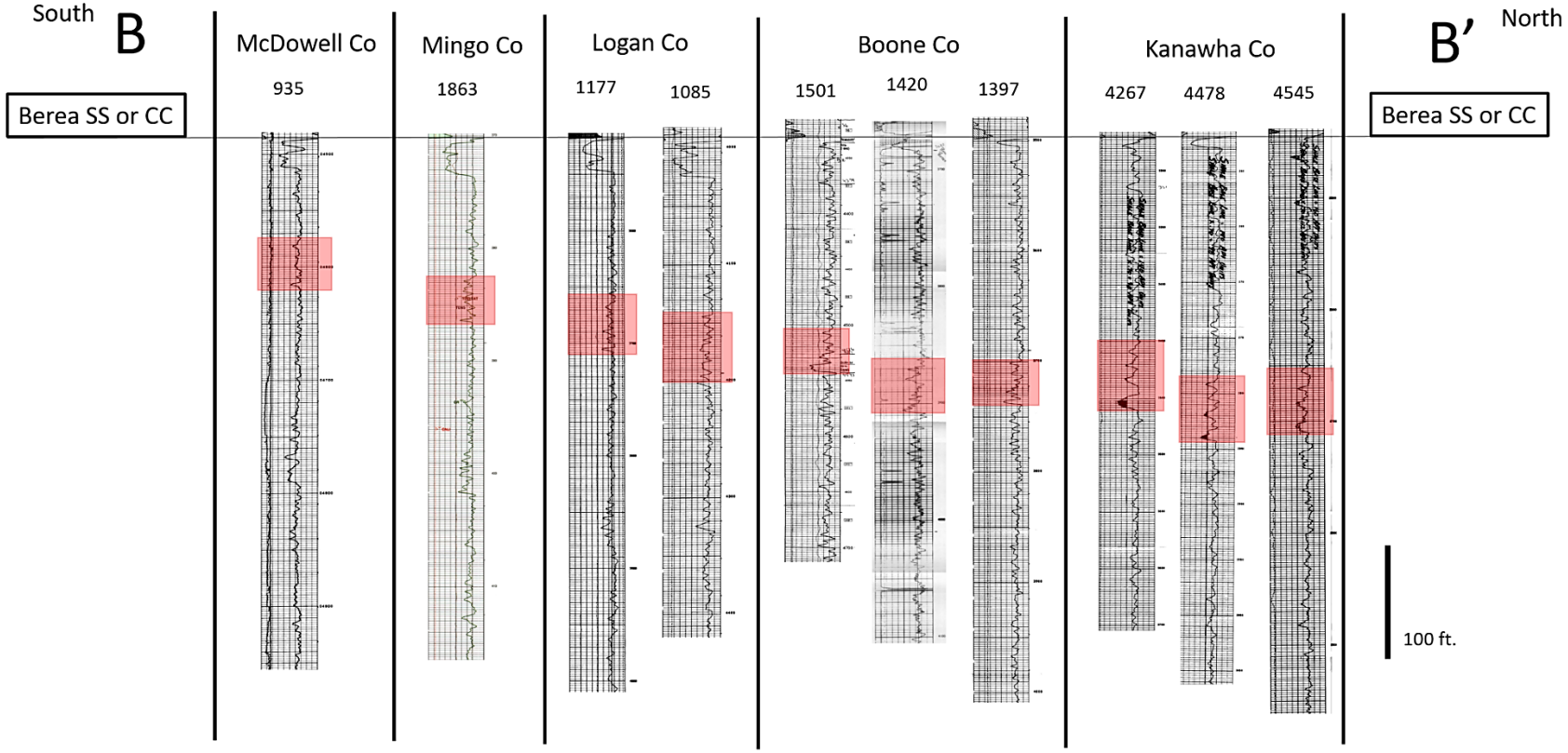

Figure 15 (Continued): Cross-sections; A, B, C, D, E show the lateral continuity of the Gordon sandstone and correlative sediments across West Virginia. No horizontal scale. Well logs are shown spaced equidistantly. See Figure 4 for location of cross-sections.

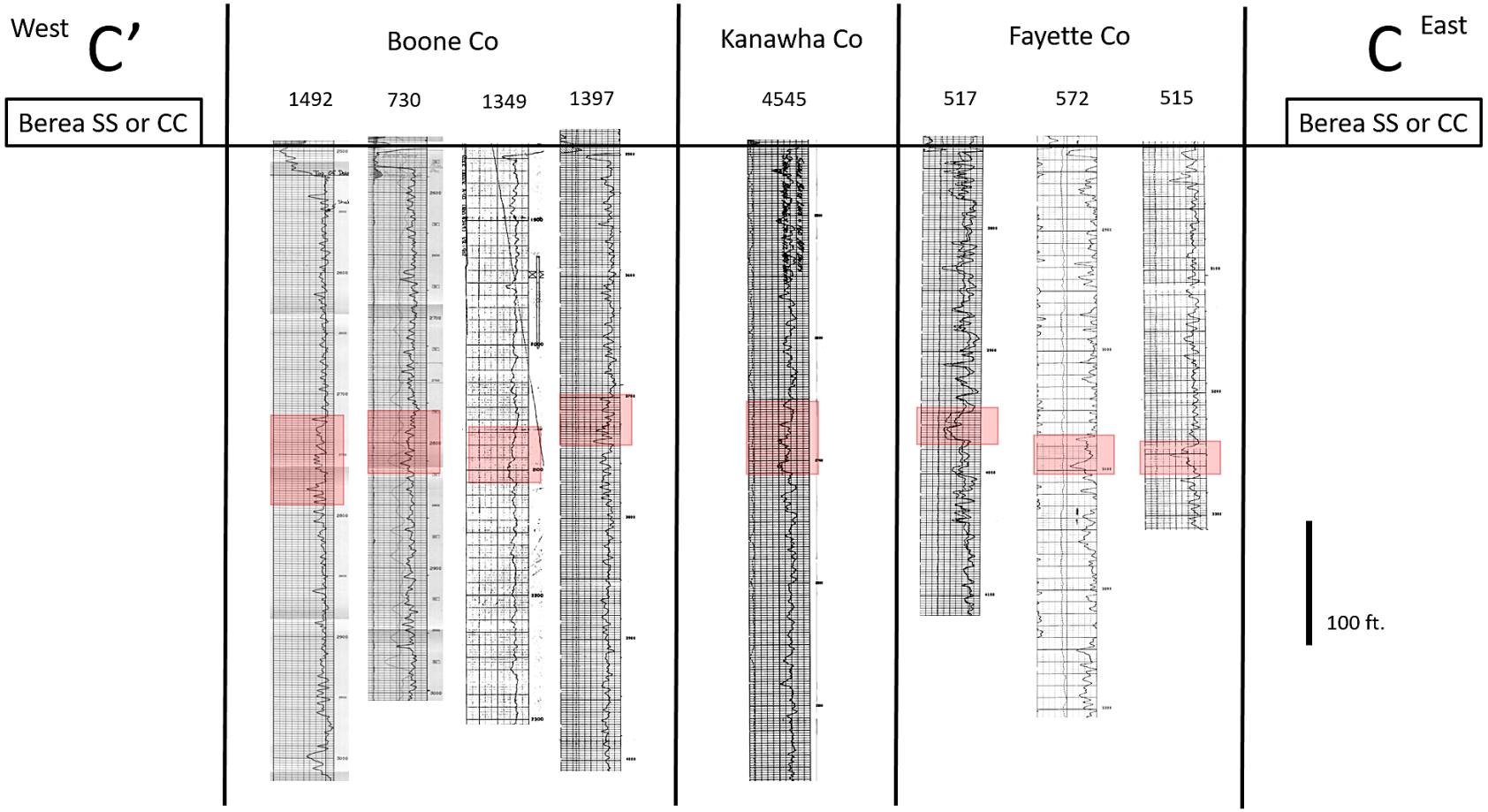

Figure 15 (Continued): Cross-sections; A, B, C, D, E show the lateral continuity of the Gordon sandstone and correlative sediments across West Virginia. No horizontal scale. Well logs are shown spaced equidistantly. See Figure 4 for location of cross-sections.

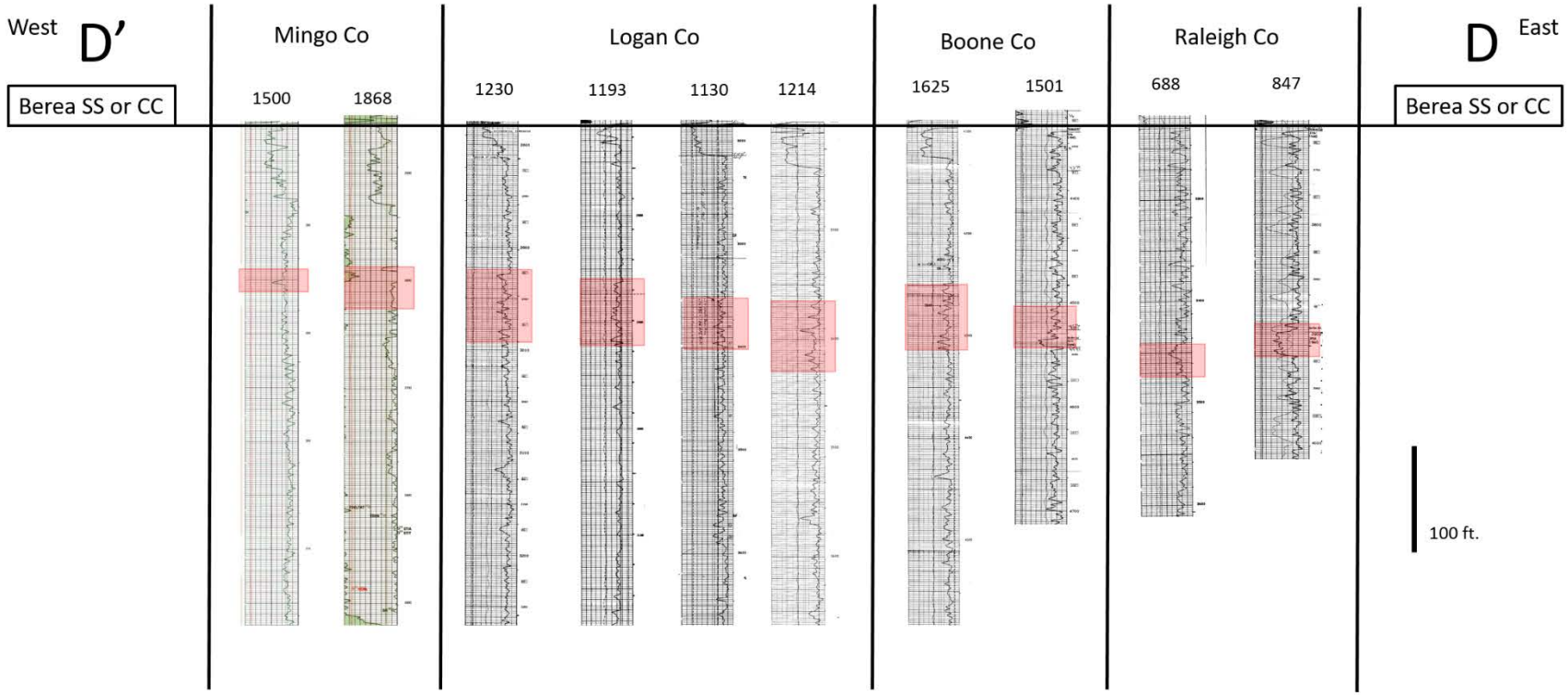

Figure 15 (Continued): Cross-sections; A, B, C, D, E show the lateral continuity of the Gordon sandstone and correlative sediments across West Virginia. No horizontal scale. Well logs are shown spaced equidistantly. See Figure 4 for location of cross-sections.

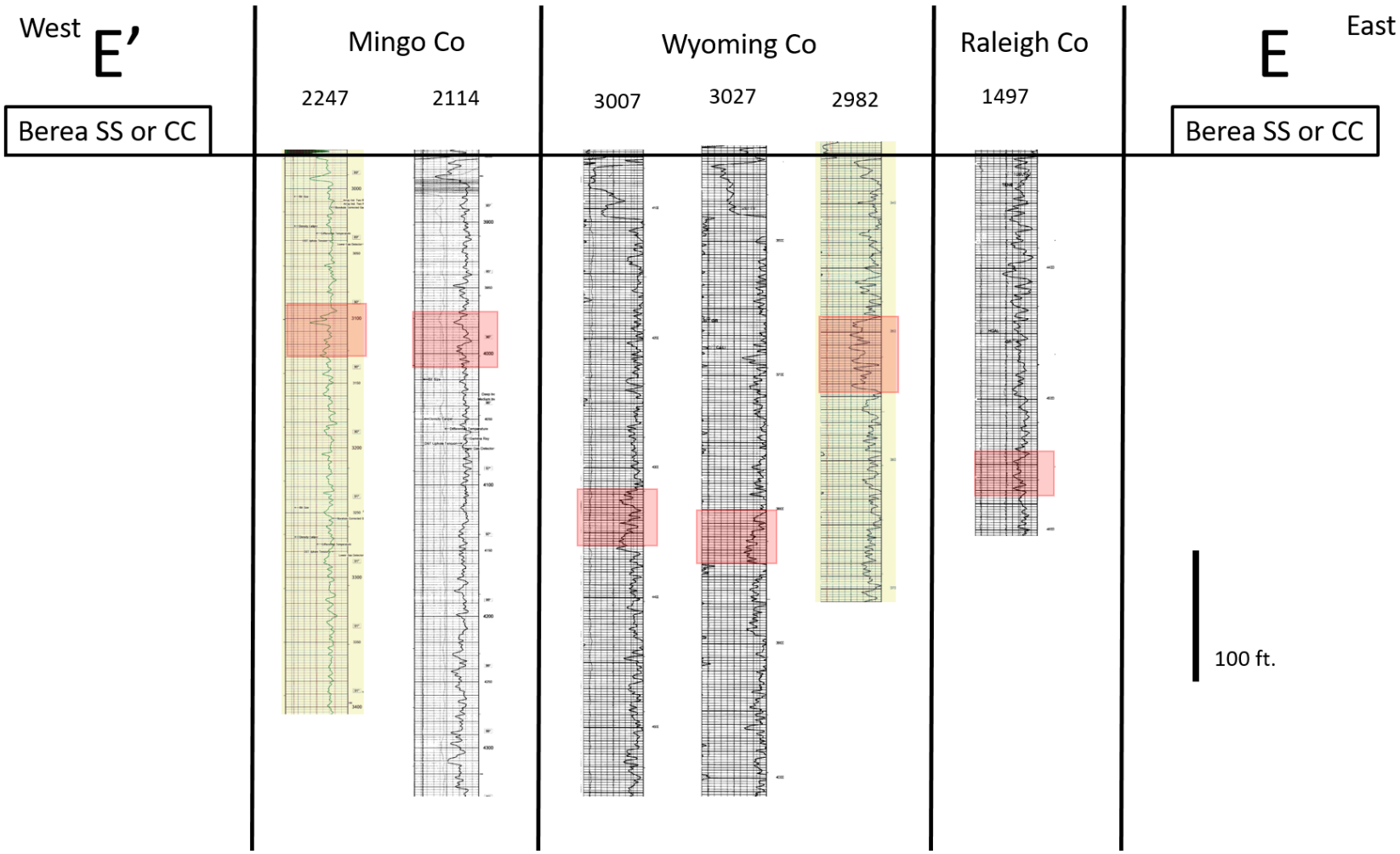

Figure 15 (Continued): Cross-sections; A, B, C, D, E show the lateral continuity of the Gordon sandstone and correlative sediments across West Virginia. No horizontal scale. Well logs are shown spaced equidistantly. See Figure 4 for location of cross-sections.

Cross-section A-A’ (Figure 15a) is the southern portion of a long cross-section A-A’-A” (Plate 1). Figure 15a exhibits a thicker Gordon interval in the south of the study area, which thins to the north. The thicker Gordon interval in the northern West Virginia cross-section (A’-A”, Plate 1) illustrates that the interval between the top of the Berea Sandstone and the top of the Gordon sandstone is thickest. In the study area, transect A-A’ (Figure 15a) illustrates that the thickest Gordon interval is in the south (McDowell 2573, 55 ft) and it thins to the north (Fayette 530, 40 ft), whereas the interval between the Berea Sandstone and the top of the Gordon is most thinnest in the south (McDowell 2573, 90 ft) and thickens to the north (Fayette 530, 248 ft).

Cross-section B-B’ (Figure 15b) illustrates that the Gordon interval from the southern end of the transect (McDowell 935, 37 ft) thickens to the northern end (Kanawha 4545, 60 ft). The top of the Gordon sandstone occurs at its shallowest depth in southern West Virginia (McDowell 935, 87 ft), and at its deepest depth in the northern part of the study area (Kanawha 4545, 208 ft), thickening in a northerly direction.

Cross-section C-C’ (Figure 15c) exhibits a thickness trend unlike others presented in this study. The thickest Gordon interval is found in the west (Boone 1492, 72 ft) and thins to the east (Fayette 515, 25 ft). The Gordon interval contains very little coarse-grained sediment which is evident by high API gamma-ray values. The interval thickness between the top of the Berea Sandstone and Gordon sandstone exhibits little variation from east (Fayette 515, 242 ft) to west (Boone 1492, 224 ft).

Cross-section D-D’ (Figure 15d), exhibits a unique trend relative to other cross-sections produced for this study. Figure 15d illustrates that the Gordon sandstone is thickest near the middle of the cross-section (Boone 1214, 66 ft), thinning and tapering to the west (Mingo 1500, 20 ft) and east (Raleigh 847, 30 ft), showing that the Gordon interval exhibits a lenticular geometry. The cross-section illustrates that the Gordon gently dips to the east, which is illustrated by the interval between the top of the Berea Sandstone and the top of the Gordon thickening in a eastward direction (Mingo 1500, 136 ft; Raleigh 847, 176 ft).

Cross-section E-E’ (Figure 15e) is the most southerly east to west striking vertical section in the study area. E-E’ illustrates minimum variability of the Gordon’s thickness from the eastern most well (Raleigh 1497, 29 ft) to the western most well (Mingo 2247, 35 ft). Figure 15e shows that the interval between the top of the Berea Sandstone and the top of the Gordon sandstone is moderately variable from east to west (Raleigh 1497, 228 ft; Wyoming 2982, 124 ft; Wyoming 3007, 139 ft; Mingo 2247, 119 ft).

Structure Contour Maps

Structure contours were evaluated for the top of the Berea Sandstone, top of the Gordon sandstone, and base of the Gordon sandstone (Figures 16, 17, 18). The western margin of the mapped study area exhibits a sub-linear structural high that corresponds with the eastern margin of the Rome Trough (Ryder et al., 2008). The low lying structural basin to the southeast of the Rome Trough eastern margin exhibits a NE-SW structural trend composed of a syncline and an anticline. Faulting is a possible cause of structural relief, but is not evident within the cross-sections (Figure 15).

Top of the Berea Sandstone

In the western margin of the mapped area a sub-linear structural high is evident oriented in a NE-SW direction. In south-central West Virginia study area, there is a NE to SW structural trend (Figure 16), located southeast of the Rome Trough eastern margin, and is composed of a syncline and anticline. In the study area, the Berea occurs at its shallowest depth of 492 ft in Fayette County well 4701900515 (Appendix II) (located along the Mann Mountain anticline crest), and at a maximum depth of 2647 ft in McDowell County well 4704701196 (Appendix II); this illustrates that the surface dips to the southwest (Figure 16).

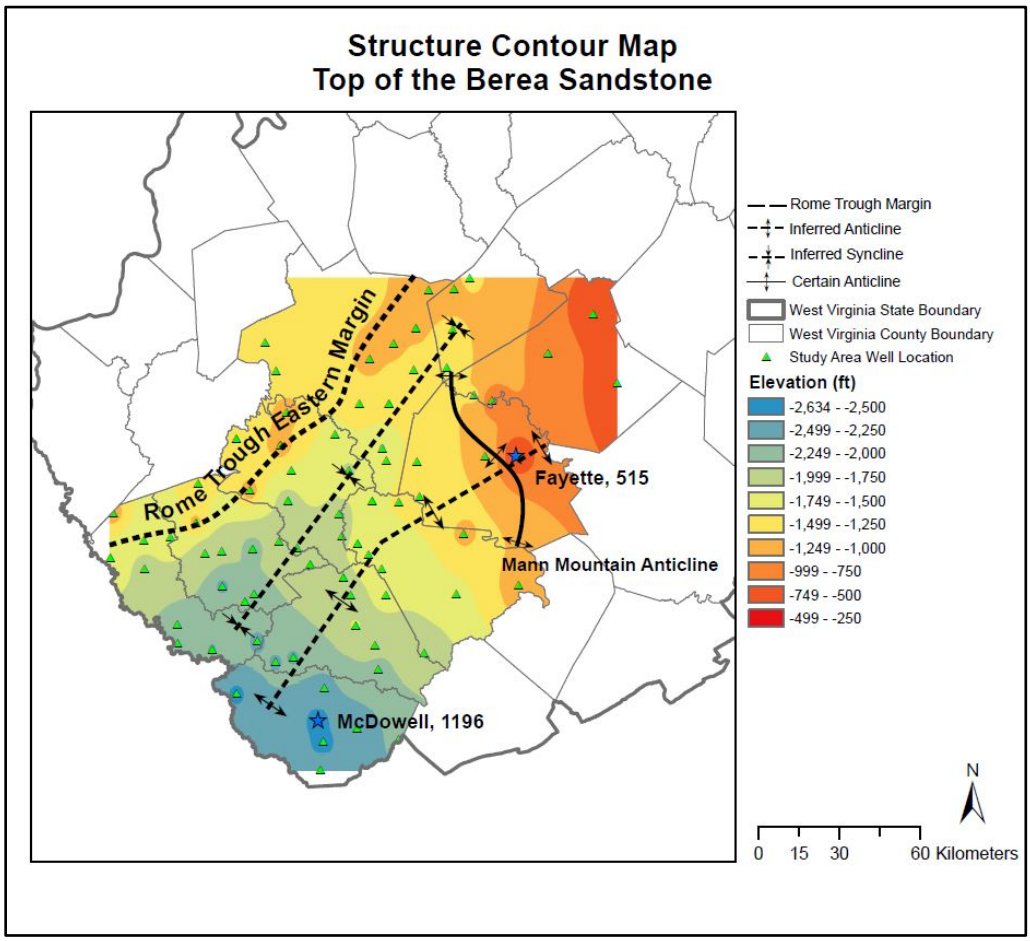

Figure 16: Detailed structure contour map of the focal study area, expressed as feet below sea level to the top of the Berea Sandstone. North-northeast to south-southwest structure trend is observed. Rome Trough margin from Ryder et al. (2008). Data used to construct this map are found in Appendix II.

Top of the Gordon Sandstone

Mimicking that of Figure 16, the top of the Gordon sandstone exhibits a sub-linear structural high along the western margin of the study area, that trends NE-SW. In the focal study area a structural basin is observed southeast of the Rome Trough eastern margin (Ryder et al., 2008) that exhibits a NE-SW structural trend (Figure 17) that is composed of a syncline and an anticline. In the focal study area located in south-central West Virginia, the Gordon sandstone occurs at its shallowest depth of 734 ft in Fayette County well 4701900515 (Appendix II) (located along the Mann Mountain anticline crest), a maximum depth 2802 ft in McDowell County well 4704700890 (Appendix II), and dips to the southwest (Figure 17).

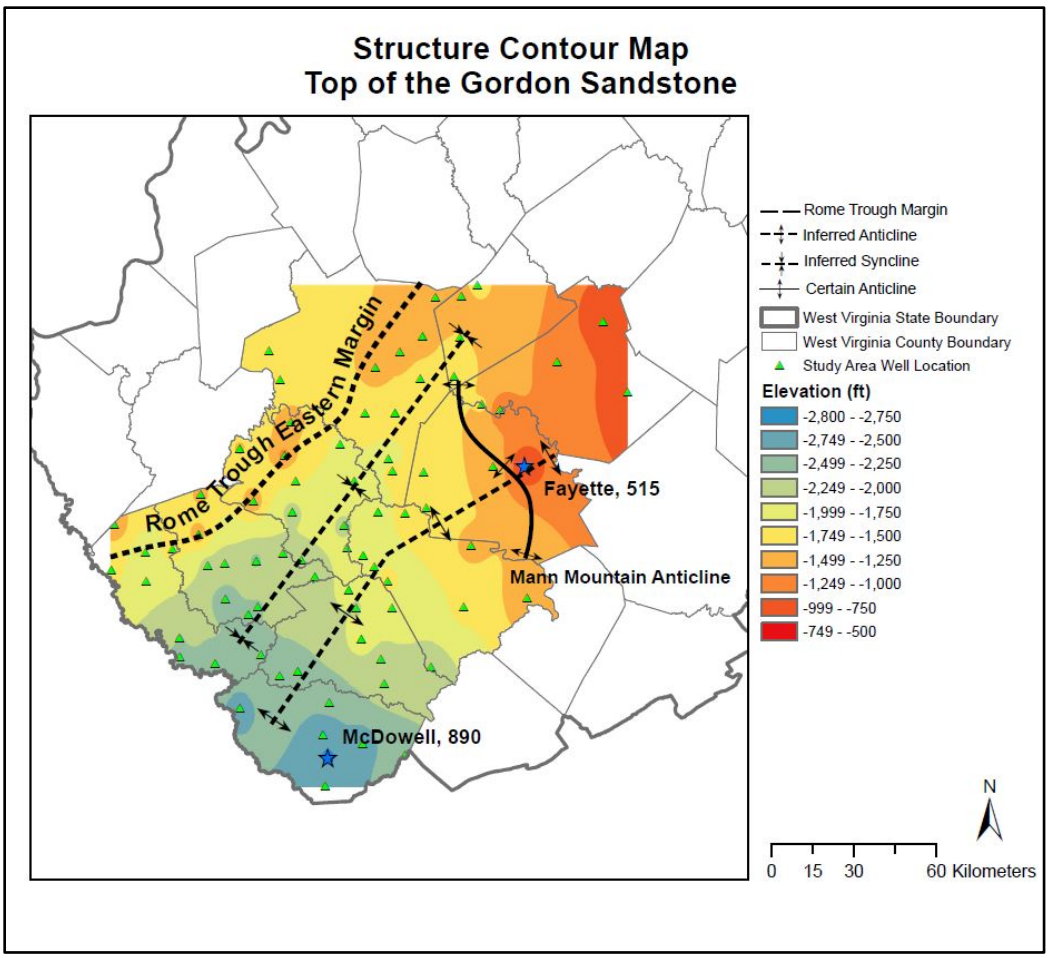

Figure 17: Detailed structure contour map of the focal study area, expressed as feet below sea level to the top of the Gordon sandstone. North-northeast to south-southwest structure trend is observed. Rome Trough margin from Ryder et al., (2008). Data used to construct this map are found in Appendix II.

Base of the Gordon Sandstone

The base of the Gordon sandstone contour map mimics the geometry of the top of the Berea Sandstone and top of the Gordon sandstone, in that the sub-linear structural high along the western margin of the mapped study area is associated with the eastern margin of the Rome Trough (Ryder et al., 2008). Southeast of the Rome Trough margin is a structural basin that exhibits a NE-SW structural trend that is composed of a syncline and an anticline. In the focal study area, the base of the Gordon sandstone occurs at its shallowest depth of 759 ft in Fayette

County well 4701500515, a maximum depth of 2856 ft in McDowell County well 4704700890, and dips to the southwest.

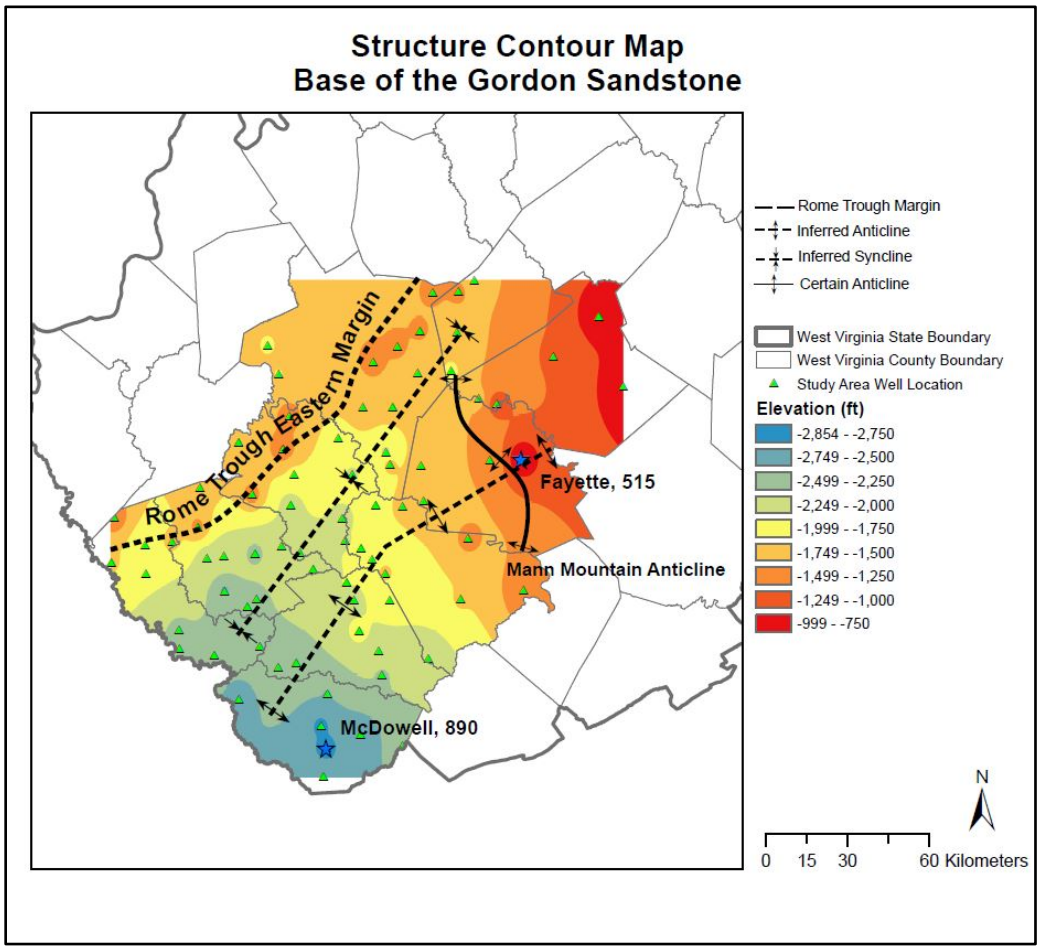

Figure 18: Detailed structure contour map of the focal study area, expressed as feet below sea level to the base of the Gordon sandstone. North-northeast to south-southwest structure trend is observed. Rome Trough margin from Ryder et al., (2008). Data used to construct this map are found in Appendix II.

Isopach Maps

In this study isopach maps were generated for the entire Gordon interval and the interval between the top of the Berea Sandstone and the top of the Gordon sandstone. A detailed version was produced to investigate the Gordon sandstone in the study area, south-central West Virginia.

Total Gordon Interval

The isopach map of the total Gordon sandstone interval (Figure 19) shows that it is thickest along the western margin of the Catskill delta complex and thins in a radial basinward direction. A dendritic geometry of thicker Gordon strata extends away from the Catskill delta complex strata into the basin (Figure 19). The total Gordon sandstone interval ranges in thickness from 10 ft to 202 ft. The Gordon sandstone thins to the south and west. Overall distribution of total Gordon strata are closely matched by that of the isolith map (Figures 22, 23).

In south-central West Virginia, total Gordon sandstone interval thickness exhibits no defined geometry (Figure 20). Localized areas of thicker strata represent all lithologies that compose the Gordon interval (e.g. sandstone, shale, siltstone), and are not directly associated with reservoir quality Gordon strata. Total Gordon interval strata thicknesses range between 18 ft and 74 ft (Figures 19, 20).

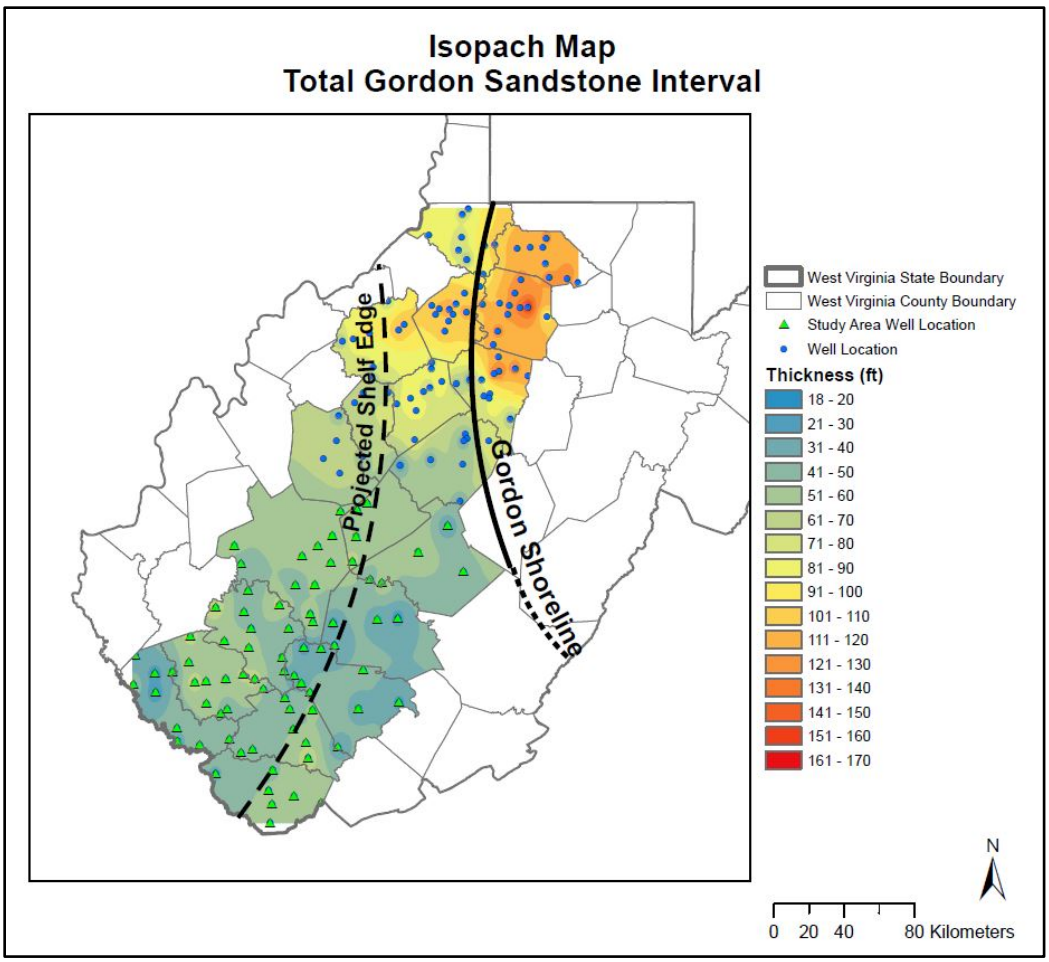

Figure 19: Isopach map of the total Gordon sandstone interval. Thickest sediments are located along the Catskill delta complex and thin in a basinward direction. Projected Gordon shoreline form Boswell and Jewell (1988). Projected Gordon shelf edge from the isolith high (Figure 21, 22). Data used to construct this map are found in Appendix III and V.

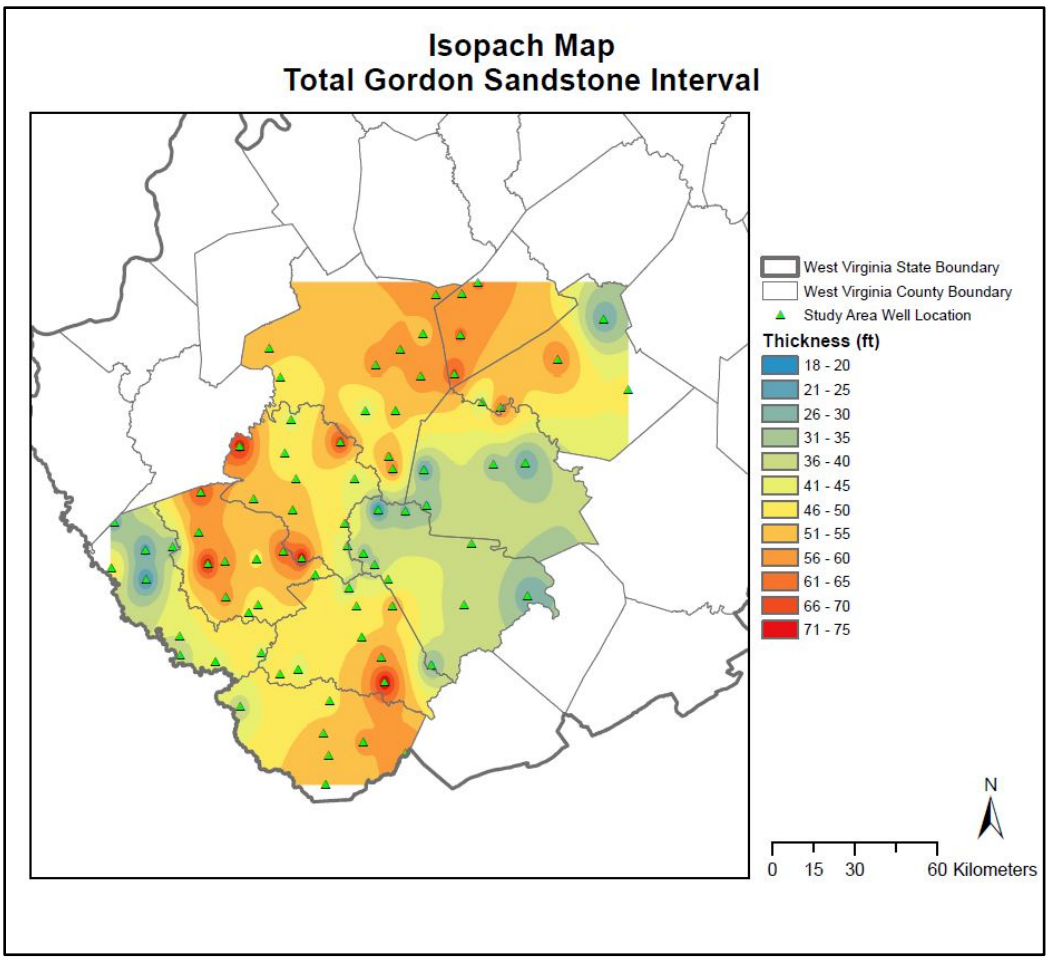

Figure 20: Detailed isopach map of the study area in south-central West Virginia. Data used to construct this map are found in Appendix III.

Isolith Maps

Isolith maps were generated for strata that is composed of ≥50% sand (Figure 21, 22). The thickest accumulation of Gordon strata that is ≥50% sand in the study area is a NNE-SSW trending linear tract located along the shelf edge margin; west of the shelf edge margin is a NNW-SSE trending linear patch (Figure 22). The eastern linear tract is located along the axis of an anticline that composes the NNE-SSW structural trend observed in the structure contour maps. The smaller western tract's thickness varies from 10 ft to 19 ft, while the larger eastern tract's thickness ranges between 21 ft to 48 ft. (Figure 22).

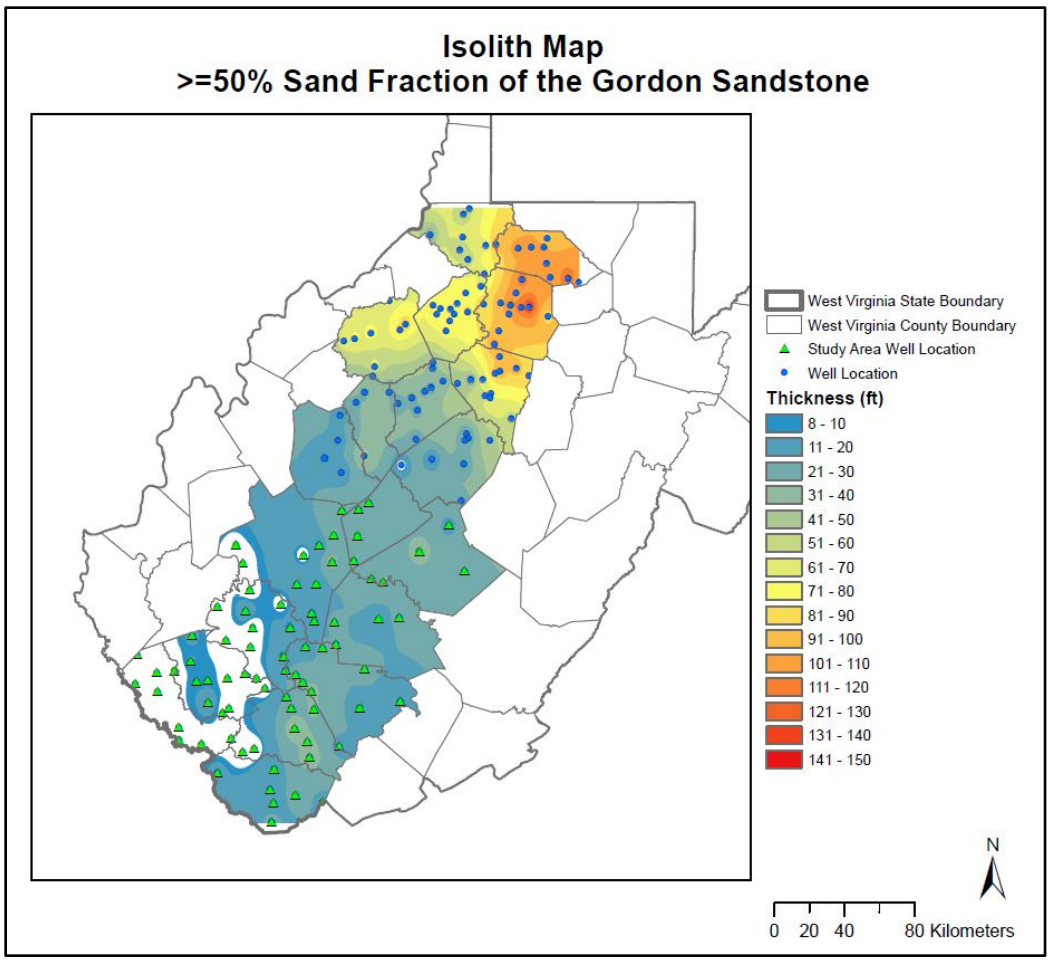

Figure 21: Isolith map showing the thickness of Gordon sediment that is composed of ≥50% sand. Thickest Gordon sediments are located along the Catskill delta complex in north-central West Virginia and thin in a radial basinward direction. Data used to construct this map are found in Appendix III and V.

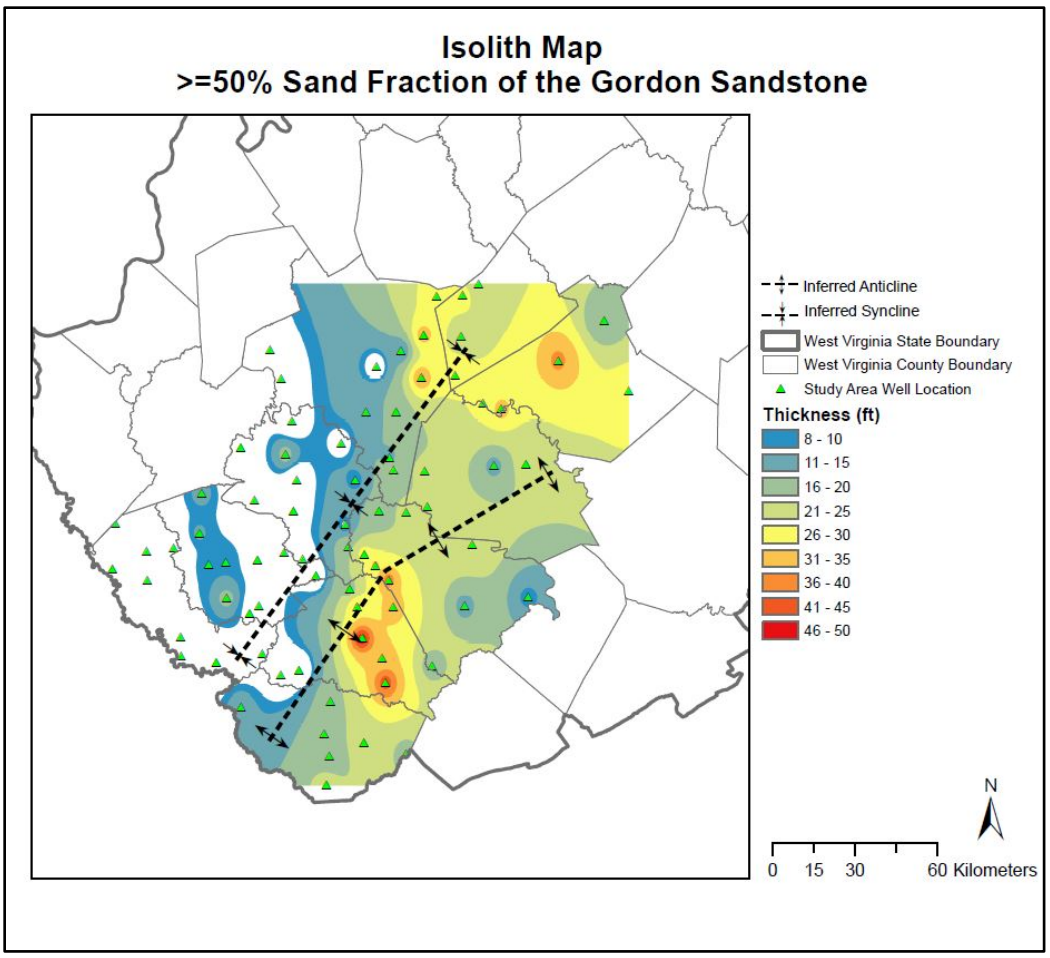

Figure 22: Detailed isolith map showing the thickness of Gordon sediment that is composed of ≥50% sand in the focal study area. Displayed are the two linear tracts of thicker Gordon sediments. The eastern tract is greater in aerial extent and thickness. Data used to construct this map are found in Appendix III.

Log Porosity Maps

Log porosity is not a measured petrophysical parameter, but rather a proxy for porosity calculated using bulk density. Higher log porosity values along the primary tract of production resulted from overall lower bulk density values collected from wireline logs. A linear tract of high porosity values is observed in south-central West Virginia (Figure 23). In the study area, the larger eastern linear tract (Figure 23) shows significantly higher log porosity values than the smaller western tract (Figure 23). Higher log porosity values are expected in the eastern tract, considering the high percentage of sand that composes the tract relative to the western tract. The eastern tract exhibits reservoir quality log porosity values ranging between 9%-16% Figure 23).

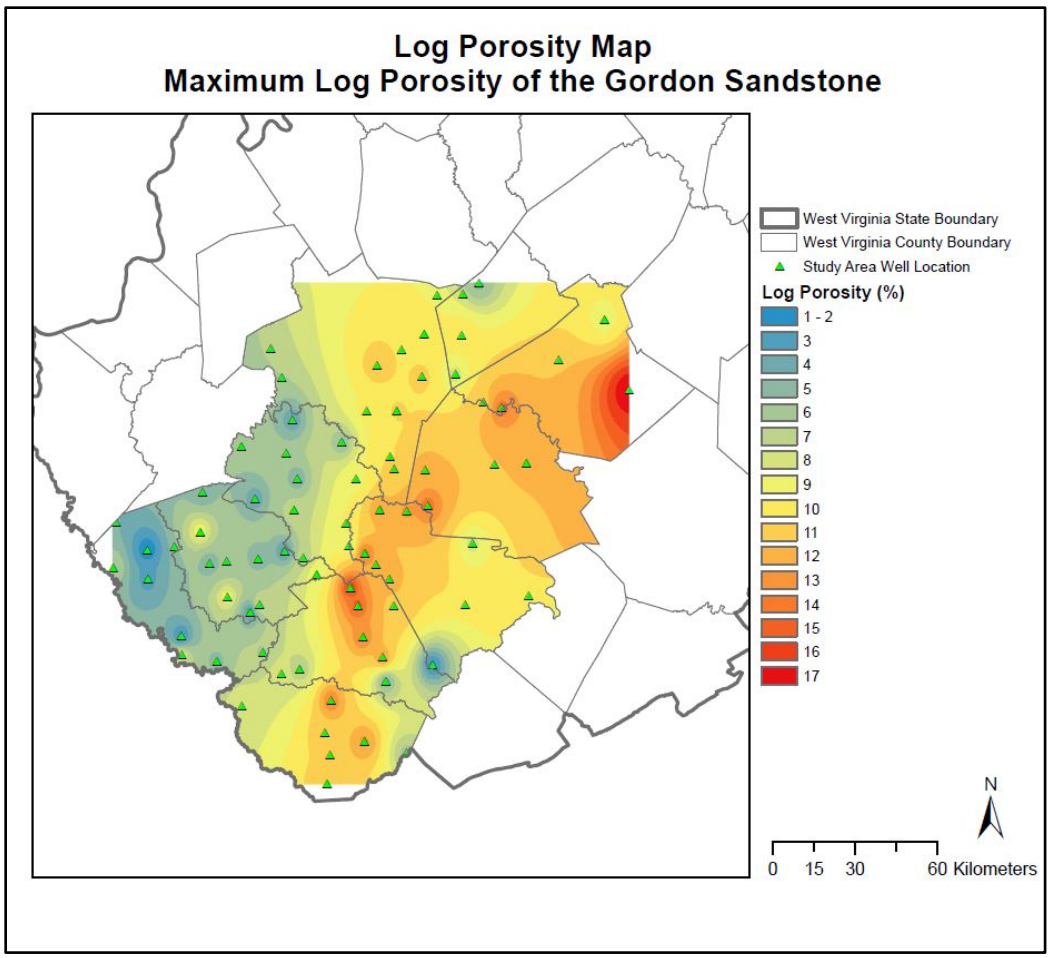

Figure 23: Detailed map of maximum log porosity expressed as percent for the Gordon sandstone interval. Highest log porosity values occur in pods, thereby compartmentalizing the reservoir. Data used to construct this map are found in Appendix IV.

Predictive Permeability Map

Whole core-measured porosity and whole core-measured permeability data (Ameri et al., 2001) show a strong positive correlation and an $R^2 = 0.835$ (Figure 24). An exponential trendline was determined and defined by the predictive permeability equation $y=0.0072^{0.4237x}$ (Figure 24) where (y) equals the predicted permeability value. Calculated maximum log porosity values (x) were input in the predictive permeability equation to best represent the permeability of the Gordon sandstone in south-central West Virginia. Resultant permeability values in the study area range from 0.01 mD-8 mD (Figure 25). Along the eastern linear tracts, permeability ranges between 0.6 mD-8 mD, which exhibits low reservoir quality, but is not quantified as tight reservoirs (Figure 25). The eastern tract exhibits consistent higher permeability relative to rocks around them (Figure 25). This zoning of the reservoir matches that of zones with higher porosity, as expected because of how the permeability was predicted.

This method of predicting permeability has its limitations. One limitation is that the core data was collected in a marginal marine environment along the Catskill Delta complex, whereas the area in which permeability is being predicting is located along the shelf edge. Therefore, the sediment characteristic for shelf edge sediments in the study area may differ from that of the sediments found in the Jacksonburg-Stringtown field in northern West Virginia. Use of the Jacksonburg-Stringtown field data in the south-central West Virginia study area is enabled by Ameri et al., (2001) classifying the pay zone as lower shoreface. Lower shoreface environments would also be located in the study area, along the shelf edge, when the delta prograded across the shelf to the point of maximum regression to the shelf edge margin.

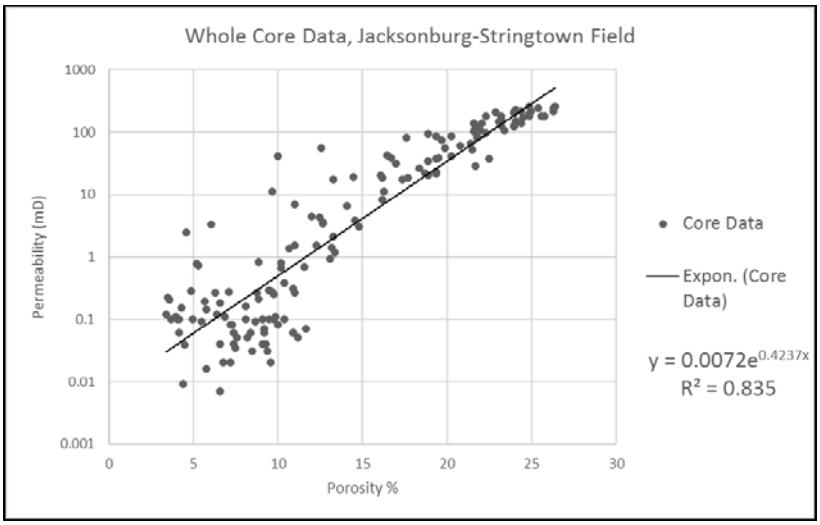

Figure 24: Cross-plots of measured porosity and permeability from cores taken at the same interval from the Jacksonburg-Stringtown oil field. A) Whole core porosity-permeability cross plot. Statistics: R^2=0.835, $y=0.0072^{0.4237x}$.

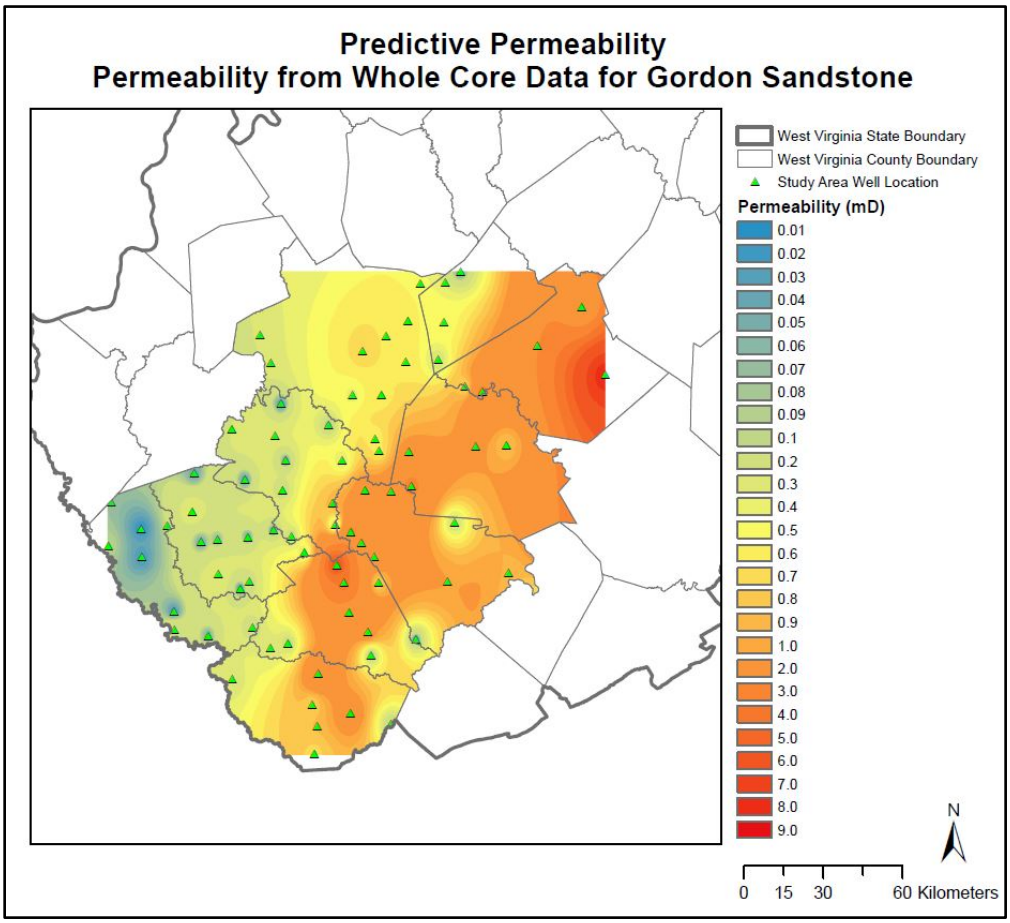

Figure 25: Map of predicted permeability. Values were calculated using the maximum predictive permeability equation and maximum log porosity values. The eastern tract exhibits compartmentalization, pod-like zones, of more permeable material. Data used to construct this map are found in Appendix IV.

DISCUSSION

Interpretations

Cross-section Interpretations

Multiple trends are observable in the cross-sections constructed for this study: 1) Gordon sediments are thickest in the northern West Virginia along the Catskill delta complex (Plate 1), which was the primary source of sediment influx, and thin in a basinward direction. 2) From the datum (top of the Berea Sandstone or the correlative conformity) to the top of the Gordon, the interval is thicker in northern West Virginia than in southern West Virginia. 3) Vertical variation of the Gordon's occurrence as subsea depths indicates that structural deformation was an ongoing process from the time the Gordon was deposited (late Devonian) until the deposition of the Berea (early Mississippian).

Structure Contour Interpretations

Each of the structure contour surfaces closely mimics the other selected surfaces. Similar structural trends, position, and location for all three structure contour maps (Figures 16, 17, 18) provide evidence that tectonic deformation of the central Appalachian basin occurred after early Mississippian, during which the Berea Sandstone, the youngest unit studied, was deposited. The westernmost NE-SW striking sub-linear structural high is spatially located above the eastern margin of the Rome Trough (Figure 18) (Ryder et al., 2008), suggesting the NE-SW striking structural high may be the result of Rome Trough reactivation during the Alleghenian orogeny. Previous studies that utilize multiple well log datasets, core data, and seismic data techniques suggest that Rome trough reactivation persisted throughout the entire Paleozoic to varying degrees (Gao, 1994; Shumaker, 1996; Shumaker and Wilson, 1996). The western NE-SW trending syncline, and eastern NE-SW trending anticline are prominent structural features in

each of the three structure contour maps. This suggests that the structural relief of the Gordon sandstone developed after the early Mississippian, based on the premise that the top of Berea Sandstone (Early Mississippian time) exhibits near matching contour geometries. The Alleghenian orogeny (Mid-Carboniferous through Late Permian) is one likely time that deformation occurred.

Depositional Environment

The Gordon sandstone in northern West Virginia has been defined traditionally as being deposited in a shallow marginal marine shore zone setting associated with the Upper Devonian Catskill delta complex (Boswell & Donaldson, 1988; Boswell & Jewell, 1988; Boswell, 1993; Ettensohn, 1995; Ameri et. al., 2001). However, in southern West Virginia, the depositional environment is much different. The gamma-ray signature of the Gordon suggests its depositional environment is continental shelf to shelf edge, and was located west of the mapped Upper Devonian Catskill shoreline (Figure 19) (Boswell & Donaldson, 1988; Boswell & Jewell, 1988). The shelf edge deposits are likely stacked progradational deltaic mouth bar or shoreline deposits (Figure 26), similar to the suggested shelf edge deposits described in Carvajal and Steel (2009). The location, of the primary production tract observed in the isolith maps (Figures 21, 22) suggests deposition occurred along the shelf edge.

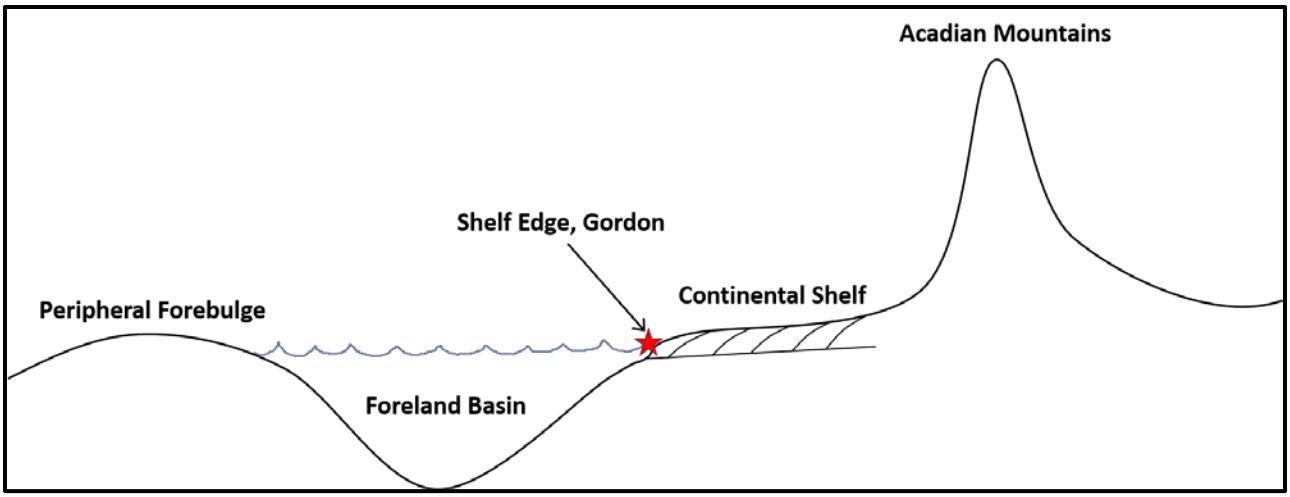

Figure 26: Schematic cross-section from the peripheral forebulge to the Acadian mountains. Red star indicates the location of Gordon deposition along the shelf edge.

These observations are similar to those of Carvajal and Steel (2009), who conducted a study in southern Wyoming, focused on the architecture of a shelf-edge, and how it was influenced by sediment supply, varying sea level, and shelf edge processes. Pertinent to this study are the geometries, relative thicknesses, and gamma-ray response of shelf edge deposits, sub-marine channels, and basin fan deposits presented in Carvajal and Steel (2009). The combination of multi-well geophysical analysis and outcrop observation, enabled them to define the location, position, and geometry of the shelf edge, while also being able to define the shelf edge depositional environment during a lowstand systems tract. Outcrop observation and analysis suggest the shelf edge deposits were composed of stacked mouth bars. Their continental shelf edge gamma-ray signatures are similar to those of the Gordon sandstone presented in this study.

The Carvajal and Steel (2009) study used vertical cross-sections to illustrate vertical stacking of continental shelf edge sand deposits. An isolith map from Carvajal and Steel (2009) illustrates the geometry of the shelf edge, and the sand masses that are localized along the shelf edge. The total Gordon interval, isolith map (Figure 22), is similar to that of the shelf edge sand

distribution presented in the Carvajal and Steel (2009) study. The similar geometries of the isolith and the basinward location of the high isolith sands fraction feature relative to the position of the shoreline, leads to the conclusion that the high isolith sand fraction feature observed for the Gordon is the shelf edge. Correlation between outcrops and downhole wireline logs (e.g. gamma-ray signatures) in the Carvajal and Steel (2009) study concluded that the deposits along the shelf edge were stacked delta mouth bars. Comparison of the shelf edge delta mouth bar gamma-ray signatures in Carvajal and Steel (2009) study and the shelf edge gamma-ray signature in this study shows they are similar (Figure 27). These similar gamma-ray signatures suggests that the defined depositional environments in Carvajal and Steel (2009) can be used to characterize the Gordon shelf edge deposits as delta mouth bars. However, reworking of mouth bar deposit sediments may develop other sand-rich coastal deposits such as beach, shoreface, Aeolian.

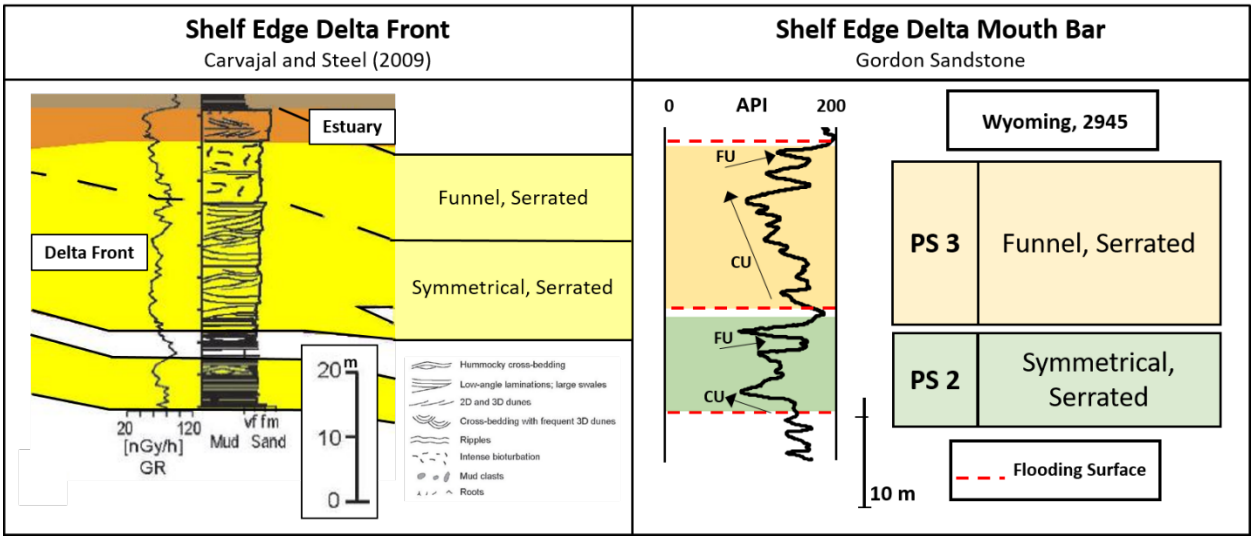

Figure 27: Illustrates the similarity between the shelf edge delta front mouth bar deposit gamma-ray signature of the Carvajal and Steel (2009) study and that of the shelf edge interpreted mouth bar deposits of the Gordon sandstone in southern West Virginia. The basal parasequence in both studies exhibit a symmetrical and serrated gamma-ray geometry. The upper parasequence in both studies exhibit a funnel and serrated gamma-ray geometry.

The marine environment in which the Gordon was deposited suggests the lithology was influenced by sea level change. The Gordon interval is composed of three parasequences. Parasequence 1 (PS 1) is the basal parasequence, PS 2 is the middle parasequence, and PS 3 is the uppermost parasequence (Figure14). Each parasequence is composed of a sand body and bounding shale beds. Each sand body likely represents a period of regression, while each shale bed likely represents a period of transgression (Figure 28). Each of the three parasequences with sediment composed of ≥50% sand thickness and maximum calculated log porosity have been mapped (Figures 30-38) and described below. The three parasequences were picked by first identifying the Gordon and second by identifying the sand bodies that compose the Gordon. The parasequences are bound by flooding surfaces (FS) (Figure 13). Once each parasequence had been identified, the isolith thickness was calculated. The Gordon parasequences are not all laterally continuous; where a parasequence could not be identified the isolith value was recorded as zero.

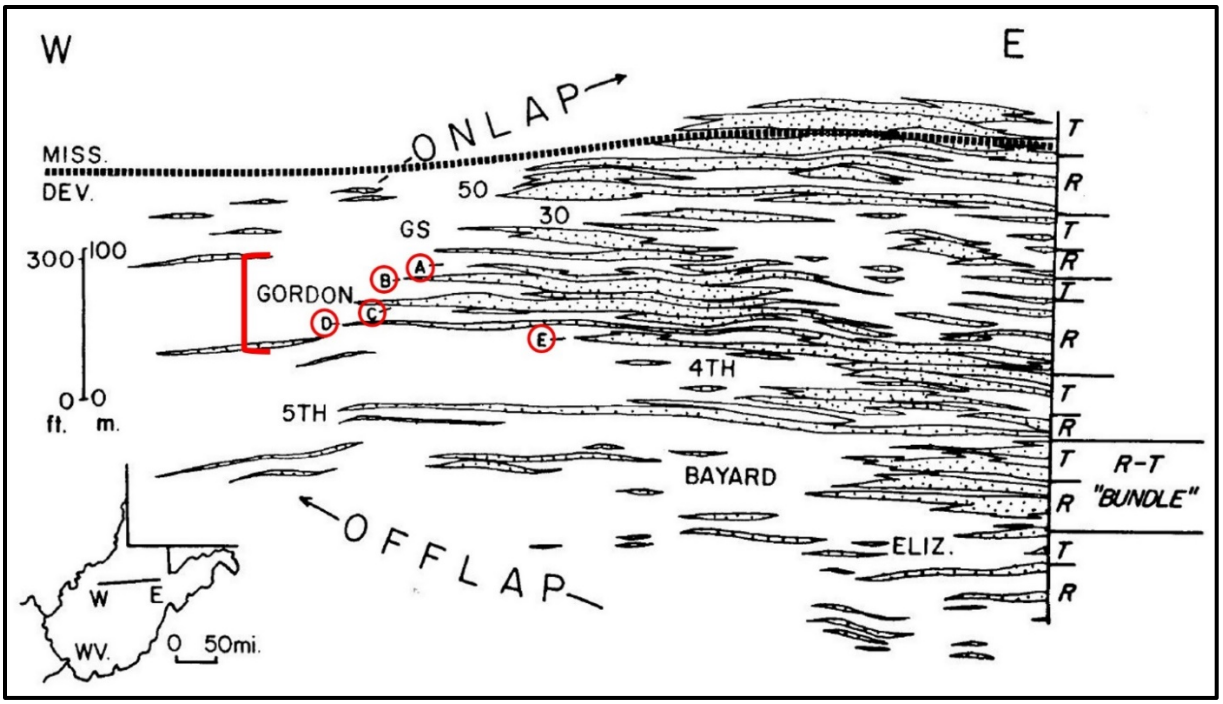

Figure 28: Schematic east-west cross-section showing the distribution of Catskill delta complex sandstones in the Upper Devonian in northern West Virginia. T= transgressive horizon; R= regressive horizon. This diagram shows the Gordon sub-divided in five sections (A, B, C, D, E). Boswell and Donaldson, (1988).

Shifts in the shoreline position, discussed as shoreline transgression and regression, represent fluctuations of relative sea level (e.g. relative sea level rise and fall) (Johnson et. al., 1985) (Figure 29). As relative sea level rises it results in a transgressive shoreline. When relative sea level falls it results in a regressive shoreline (Figure 29). A close association between relative sea level rise and fall, and the resultant shoreline migration is evident in Figure 29.

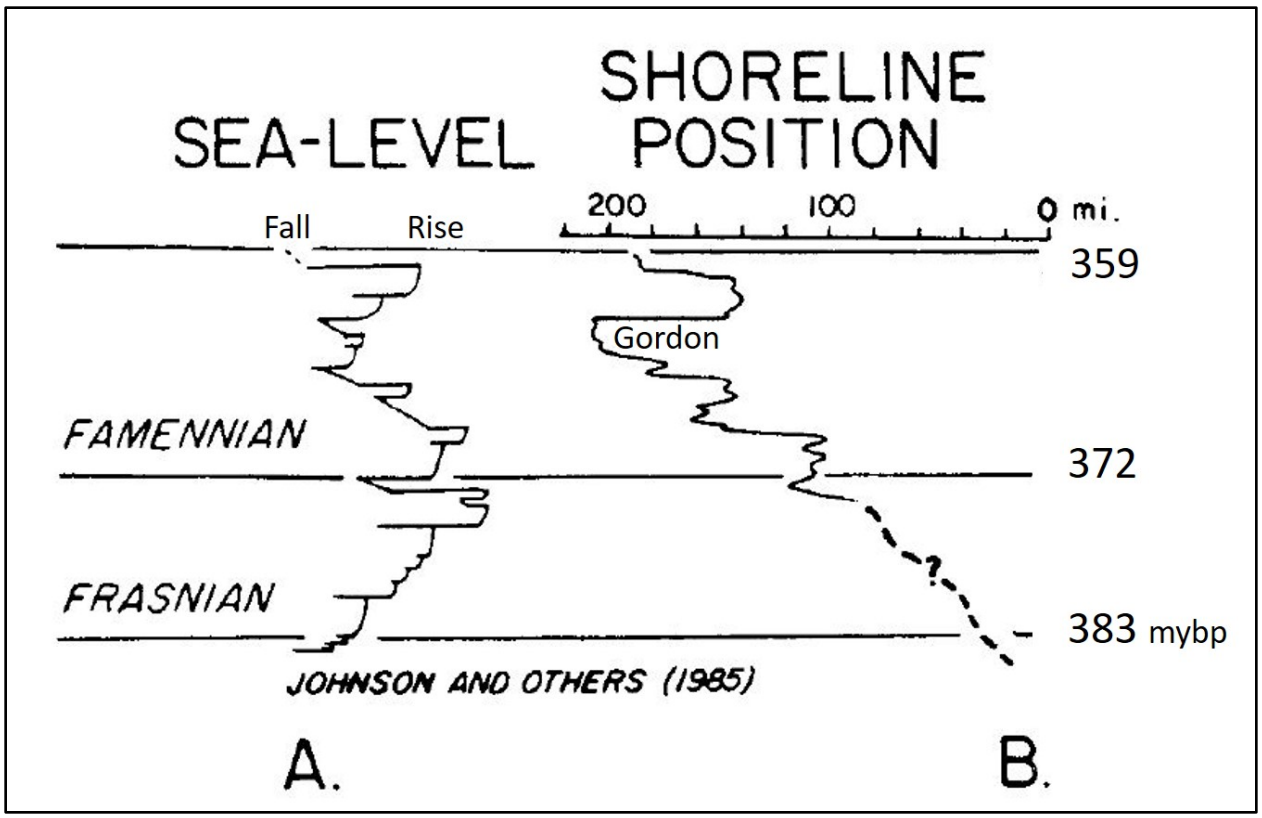

Figure 29: Graphic correlation between relative sea level and shoreline position by correlating conodont biostratigraphy zones. Curve A- Relative sea level curve; Curve B- Position of strike-trending sandstones in northern and central West Virginia, produced by Johnson and others (1985). Source of ages are from the Geological Society of America. Adapted from Boswell and Donaldson, 1988.

Parasequence 1

An isolith map for parasequence 1 (PS 1) indicates that localized thicker strata (Figure 30) occurred largely along the primary tract (Figure 5) to the north and south. Sedimentation also occurred to the east of the northern sedimentation lobe (Figure 30). Deposition in the secondary, western, tract (Figure 5) did occur but was thin and sparse (Figure 30). PS 1 exhibits a weak positive correlation between isolith thickness and log porosity, with an R^2=0.392 (Figure 31) that suggests areas that exhibit increased isolith thickness, also exhibit higher log porosity. Log porosity maps of PS 1 (Figure 32) closely match that of the isolith map for PS 1 (Figure 30).

Localized higher porosity areas (Figure 32) are restricted to the two lobes of thicker sedimentation (Figure 30), north and south sections, of the primary tract (Figure 5).

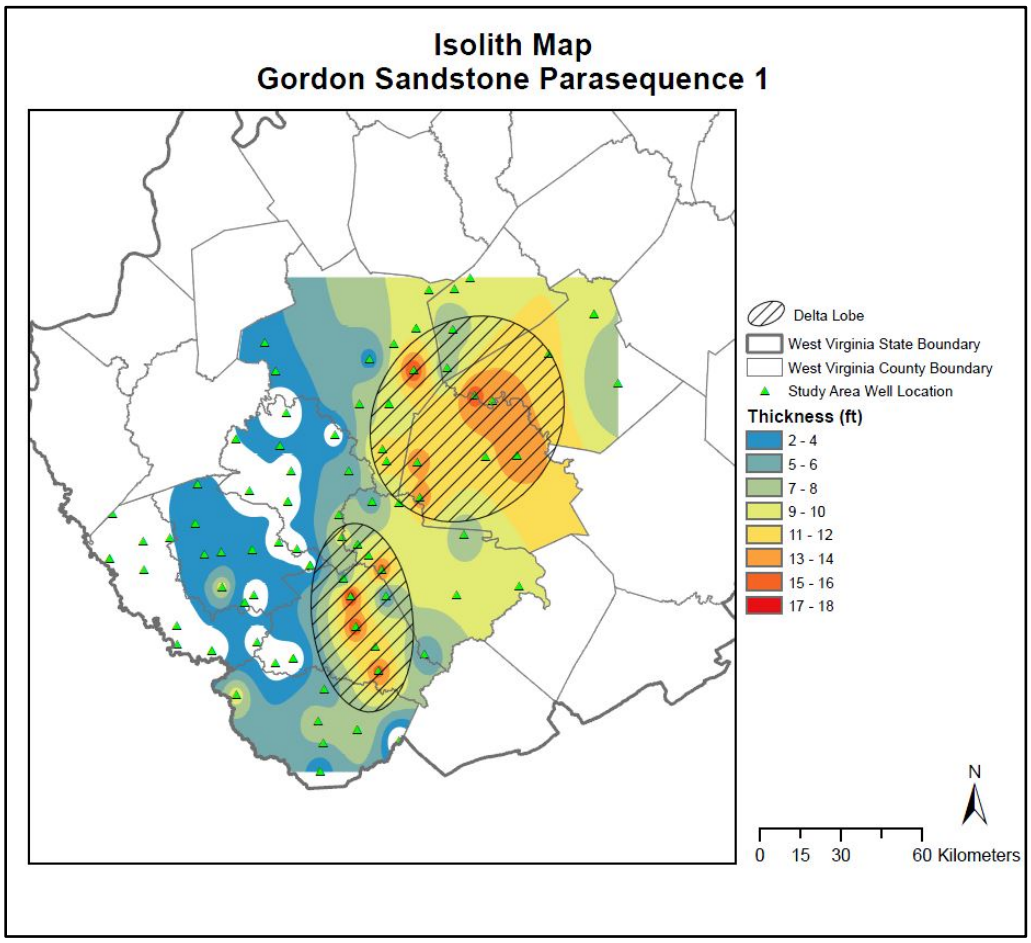

Figure 30: Detailed isolith map of Gordon parasequence 1 sediment that is ≥50% sand in the focal study area.

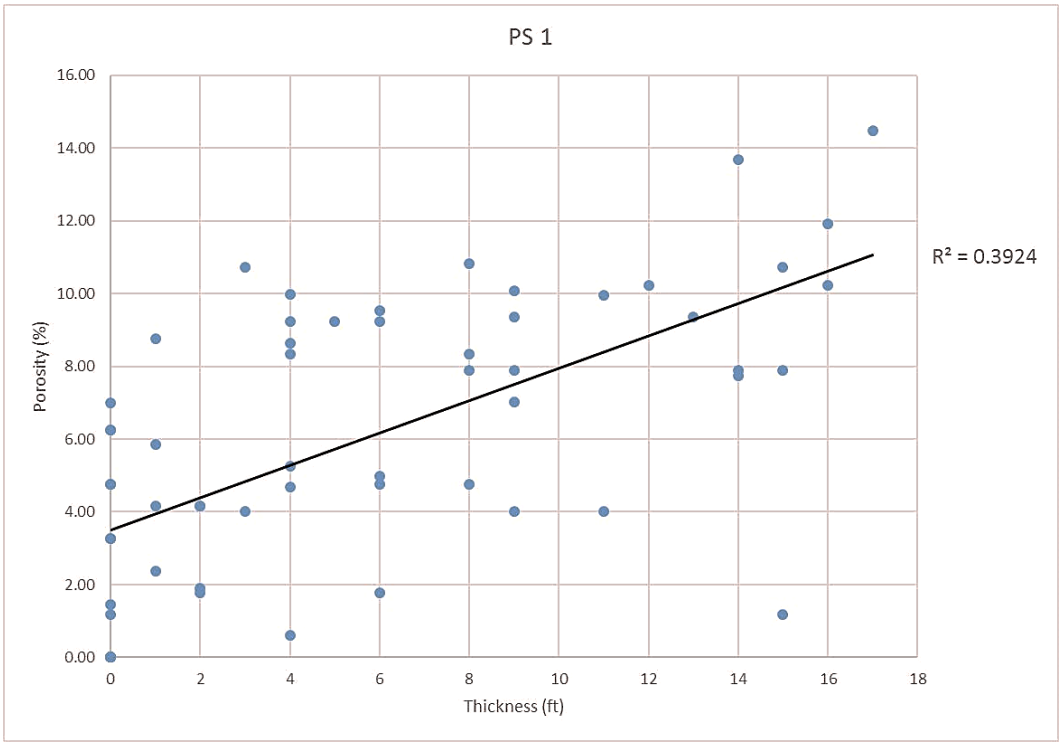

Figure 31: Cross-plot of parasequence 1 thickness and parasequence 1 maximum log porosity in the focal study area. Statistics: R^2= 0.392.

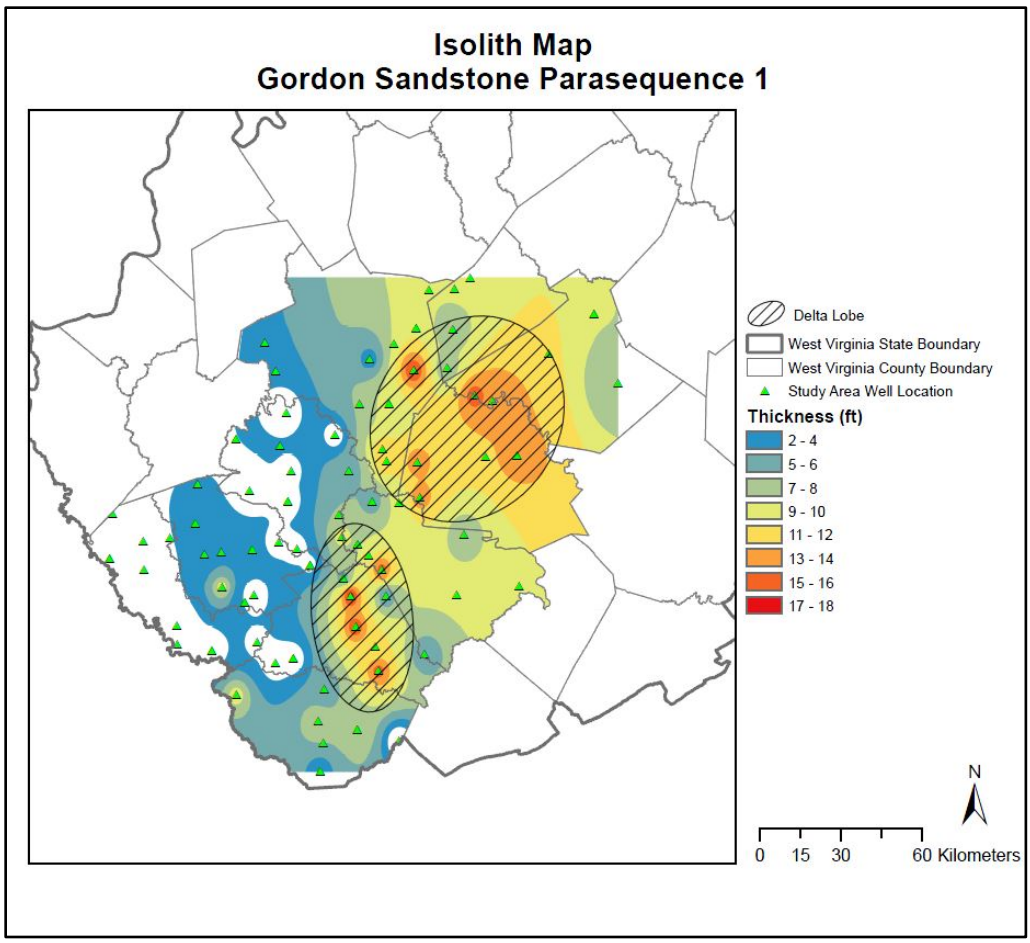

Figure 32: Detailed maximum log porosity map for the Gordon sandstone parasequence 1 in the focal study area.

Parasequence 2

The parasequence 2 (PS 2) isolith map (Figure 33) shows that thickest sedimentation largely occurred to the central and southern areas of the primary tract. A very localized pod of thicker sedimentation occurred in the northern section of the primary tract (Figure 33). The secondary tract (Figure 5) exhibits a very localized lobe of thin strata just west of the area along the primary tract (Figure 5) that exhibits thicker sediments (Figure 33). PS 2 exhibits a weak positive correlation between isolith thickness and log porosity with an R^2= 0.438 (Figure 34) that suggests areas that exhibit increased isolith thickness also exhibit areas of high log porosity.

Similar to PS 1, PS 2 highest log porosity values (Figure 35) closely match areas of thickest isolith strata (Figure 33). Therefore, PS 2 highest porosity values are located in the central and southern sections of the primary tract, and a localized pod of higher porosity (Figure 35) that is associated with the small area of thicker strata located in the northern section of the primary tract (Figure 33).

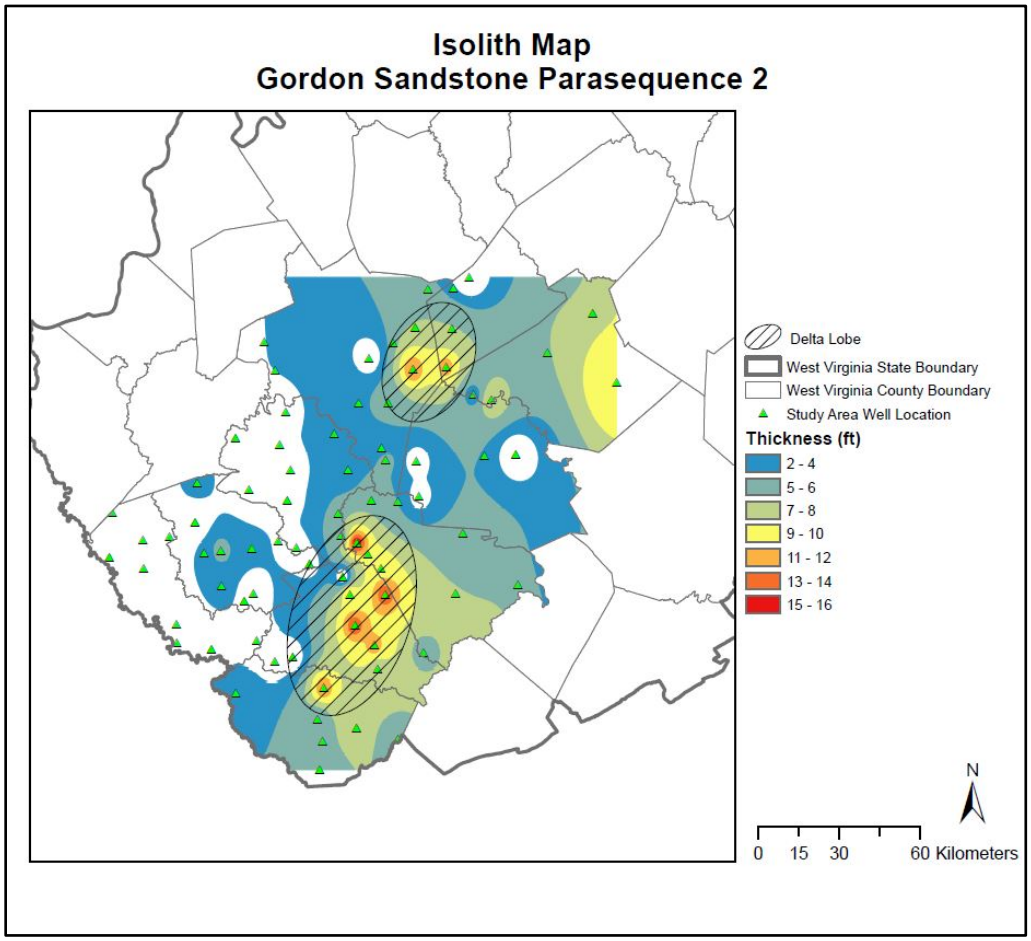

Figure 33: Detailed isolith map of Gordon parasequence 2 sediment that is ≥50% sand in the focal study area.

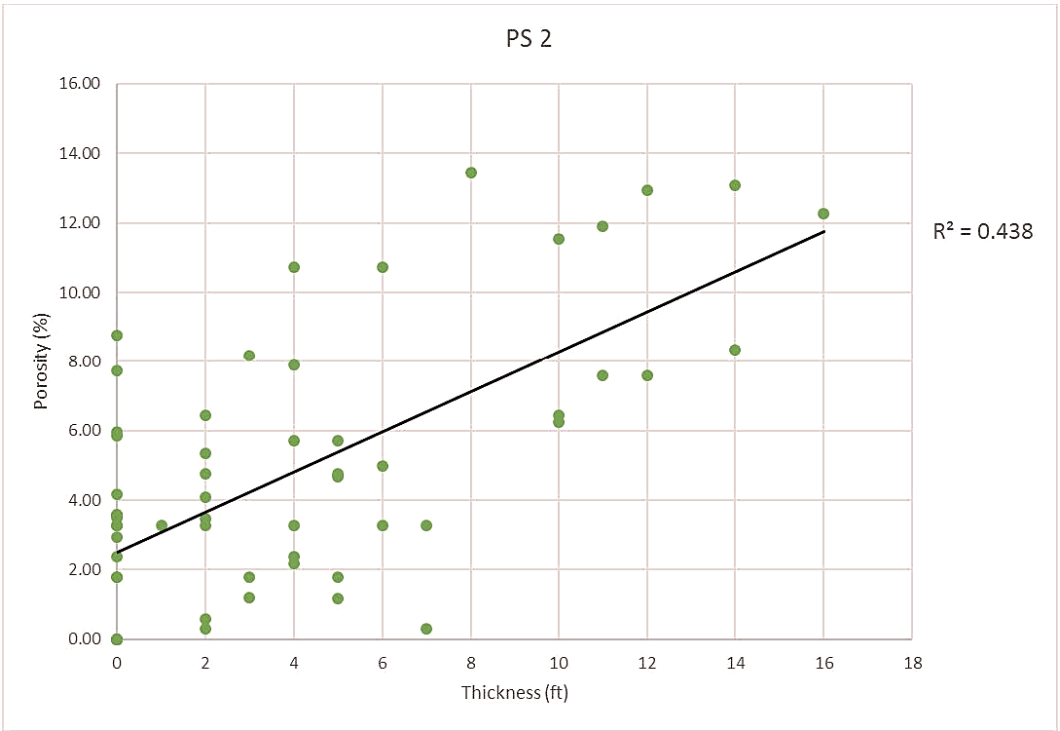

Figure 34: Cross-plot of parasequence 2 thickness and parasequence 2 maximum log porosity in the focal study area. Statistics: R^2= 0.438

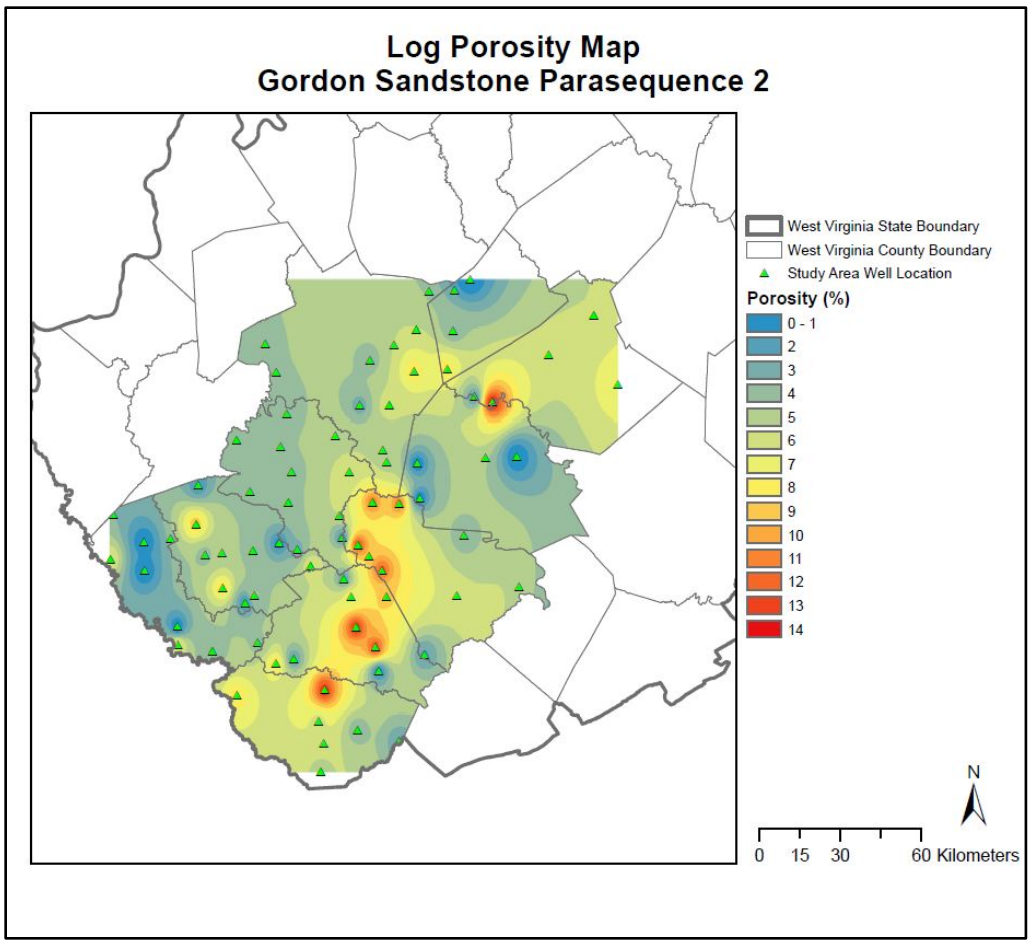

Figure 35: Detailed maximum log porosity map for the Gordon sandstone parasequence 2 in the focal study area.

Parasequence 3

An isolith map of parasequence 3 (PS 3) (Figure 36) indicates that thickest sedimentation occurred in the southern section of the primary tract (Figure 5), while thinning of PS 3 strata occurs in a northerly direction (Figure 36) along the primary tract (Figure 5). Thin, but rather expansive, sedimentation occurred along the entire length of the secondary tract (Figure 5). However, a wide swath of no sedimentation occurred in the area separating the primary and secondary tracts, oriented in a north-south direction. (Figure 36). PS 3 exhibits a very weak, but positive correlation between isolith thickness and log porosity, with an R^2= 0.177 (Figure 38),

that suggests areas with increased isolith thickness do not always exhibit higher log porosity. Highest log porosity values (Figure 38) along the primary tract (Figure 5) are located in the gradational zone of thinning strata (Figure 36). An anomaly of high log porosity (Figure 38) is located along the eastern margin of the mapped area, where Gordon PS 3 sediment is 6-8 ft thick (Figure 36).

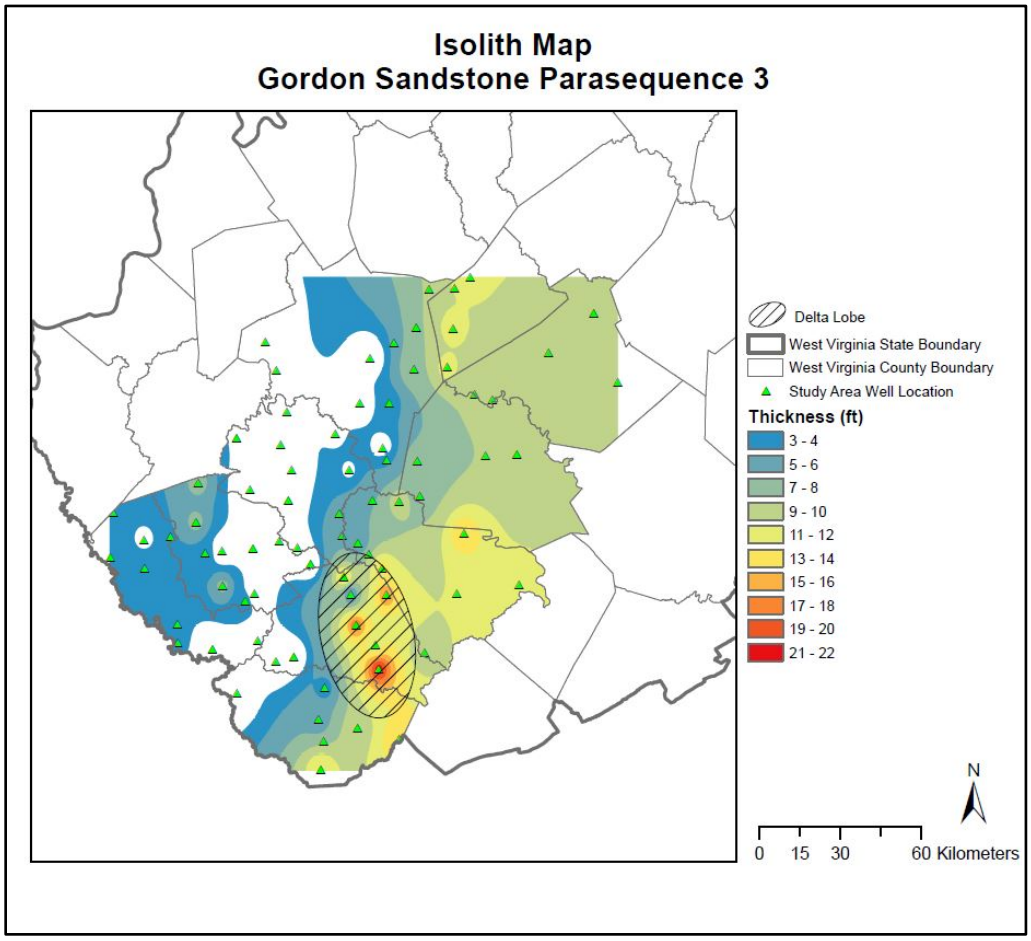

Figure 36: Detailed isolith map of Gordon parasequence 3 sediment that is ≥50% sand in the focal study area.

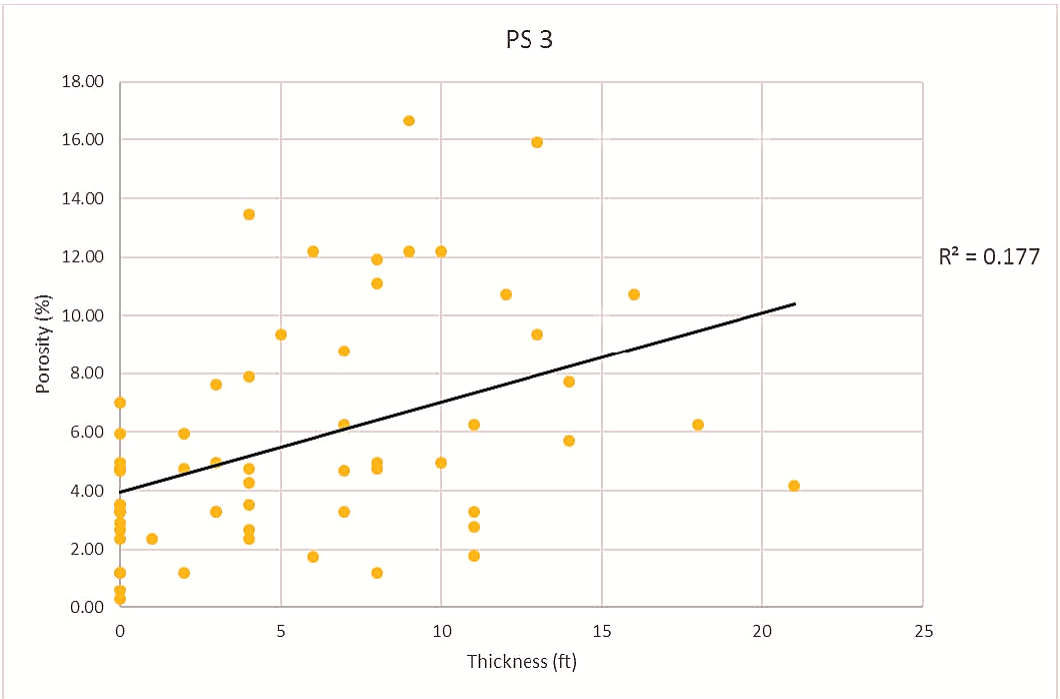

Figure 37: Cross-plot of parasequence 3 thickness and parasequence 3 maximum log porosity in the focal study area. Statistics: R^2= 0.177.

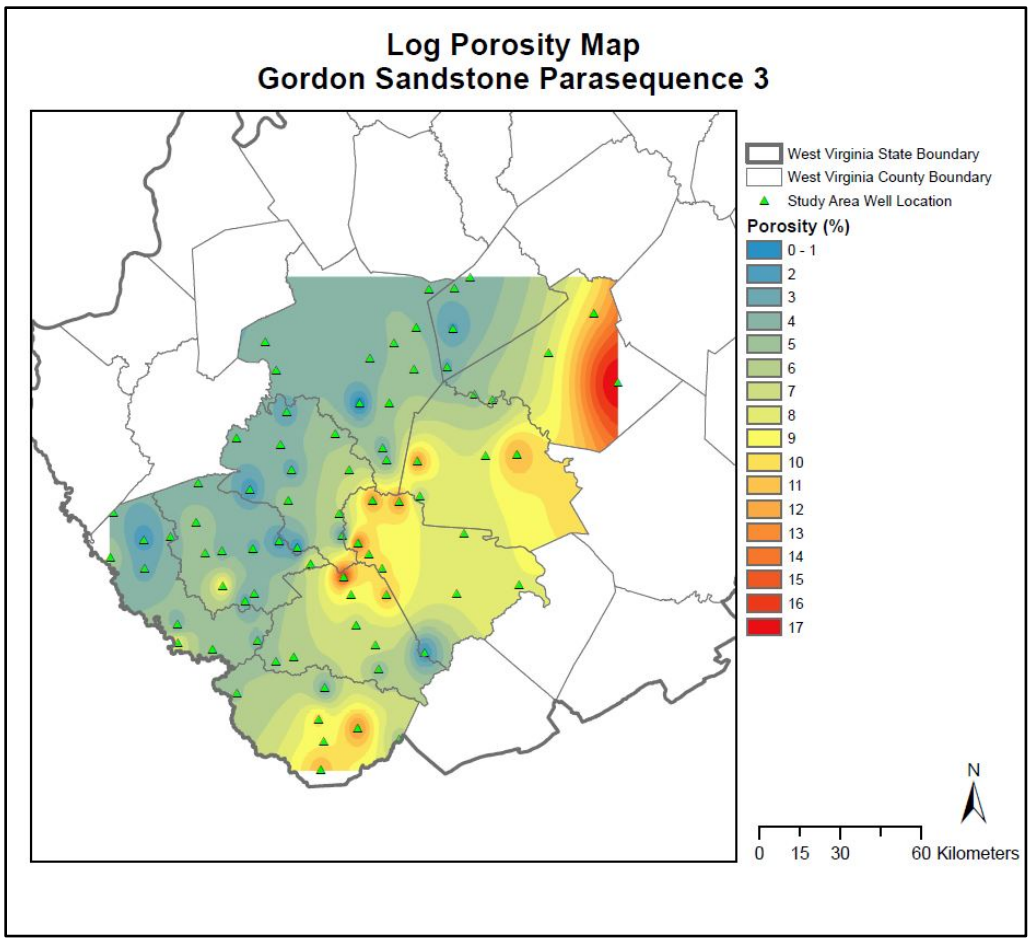

Figure 38: Detailed maximum log porosity map for the Gordon sandstone parasequence 3 in the focal study area.

Isolith maps (Figures 30, 33, 36) illustrate the localized lobes increased isolith thickness per parasequence that compose the Gordon sandstone. The lobes are geographically located along the shelf edge and the primary tract (Figure 5). The sum of the parasequence isolith thicknesses (Figure 22) illustrate the sub-linear geometry of increased isolith thickness west (basinward) of the projected Gordon shoreline produced in Boswell and Jewell (1988) and Boswell and Donaldson (1988). The location (basinward) and geometry of the sub-linear tract that exhibits increased isolith thickness is consistent with a basinward location and geometry for

what was considered as the shelf edge margin in Carvajal and Steel (2009) (Figure 39) from similar isolith map and outcrop analysis.

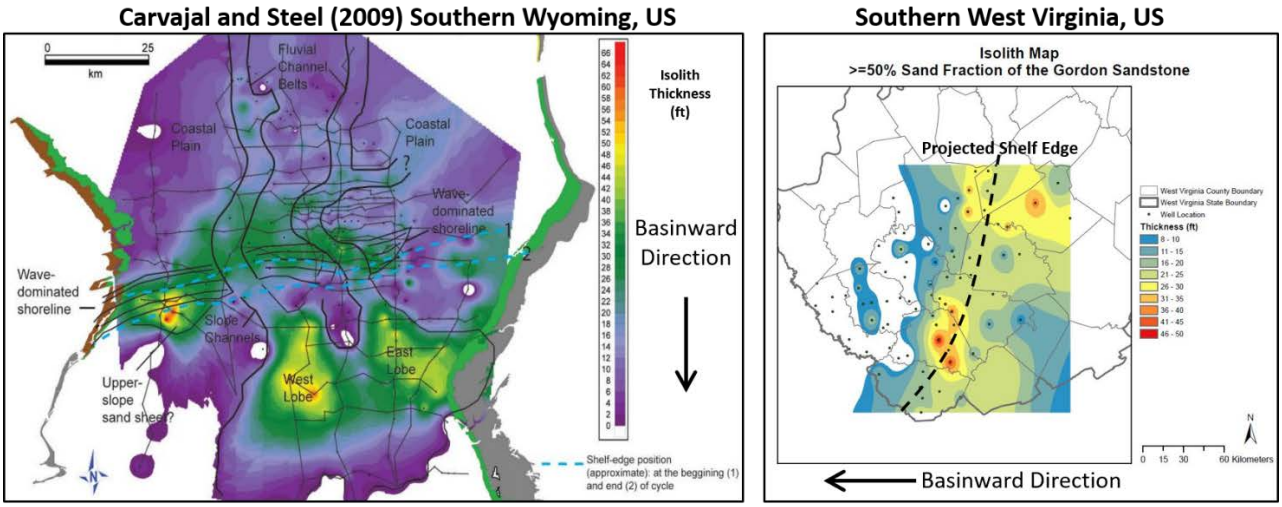

Figure 39: Carvajal and Steel (2009) mapped isolith thickness of the ≥50% sand fraction in southern Wyoming, US. Blue dash lines from Carvajal and Steel (2009) indicate the shelf edge margin for cycles 1 and 2. Southern West Virginia, US isolith of the Upper Devonian Gordon shelf edge.

The smaller secondary tract (Figure 5) is interpreted as lower slope deposits, due to its basinward location of the projected Gordon shelf edge margin. Such deposits can accumulate thick packages of fine-grained sediment (i.e.: silt, clay, pelagic muds) with a small amount of coarse siliciclastic sediment. This is observed in the total Gordon interval maps that illustrate the secondary tract as having a thick Gordon interval, whereas total Gordon interval isolith maps and individual parasequence isolith maps show very thin Gordon sediments that are ≥50% sand.

Petroleum development of the secondary tract likely occurred in response to encountering petroleum in a few localized wells where the Gordon may be sandier (e.g. dip-trending sub-marine channel composed of coarse siliciclastic material) than the dominant lower slope depositional environment. As petroleum developers moved laterally, along strike, encountering Gordon intervals composed of lesser volumes of sand, development ceased. Lower slope

maximum regressive deposits are typically composed of turbidite deposits (Catuneanu, 2006); however, the gamma-ray response to the Gordon interval that composes the secondary tract indicates that is not the case in south-central West Virginia. The gamma-ray signature of the Gordon for the secondary tract is funnel-shaped to symmetrical (Figure 40), whereas turbidite deposit gamma-ray signatures are bell-shaped (Serra and Sulpice, 1975; Catuneanu, 2006; Muslim 2014) (Figure 13).

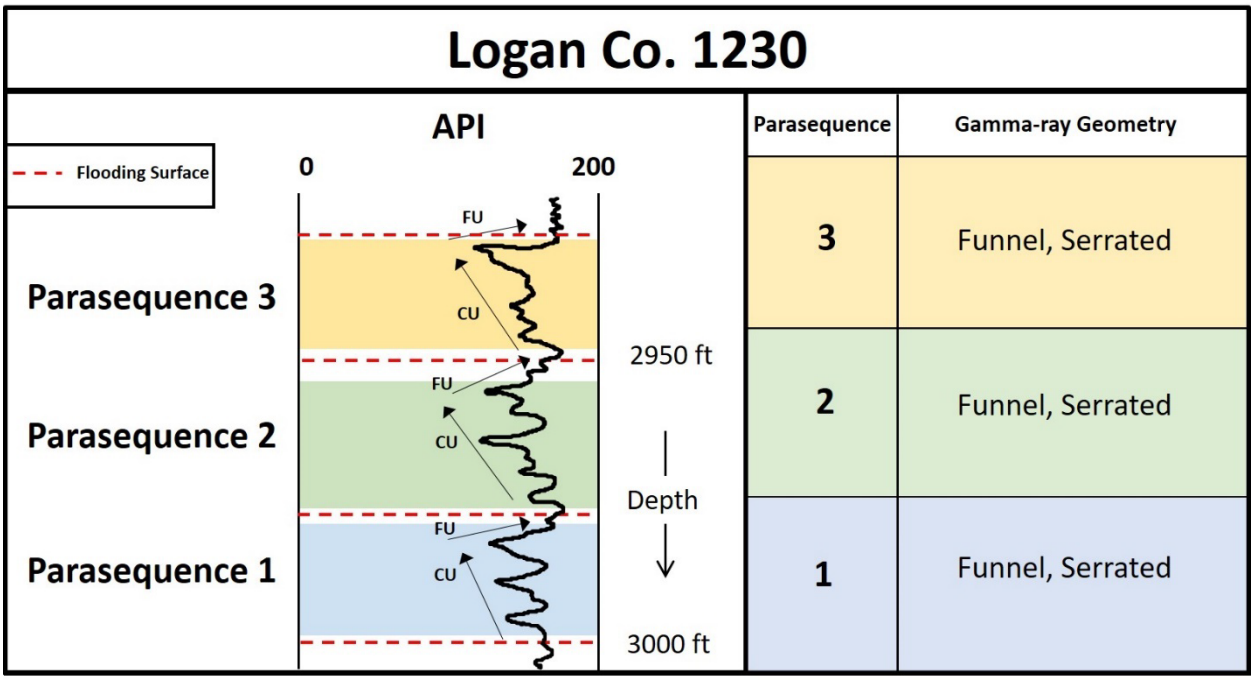

Figure 40: The gamma-ray signature for the Logan Co. 1230 well located along the lower slope, basinward of the projected shelf edge. The gamma-ray signature of the Gordon interval is divided in three distinct parasequences, and each parasequence exhibits a serrated funnel geometry.

Petroleum Geology

In the study area, south-central West Virginia, the gas is primarily distributed across the primary tract, which is a NNE-SSW trending tract of closely-spaced producing wells (Figure 5). Within the study area, the highest log porosity values are located within the area of the primary tract. Overall, the primary tract is vertically sub-divided into three parasequences. Each

parasequence is characterized as shelf edge delta mouth bar deposits, when compared to isolith maps and gamma-ray signatures of the Carvajal and Steel (2009) study. The parasequences are sub-divided into lobes of increased isolith thickness and relative higher log porosity. The increased isolith thickness and porosity developed by active lobe sedimentation from the delta that prograded across the continental shelf during the Late Devonian.

The controls on natural gas production of the Gordon sandstone are controlled structurally and stratigraphically. The depositional history of the Gordon has the largest influence on the stratigraphic controls of natural gas production. Post-deposition deformation from the Alleghenian orogeny generated structural relief for the Gordon interval. The primary tract of production is located along the crest of an anticline (Figures 16, 17, 18), which aided in the migration of petroleum resources from surrounding areas into the anticline crest which is composed of the higher porosity and permeability shelf edge sediments.

Stratigraphic Controls

Production of petroleum from the primary, eastern, tract is partially controlled by the stratigraphy of the Gordon. Within the primary tract, the Gordon is thicker and composed of a higher fraction of sand than in adjacent depocenters. The eastern tract is interpreted as three stacked mouth bar, deltaic shelf edge, lowstand normal regressive paraseqeuences as defined by Catuneanu, (2006) (Figures 30, 33, 36). Individual parasequences show local areas along the primary tract that exhibited higher amounts of sedimentation relative to the secondary tract (Figures 30, 33, 36). Localized increased thickness of sedimentation per parasequence is thought to be driven by active lobes of the delta at the time of deposition, channel avulsion, and active lobe migration. Channel avulsion and active lobe migration (Slingerland and Smith, 2004) occurred during short periods of transgression flooding of the delta that separate parasequences.

As a result of transgression, the delta flooded back filling the parent channels with sediment (Slingerland and Smith, 2004). Following transgression and flooding of the delta, regression ensues and the back filled parent channel no longer exists; forcing channel avulsion as newly generated fluvial systems source sediment to the basin (Slingerland and Smith (2004). These periods of transgression are preserved and observed as shale intervals in the gamma-ray signature of the Gordon. Each parasequence shows a positive correlation (Figures 31, 34, 37) between increased thickness and increased log porosity (Figures 32, 35, 38). The positive correlation between isolith thickness and log porosity indicated that areas with increased isolith thicknesses also exhibit higher log porosity.

Ettensohn (2005), Boswell & Jewell (1988), and Boswell (1993) explicitly state that the Upper Devonian Catskill delta shoreline experienced multiple periods of shoreline migration, referred to as shoreline transgression and regression. The Gordon gamma-ray signature sand bodies reflect a period of regression, and the bounding shale beds reflect periods of transgression. Deltaic lobes, expressed as localized areas of increased thickness in the parasequence isolith maps (Figures 30, 33, 36), migrate laterally between PS 1, PS 2, and PS 3. Lateral migration of the deltaic lobes occurred during periods of transgression, as a process of channel avulsion, and is illustrated in the isolith maps of deltaic lobes composed of sand along the shelf edge during periods of regression for each parasequence.

Structural Controls

Production from the primary, eastern tract of the Gordon sandstone is also partially controlled by the structural relief generated due to post-depositional deformation. The primary tract, identified as the shelf edge, structurally evolved into an anticline from its original horizontal depositional position (Figure 17). Being that the three stacked deltaic mouth bar, shelf

edge, lowstand normal regressive parasequences lie along the axis of an anticline, aided in the migration of petroleum resources to the anticline crest, which is composed of material that exhibits higher log porosity values than adjacent environments. The migration and accumulation of petroleum resources along the anticline crest explains why so many wells are located along the primary tract in south-central West Virginia.

Structure contour maps of the study area indicate that an anticline crest is geographically located in the same area as the stacked continental shelf edge sand bodies, which act as a superior reservoir relative to adjacent non-shelf edge deposits (Figure 16, 17, 18). The western falling limb of the anticline transitions into a syncline. The structural relief, and connectivity from the syncline to reservoir quality sand bodies that comprise the sediments along the anticline crest aid in the migration and storage of petroleum resources along strike of the anticline crest (Figures 16, 17, 18, 30, 33, 36).

SUMMARY

1. The Gordon sandstone in south-central West Virginia has been identified as continental shelf sheet sands, formed by deltaic progradation during falling stage system tracts, transitioning into lowstand system tracts.

2. The primary tract of production has been identified as stacked lowstand normal regression deltaic mouth bars that developed through three parasequences.

3. Localized increased thickness per parasequence has been identified as the active lobes of sedimentation during the time of each individual parasequence.

4. Lateral migration of the active lobes along strike of the primary tract is likely due to channel avulsion during periods of transgression that separate the Gordon parasequences and are marked by shale beds in the gamma-ray log signature.

5. The secondary tract has been identified as continental shelf slope deposits that resulted from deepwater sedimentation at the point of maximum regression per parasequence.

6. The primary tract is located along the axis of an anticline. The structural relief was generated from post depositional deformation which aided in the migration of petroleum to the anticline crest that is composed of the higher log porosity materials relative to adjacent environments.

REFERENCES

Ameri, S., Aminian, K., Avary, K.L., Bilgesu, H.I., Hohn, M.E., McDowell, R.R., and Matchen, D.L., 2001. Reservoir Characterization of the Upper Devonian Gordon Sandstone, Jacksonburg Stringtown Oil Field, Northwestern West Virginia, Final Report, Performed under Contract No. DE-AC26-98BC15104, DOE Report 884841, October 2001, 86 p.

Beaumont, C., Quinlan, G. M., and Hamilton, J., 1988, Orogeny and stratigraphy: numerical models of the Paleozoic in the eastern interior of North America. Tectonics, v. 7, pp. 389–416.

Boswell, R.M. and Donaldson, A.C., 1988. Depositional architecture of the Upper Devonian Catskill Delta complex: Central Appalachian Basin, USA. *in*: McMillan, N.J., Embry, A.F., Glass, G.J., (Eds.), Devonian of the World, Proceedings of the Second International Symposium on the Devonian System. Canadian Society of Petroleum Geologists Memoir 14, 2, pp.65–84.

Boswell, R. M. and G. Jewell, 1988, Atlas of Upper Devonian-Lower Mississippian sandstone in the subsurface of northern West Virginia: Southeastern Geology. v. 29, n.2, p.105-131.

Boswell, R. M., Pool, S., Pratt, S., and Matchen, D., 1993. Appalachian Basin Low- Permeability Sandstone Reservoir Characterizations. United States; Report No. 94CC-R91-003, 73 p. doi:10.2172/1030788

Burns, P. J., and Claus, R. C., 1985, An overview of hydrocarbon production in Appalachian basin —a glance at the forest. Oil & Gas Journal, v. 83, pp. 116–122.

Carvajal, C., and R. Steel, 2009, Shelf-Edge Architecture and Bypass of Sand to Deep Water: Influence of Shelf-Edge Processes, Sea Level, and Sediment Supply: Journal of Sedimentary Research, v. 79, no. 9, p. 652–672, doi:10.2110/jsr.2009.074.

Catuneanu, O. (2006) Principles of Sequence Stratigraphy, 1st edn. Elsevier, Amsterdam, 375p.

Cecil, C. B., Ahlbrandt, T. S., and Heald, M. T., 1991, Paleoclimate implications for the origin of Paleozoic quartz arenites in the Appalachian basin. Geological Society of America Abstracts with Programs, v. 23, pp. A-72.

Cecil, C. B., Brezinski, D., and DuLong, F., 2004, The Paleozoic record of changes in global climate and sea level: central Appalachian basin, *in* Southworth, S. and Burton, W. eds., Geology of the National Capital Region—field trip guidebook, U.S. Geological Survey Circular 1264, pp. 77–135.

Colton, G. W., 1970, The Appalachian Basin – its depositional sequences and their geologic relationships, *in* Fisher, G. W., Pettijohn, F. J., Reed, J. C. Jr., and Weaver, K. N. eds., Studies of Appalachian geology: central and southern, Interscience Publishers, New York, pp. 5–47.

Dennison, J. M., 1989, Paleozoic sea-level changes in the Appalachian basin, 28th International Geological Congress Field Trip Guidebook T354, Washington, DC, American Geophysical Union, 56 pp.

Dewey, J. F., and Burke, K., 1974, Hot spots and continental break-up: implications for collisional orogeny. Geology, v. 2, pp. 57–60.

Dewey, J. F., and Kidd, W. S. F., 1974, Continental collisions in the Appalachian–Caledonian belt: variations related to complete and incomplete suturing. Geology, v. 2, pp. 543–546.

Dickinson, W. R., Soreghan, G. S., and Giles, K. A., 1994, Glacio-eustatic origin of Permo-Carboniferous stratigraphic cycles: evidence from the southern Cordilleran foreland region, *in* Dennison, J. M. and Ettensohn, F. R. eds., Tectonic and eustatic controls on sedimentary cycles, SEPM Concepts in Sedimentology and Paleontology 4, pp. 25–34.

Ettensohn, F. R., 1985, The Catskill Delta complex and the Acadian orogeny: a model, *in* Woodrow, D. L. and Sevon, W. D. eds., The Catskill Delta, Geological Society of America (Special Paper 201), Boulder, CO, pp. 39–49.

Ettensohn, F. R., 1991, Flexural interpretation of relationships between Ordovician tectonism and stratigraphic sequences, central and southern Appalachians, U.S.A., *in* Barnes, C. R. and Williams, S. H. eds., Advances in Ordovician geology, Geological Survey of Canada (Paper 90-9), pp. 213–224.

Ettensohn, F. R., 1994, Tectonic control on the formation and cyclicity of major Appalachian unconformities and associated stratigraphic sequences, *in* Dennison, J. M., and Ettensohn, F. R. eds., Tectonic and eustatic controls on sedimentary cycles, SEPM Concepts in Sedimentology and Paleontology 4, pp. 217–242.

Ettensohn, F. R., 2005, The sedimentary record of foreland-basin, tectophase cycles: examples from the Appalachian basin; Chapter 5, in Mabesoone, J. M. and Neuman, V. H. eds., Cyclic development of sedimentary basins, Developments in Sedimentology, v. 57, Amsterdam, Elsevier, pp. 139–172.

Frakes, F. A., Frances, J. E., and Syktus, J. I., 1992, Climate modes of the Phanerozoic, Cambridge, Cambridge University Press, 274 pp.

Gao, Dengliang, 1994, Subsurface geometry and growth history of the Warfield structure in south-central West Virginia, central Appalachian Basin [M.S. thesis]: Morgantown, West Virginia University, 243 p.

Gradstein, F. M., Ogg, J. G., and Smith, A. G., eds., 2004a, A geologic time scale 2004. Cambridge University Press, Cambridge, 589 p.

Hatcher, R. D. Jr., and Odom, A. L. 1980. Timing of thrusting in the southern Appalachians, USA: model for orogeny? J. Geol. Soc. London 137: 321-27.

Milici, R. C., and de Witt, W., Jr., 1988, The Appalachian basin, *in* Sloss, L. L. ed., Sedimentary cover—North American craton, Geological Society of America, The Geology of North America, Boulder CO, v. D-2, pp. 427–469.

Muslim, Mohanad, 2014, A Sequence Stratigraphic Analysis of the Berea Sandstone in Athens County, Ohio [M.S. thesis] Athens, Ohio University, p.

Read, J. F., 1989, Controls on evolution of Cambrian–Ordovician passive margin, U.S. Appalachians, *in* Crevello, P. D., Wilson, J. L., Sarg, J. F., and Read, J. F. eds., Controls on carbonate platform and basin development, SEPM (Special Publication 44), Tulsa, pp. 147–165.

Ross, C. A., and Ross, J. R. P., 1988, Late Paleozoic transgressive-regressive deposition, *in* Wilgus, C. K., Hastings, B. S., Posamentier, H. W., Ross, C. A., and Van Wagoner, J. C. eds., Sea-level changes: an integrated approach, SEPM (Special Paper 42), Tulsa, pp. 227–247.

Schlumberger, 1989, Log Interpretation Principles and Applications: Schlumberger Education Services, p.

Scotese, C. R., 2003, Paleogeographic Map archive, PALEOMAP project, Arlington, Department of Geology, University of Texas at Arlington.

Serra, O. and Sulpice, L., 1975, Sedimentological analysis of shale-sand series from well logs: Transactions of the SPWLA 16th Annual Logging Symposium, paper W., p.

Shumaker, R. C., 1986b, The effect of basement structure on sedimentation and detached structural trends within the Appalachian basin, *in* McDowell, R. C., and Glover. L., eds., The Lowry Volume, Studies in Appalachian geology: Virginia Polytechnic Institute and State University, Department of Geological Sciences Memoir 3, p. 67-8 1 .

Shumaker, R. C., and Wilson T. H., 1996, Basement structure of the Appalachian foreland in West Virginia: Its style and effect on sedimentation, *in* van der Pluijm, B. A., and Catacosinos, P. A., eds., Basement Basins of Eastern North American: Boulder, Colorado, Geological Society of America Special Paper 308, p. 141-155.

Slingerland, R. and Smith, N. D., 2004, River Avulsion and Their Deposits: Annual Review of Earth and Planetary Sciences, v. 32, p. 257-285.

Tankard, A. J., 1986, Depositional response to foreland deformation in the Carboniferous of eastern Kentucky. American Association of Petroleum Geologists Bulletin, v. 70, pp. 853–868

Thomas, W. A., 1993, Low-angle detachment geometry of the Late Precambrian–Cambrian Appalachian–Ouachita rifted margin of southeastern North America. Geology, v. 21, pp. 921–924.

Thomas, W. A., 2006, Tectonic inheritance at a continental margin. GSA Today, v. 16, pp. 4–11.

APPENDICES

APPENDIX I

Data were used to calculate the structure surface elevations for the top of the Berea Sandstone, top of the Gordon sandstone, and base of the Gordon sandstone. Data are measure depths, determined from gamma-ray logs.

Well API #	Longitude	Latitude	County	Datum	Top of Berea (ft)	Top of Gordon (ft)	Bottom of Gordon (ft)
4704702533	-81.63	37.46	McDowell	1784	4102	4240	4289
4704701196	-81.65	37.38	McDowell	1575	4210	4340	4390
4704700890	-81.63	37.32	McDowell	2420	4993	5222	5276
4704702573	-81.64	37.25	McDowell	1751	4215	4305	4360
4704700935	-81.92	37.45	McDowell	1919	4486	4573	4610
4704702593	-81.52	37.36	McDowell	2066	4551	4704	4760
4704702647	-81.38	37.33	McDowell	2066	4300	4472	4532
4710902979	-81.56	37.75	Wyoming	1746	3530	3704	3740
4710901097	-81.54	37.71	Wyoming	1733	3602	3756	3804
4710901081	-81.52	37.63	Wyoming	1745	3462	3590	3640
4710902982	-81.46	37.57	Wyoming	1452	3364	3488	3548
4710902945	-81.45	37.51	Wyoming	2196	4278	4402	4476
4710903007	-81.79	37.53	Wyoming	1802	4066	4200	4248
4710903027	-81.73	37.54	Wyoming	1268	3539	3672	3714
4710901024	-81.42	37.71	Wyoming	1902	3565	3704	3760
4708100688	-81.16	37.87	Raleigh	2057	3232	3436	3476
4708100775	-81.19	37.71	Raleigh	2377	3900	4080	4115
4708101497	-81.29	37.55	Raleigh	2404	4314	4542	4571
4708100710	-81.47	37.95	Raleigh	1007	2736	2950	2968
4708100585	-81.38	37.95	Raleigh	1841	3262	3454	3482
4708100847	-81.52	37.84	Raleigh	2032	3714	3890	3920
4708100708	-81.48	37.81	Raleigh	1587	3135	3316	3349
4708100737	-81.44	37.78	Raleigh	2280	3760	3923	3964
4708100296	-80.98	37.73	Raleigh	2828	3934	4126	4154
4705900991	-82.33	37.92	Mingo	1369	2494	2624	2652
4705901772	-82.23	37.85	Mingo	986	2715	2855	2878
4705901500	-82.22	37.77	Mingo	883	2704	2840	2860
4705901144	-82.11	37.63	Mingo	1302	3428	3557	3597
4705902114	-82.00	37.56	Mingo	1591	3852	3940	3983
4705901863	-81.85	37.58	Mingo	1403	3702	3825	3868
4705901868	-82.34	37.81	Mingo	919	2454	2586	2635

4705901427	-82.14	37.86	Mingo	1569	3182	3220	3250
4705902247	-82.11	37.58	Mingo	794	2976	3095	3130
4704502023	-82.05	38.00	Logan	932	2174	2364	2430
4704502002	-82.05	37.90	Logan	1037	2191	2368	2428
4704501230	-82.02	37.81	Logan	872	2781	2925	2998
4704501125	-81.96	37.73	Logan	1271	3603	3762	3820
4704501232	-81.89	37.69	Logan	979	3158	3290	3340
4704501085	-81.67	37.79	Logan	2007	3994	4155	4204
4704501177	-81.86	37.71	Logan	1398	3519	3662	3708
4704501193	-81.97	37.82	Logan	711	2714	2862	2920
4704501130	-81.86	37.83	Logan	1050	3183	3352	3400
4704501214	-81.78	37.85	Logan	1271	3210	3364	3430
4700501520	-81.75	38.18	Boone	963	2032	2274	2316
4700501349	-81.77	38.10	Boone	902	1847	2066	2110
4700500730	-81.74	38.03	Boone	1037	2565	2774	2824
4700500885	-81.75	37.95	Boone	1136	3048	3248	3300
4700501625	-81.72	37.83	Boone	2163	4095	4238	4312
4700501397	-81.54	38.03	Boone	1685	3498	3698	3739
4700501420	-81.58	37.92	Boone	1786	3667	3862	3909
4700501501	-81.57	37.86	Boone	2493	4334	4504	4543
4700501492	-81.92	38.12	Boone	1235	2494	2718	2790
4700502319	-81.59	38.13	Boone	1060	2622	2838	2906
4700502218	-81.87	37.98	Boone	1542	2617	2828	2882
4703901093	-81.28	38.50	Kanawha	959	2130	2377	2434
4703904172	-81.32	38.41	Kanawha	845	2038	2262	2316
4703904545	-81.33	38.29	Kanawha	1094	2442	2650	2710
4703904478	-81.41	38.21	Kanawha	1104	2568	2790	2842
4703904267	-81.42	38.06	Kanawha	1827	3270	3450	3510
4703904499	-81.82	38.37	Kanawha	708	2167	2415	2470
4703905503	-81.48	38.32	Kanawha	1188	2260	2492	2550
4703903825	-81.40	38.36	Kanawha	1013	2174	2398	2455
4703903767	-81.79	38.29	Kanawha	794	2275	2505	2550
4703904321	-81.51	38.21	Kanawha	631	1948	2184	2224
4703904066	-81.43	38.09	Kanawha	1080	2884	3094	3150
4706700835	-80.73	38.44	Nicholas	2451	2988	3265	3292
4706700736	-80.88	38.34	Nicholas	2189	3102	3356	3414
4706700656	-81.07	38.22	Nicholas	1436	2237	2480	2540
4706700910	-80.65	38.26	Nicholas	2452	2980	3278	3324
4701900530	-81.13	38.23	Fayette	759	2054	2302	2342
4701900517	-81.32	38.05	Fayette	2290	3736	3950	3973
4701900510	-81.31	37.97	Fayette	1636	2940	3136	3165

4701900572	-81.09	38.07	Fayette	1717	2831	3072	3104
4701900515	-80.99	38.07	Fayette	2508	3000	3242	3267
4701502500	-81.14	38.53	Clay	1207	2512	2763	2824
4701502655	-81.19	38.50	Clay	1149	2314	2562	2617
4701502672	-81.20	38.40	Clay	1339	2608	2843	2904
4701502376	-81.22	38.30	Clay	1431	2966	3190	3256

APPENDIX II

Data were used to generate structure contour maps for the top of the Berea Sandstone, top of the Gordon sandstone, and base of the Gordon sandstone. Data are subsea depths, calculated using the measured depth read from the logs (Appendix I) and the elevation of the datum the log was measured from.

Well API #	Longitude	Latitude	County	Datum	Structure Top of Berea (ft)	Structure Top of Gordon (ft)	Structure Base of Gordon (ft)
4704702533	-81.63	37.46	McDowell	1784	-2318	-2456	-2505
4704701196	-81.65	37.38	McDowell	1575	-2635	-2765	-2815
4704700890	-81.63	37.32	McDowell	2420	-2573	-2802	-2856
4704702573	-81.64	37.25	McDowell	1751	-2464	-2554	-2609
4704700935	-81.92	37.45	McDowell	1919	-2567	-2654	-2691
4704702593	-81.52	37.36	McDowell	2066	-2485	-2638	-2694
4704702647	-81.38	37.33	McDowell	2066	-2234	-2406	-2466
4710902979	-81.56	37.75	Wyoming	1746	-1784	-1958	-1994
4710901097	-81.54	37.71	Wyoming	1733	-1869	-2023	-2071
4710901081	-81.52	37.63	Wyoming	1745	-1717	-1845	-1895
4710902982	-81.46	37.57	Wyoming	1452	-1912	-2036	-2096
4710902945	-81.45	37.51	Wyoming	2196	-2082	-2206	-2280
4710903007	-81.79	37.53	Wyoming	1802	-2264	-2398	-2446
4710903027	-81.73	37.54	Wyoming	1268	-2271	-2404	-2446
4710901024	-81.42	37.71	Wyoming	1902	-1663	-1802	-1858
4708100688	-81.16	37.87	Raleigh	2057	-1175	-1379	-1419
4708100775	-81.19	37.71	Raleigh	2377	-1523	-1703	-1738
4708101497	-81.29	37.55	Raleigh	2404	-1910	-2138	-2167
4708100710	-81.47	37.95	Raleigh	1007	-1729	-1943	-1961
4708100585	-81.38	37.95	Raleigh	1841	-1421	-1613	-1641
4708100847	-81.52	37.84	Raleigh	2032	-1682	-1858	-1888
4708100708	-81.48	37.81	Raleigh	1587	-1548	-1729	-1762
4708100737	-81.44	37.78	Raleigh	2280	-1480	-1643	-1684
4708100296	-80.98	37.73	Raleigh	2828	-1106	-1298	-1326
4705900991	-82.33	37.92	Mingo	1369	-1125	-1255	-1283
4705901772	-82.23	37.85	Mingo	986	-1729	-1869	-1892
4705901500	-82.22	37.77	Mingo	883	-1821	-1957	-1977
4705901144	-82.11	37.63	Mingo	1302	-2126	-2255	-2295
4705902114	-82.00	37.56	Mingo	1591	-2261	-2349	-2392
4705901863	-81.85	37.58	Mingo	1403	-2299	-2422	-2465
4705901868	-82.34	37.81	Mingo	919	-1535	-1667	-1716

4705901427	-82.14	37.86	Mingo	1569	-1613	-1651	-1681
4705902247	-82.11	37.58	Mingo	794	-2182	-2301	-2336
4704502023	-82.05	38.00	Logan	932	-1242	-1432	-1498
4704502002	-82.05	37.90	Logan	1037	-1154	-1331	-1391
4704501230	-82.02	37.81	Logan	872	-1909	-2053	-2126
4704501125	-81.96	37.73	Logan	1271	-2332	-2491	-2549
4704501232	-81.89	37.69	Logan	979	-2179	-2311	-2361
4704501085	-81.67	37.79	Logan	2007	-1987	-2148	-2197
4704501177	-81.86	37.71	Logan	1398	-2121	-2264	-2310
4704501193	-81.97	37.82	Logan	711	-2003	-2151	-2209
4704501130	-81.86	37.83	Logan	1050	-2133	-2302	-2350
4704501214	-81.78	37.85	Logan	1271	-1939	-2093	-2159
4700501520	-81.75	38.18	Boone	963	-1069	-1311	-1353
4700501349	-81.77	38.10	Boone	902	-945	-1164	-1208
4700500730	-81.74	38.03	Boone	1037	-1528	-1737	-1787
4700500885	-81.75	37.95	Boone	1136	-1912	-2112	-2164
4700501625	-81.72	37.83	Boone	2163	-1932	-2075	-2149
4700501397	-81.54	38.03	Boone	1685	-1813	-2013	-2054
4700501420	-81.58	37.92	Boone	1786	-1881	-2076	-2123
4700501501	-81.57	37.86	Boone	2493	-1841	-2011	-2050
4700501492	-81.92	38.12	Boone	1235	-1259	-1483	-1555
4700502319	-81.59	38.13	Boone	1060	-1562	-1778	-1846
4700502218	-81.87	37.98	Boone	1542	-1075	-1286	-1340
4703901093	-81.28	38.50	Kanawha	959	-1171	-1418	-1475
4703904172	-81.32	38.41	Kanawha	845	-1193	-1417	-1471
4703904545	-81.33	38.29	Kanawha	1094	-1348	-1556	-1616
4703904478	-81.41	38.21	Kanawha	1104	-1464	-1686	-1738
4703904267	-81.42	38.06	Kanawha	1827	-1443	-1623	-1683
4703904499	-81.82	38.37	Kanawha	708	-1459	-1707	-1762
4703905503	-81.48	38.32	Kanawha	1188	-1072	-1304	-1362
4703903825	-81.40	38.36	Kanawha	1013	-1161	-1385	-1442
4703903767	-81.79	38.29	Kanawha	794	-1481	-1711	-1756
4703904321	-81.51	38.21	Kanawha	631	-1317	-1553	-1593
4703904066	-81.43	38.09	Kanawha	1080	-1804	-2014	-2070
4706700835	-80.73	38.44	Nicholas	2451	-537	-814	-841
4706700736	-80.88	38.34	Nicholas	2189	-913	-1167	-1225
4706700656	-81.07	38.22	Nicholas	1436	-801	-1044	-1104
4706700910	-80.65	38.26	Nicholas	2452	-528	-826	-872
4701900530	-81.13	38.23	Fayette	759	-1295	-1543	-1583
4701900517	-81.32	38.05	Fayette	2290	-1446	-1660	-1683
4701900510	-81.31	37.97	Fayette	1636	-1304	-1500	-1529

4701900572	-81.09	38.07	Fayette	1717	-1114	-1355	-1387
4701900515	-80.99	38.07	Fayette	2508	-492	-734	-759
4701502500	-81.14	38.53	Clay	1207	-1305	-1556	-1617
4701502655	-81.19	38.50	Clay	1149	-1165	-1413	-1468
4701502672	-81.20	38.40	Clay	1339	-1269	-1504	-1565
4701502376	-81.22	38.30	Clay	1431	-1535	-1759	-1825

APPENDIX III

Data were used to generate isopach and isolith maps in the study area. Data were interpreted from gamma-ray logs.

Well API #	Longitude	Latitude	County	Total Gordon Interval	50% Isolith Thickness
4704702533	-81.63	37.46	McDowell	49	19
4704701196	-81.65	37.38	McDowell	50	17
4704700890	-81.63	37.32	McDowell	54	15
4704702573	-81.64	37.25	McDowell	55	23
4704700935	-81.92	37.45	McDowell	37	13
4704702593	-81.52	37.36	McDowell	56	24
4704702647	-81.38	37.33	McDowell	60	18
4710902979	-81.56	37.75	Wyoming	36	18
4710901097	-81.54	37.71	Wyoming	48	31
4710901081	-81.52	37.63	Wyoming	50	48
4710902982	-81.46	37.57	Wyoming	60	33
4710902945	-81.45	37.51	Wyoming	74	43
4710903007	-81.79	37.53	Wyoming	48	0
4710903027	-81.73	37.54	Wyoming	42	0
4710901024	-81.42	37.71	Wyoming	56	34
4708100688	-81.16	37.87	Raleigh	40	24
4708100775	-81.19	37.71	Raleigh	35	13
4708101497	-81.29	37.55	Raleigh	29	17
4708100710	-81.47	37.95	Raleigh	18	16
4708100585	-81.38	37.95	Raleigh	28	22
4708100847	-81.52	37.84	Raleigh	30	28
4708100708	-81.48	37.81	Raleigh	33	31
4708100737	-81.44	37.78	Raleigh	41	38
4708100296	-80.98	37.73	Raleigh	28	9
4705900991	-82.33	37.92	Mingo	28	0
4705901772	-82.23	37.85	Mingo	23	2
4705901500	-82.22	37.77	Mingo	20	4
4705901144	-82.11	37.63	Mingo	40	3
4705902114	-82.00	37.56	Mingo	43	0
4705901863	-81.85	37.58	Mingo	43	1
4705901868	-82.34	37.81	Mingo	49	4
4705901427	-82.14	37.86	Mingo	30	0
4705902247	-82.11	37.58	Mingo	35	5
4704502023	-82.05	38.00	Logan	66	12
4704502002	-82.05	37.90	Logan	60	11
4704501230	-82.02	37.81	Logan	73	10
4704501125	-81.96	37.73	Logan	58	19
4704501232	-81.89	37.69	Logan	50	8
4704501085	-81.67	37.79	Logan	49	1
4704501177	-81.86	37.71	Logan	46	0

4704501193	-81.97	37.82	Logan	58	10
4704501130	-81.86	37.83	Logan	48	4
4704501214	-81.78	37.85	Logan	66	3
4700501520	-81.75	38.18	Boone	42	2
4700501349	-81.77	38.10	Boone	44	18
4700500730	-81.74	38.03	Boone	50	1
4700500885	-81.75	37.95	Boone	52	0
4700501625	-81.72	37.83	Boone	74	0
4700501397	-81.54	38.03	Boone	41	8
4700501420	-81.58	37.92	Boone	47	7
4700501501	-81.57	37.86	Boone	39	20
4700501492	-81.92	38.12	Boone	72	0
4700502319	-81.59	38.13	Boone	68	4
4700502218	-81.87	37.98	Boone	54	0
4703901093	-81.28	38.50	Kanawha	57	28
4703904172	-81.32	38.41	Kanawha	54	33
4703904545	-81.33	38.29	Kanawha	60	36
4703904478	-81.41	38.21	Kanawha	52	17
4703904267	-81.42	38.06	Kanawha	60	21
4703904499	-81.82	38.37	Kanawha	55	7
4703905503	-81.48	38.32	Kanawha	58	3
4703903825	-81.40	38.36	Kanawha	57	10
4703903767	-81.79	38.29	Kanawha	45	2
4703904321	-81.51	38.21	Kanawha	40	10
4703904066	-81.43	38.09	Kanawha	56	13
4706700835	-80.73	38.44	Nicholas	27	15
4706700736	-80.88	38.34	Nicholas	58	36
4706700656	-81.07	38.22	Nicholas	60	32
4706700910	-80.65	38.26	Nicholas	46	27
4701900530	-81.13	38.23	Fayette	40	26
4701900517	-81.32	38.05	Fayette	23	22
4701900510	-81.31	37.97	Fayette	29	21
4701900572	-81.09	38.07	Fayette	32	13
4701900515	-80.99	38.07	Fayette	25	21
4701502500	-81.14	38.53	Clay	61	20
4701502655	-81.19	38.50	Clay	55	27
4701502672	-81.20	38.40	Clay	61	23
4701502376	-81.22	38.30	Clay	66	28

APPENDIX IV

Data were used to calculate log porosity (%) and predictive permeability values. Log porosity and permeability values were used to generate maps in the study area. Matrix density, bulk density, and fluid density data were obtained from the well log; log porosity was calculated using the Archie equation. Permeability was derived from a calculated relationship between porosity and permeability.

Well API #	Longitude	Latitude	County	P_{ma}	P_b	P_f	ϕ, Porosity (%)	Predictive Permeability (mD)
4704702533	-81.63	37.46	McDowell	2.68	2.4625	1	12.95	5.20
4704701196	-81.65	37.38	McDowell	2.71	2.525	1	10.82	2.72
4704700890	-81.63	37.32	McDowell	-	-	-	-	-
4704702573	-81.64	37.25	McDowell	2.68	2.5	1	10.71	2.64
4704700935	-81.92	37.45	McDowell	2.71	2.575	1	7.89	1.12
4704702593	-81.52	37.36	McDowell	2.68	2.475	1	12.20	4.15
4704702647	-81.38	37.33	McDowell	2.71	2.6125	1	5.70	0.58
4710902979	-81.56	37.75	Wyoming	2.68	2.4125	1	15.92	12.84
4710901097	-81.54	37.71	Wyoming	2.71	2.4625	1	14.47	8.27
4710901081	-81.52	37.63	Wyoming	2.68	2.46	1	13.10	5.44
4710902982	-81.46	37.57	Wyoming	2.68	2.48	1	11.90	3.79
4710902945	-81.45	37.51	Wyoming	2.68	2.61	1	4.17	0.36
4710903007	-81.79	37.53	Wyoming	2.68	2.55	1	7.74	1.07
4710903027	-81.73	37.54	Wyoming	2.68	2.58	1	5.95	0.62
4710901024	-81.42	37.71	Wyoming	2.68	2.5	1	10.71	2.64
4708100688	-81.16	37.87	Raleigh	2.68	2.55	1	7.74	1.07
4708100775	-81.19	37.71	Raleigh	-	-	-	-	-
4708101497	-81.29	37.55	Raleigh	2.68	2.65	1	1.79	0.18
4708100710	-81.47	37.95	Raleigh	2.68	2.475	1	12.20	4.15
4708100585	-81.38	37.95	Raleigh	2.68	2.475	1	12.20	4.15
4708100847	-81.52	37.84	Raleigh	2.71	2.48	1	13.45	6.06
4708100708	-81.48	37.81	Raleigh	-	-	-	-	-
4708100737	-81.44	37.78	Raleigh	2.71	2.5125	1	11.55	3.40
4708100296	-80.98	37.73	Raleigh	-	-	-	-	-
4705900991	-82.33	37.92	Mingo	-	-	-	-	-
4705901772	-82.23	37.85	Mingo	2.68	2.66	1	1.19	0.15
4705901500	-82.22	37.77	Mingo	2.68	2.635	1	2.68	0.23
4705901144	-82.11	37.63	Mingo	2.68	2.65	1	1.79	0.18
4705902114	-82.00	37.56	Mingo	2.71	2.63	1	4.68	0.42
4705901863	-81.85	37.58	Mingo	2.71	2.61	1	5.85	0.60
4705901868	-82.34	37.81	Mingo	2.68	2.58	1	5.95	0.62
4705901427	-82.14	37.86	Mingo	-	-	-	-	-
4705902247	-82.11	37.58	Mingo	2.71	2.58	1	7.60	1.03
4704502023	-82.05	38.00	Logan	2.68	2.61	1	4.17	0.36
4704502002	-82.05	37.90	Logan	2.71	2.56	1	8.77	1.46

4704501230	-82.02	37.81	Logan	2.68	2.6125	1.1	4.27	0.37
4704501125	-81.96	37.73	Logan	2.71	2.56	1	8.77	1.46
4704501232	-81.89	37.69	Logan	2.68	2.64	1	2.38	0.21
4704501085	-81.67	37.79	Logan	2.71	2.56	1	8.77	1.46
4704501177	-81.86	37.71	Logan	2.68	2.5625	1	6.99	0.85
4704501193	-81.97	37.82	Logan	2.71	2.625	1	4.97	0.46
4704501130	-81.86	37.83	Logan	2.68	2.61	1	4.17	0.36
4704501214	-81.78	37.85	Logan	2.68	2.64	1	2.38	0.21
4700501520	-81.75	38.18	Boone	2.68	2.625	1	3.27	0.28
4700501349	-81.77	38.10	Boone	-	-	-	-	-
4700500730	-81.74	38.03	Boone	2.68	2.61	1	4.17	0.36
4700500885	-81.75	37.95	Boone	2.68	2.575	1	6.25	0.68
4700501625	-81.72	37.83	Boone	2.68	2.575	1	6.25	0.68
4700501397	-81.54	38.03	Boone	2.68	2.535	1	8.63	1.40
4700501420	-81.58	37.92	Boone	-	-	-	-	-
4700501501	-81.57	37.86	Boone	2.71	2.575	1	7.89	1.12
4700501492	-81.92	38.12	Boone	-	-	-	-	-
4700502319	-81.59	38.13	Boone	2.68	2.6	1	4.76	0.43
4700502218	-81.87	37.98	Boone	2.68	2.625	1	3.27	0.28
4703901093	-81.28	38.50	Kanawha	-	-	-	-	-
4703904172	-81.32	38.41	Kanawha	-	-	-	-	-
4703904545	-81.33	38.29	Kanawha	2.71	2.535	1	10.23	2.28
4703904478	-81.41	38.21	Kanawha	2.71	2.5375	1	10.09	2.18
4703904267	-81.42	38.06	Kanawha	2.71	2.535	1	10.23	2.28
4703904499	-81.82	38.37	Kanawha	-	-	-	-	-
4703905503	-81.48	38.32	Kanawha	2.68	2.5	1	10.71	2.64
4703903825	-81.40	38.36	Kanawha	-	-	-	-	-
4703903767	-81.79	38.29	Kanawha	-	-	-	-	-
4703904321	-81.51	38.21	Kanawha	2.68	2.525	1	9.23	1.68
4703904066	-81.43	38.09	Kanawha	2.71	2.54	1	9.94	2.09
4706700835	-80.73	38.44	Nicholas	2.71	2.5625	1	8.63	1.40
4706700736	-80.88	38.34	Nicholas	-	-	-	-	-
4706700656	-81.07	38.22	Nicholas	2.71	2.48	1	13.45	6.06
4706700910	-80.65	38.26	Nicholas	2.68	2.4	1	16.67	16.10
4701900530	-81.13	38.23	Fayette	2.68	2.5	1	10.71	2.64
4701900517	-81.32	38.05	Fayette	2.68	2.48	1	11.90	3.79
4701900510	-81.31	37.97	Fayette	2.68	2.45	1	13.69	6.52
4701900572	-81.09	38.07	Fayette	-	-	-	-	-
4701900515	-80.99	38.07	Fayette	2.71	2.52	1	11.11	2.98
4701502500	-81.14	38.53	Clay	2.68	2.6	1	4.76	0.43
4701502655	-81.19	38.50	Clay	-	-	-	-	-
4701502672	-81.20	38.40	Clay	2.68	2.52	1	9.52	1.84
4701502376	-81.22	38.30	Clay	2.71	2.58	1	7.60	1.03

APPENDIX V

Data in this appendix and Appendix I were used to generate isopach and isolith maps across West Virginia to evaluate Gordon distribution and the distribution of sand-rich Gordon strata. Data were obtained from gamma-ray logs.

Well API #	Longitude	Latitude	County	Total Gordon Interval	50% Isolith Thickness
4710302236	-80.63	39.70	Wetzel	76	60
4710301305	-80.66	39.68	Wetzel	75	49
4710301719	-80.66	39.59	Wetzel	72	62
4710301194	-80.68	39.54	Wetzel	67	45
4710302326	-80.63	39.50	Wetzel	52	48
4710300605	-80.55	39.44	Wetzel	83	64
4710301274	-80.83	39.59	Wetzel	80	31
4710302535	-80.54	39.55	Wetzel	95	61
4704902038	-80.23	39.58	Marion	124	86
4704901563	-80.25	39.55	Marion	115	104
4704900705	-80.24	39.48	Marion	111	107
4704900253	-80.22	39.43	Marion	125	103
4704901445	-80.49	39.56	Marion	110	105
4704901478	-80.38	39.54	Marion	120	110
4704901509	-80.31	39.55	Marion	117	109
4704900731	-80.12	39.42	Marion	133	125
4704900986	-80.07	39.41	Marion	111	101
4708508062	-81.04	39.33	Ritchie	67	67
4708506259	-81.13	39.21	Ritchie	100	77
4708509159	-81.11	39.08	Ritchie	84	70
4708505863	-81.27	39.18	Ritchie	62	62
4708506821	-81.21	39.19	Ritchie	94	74
4708508169	-80.98	39.22	Ritchie	114	84
4708507766	-80.95	39.24	Ritchie	112	90
4703303847	-80.36	39.42	Harrison	127	119
4703302648	-80.39	39.37	Harrison	130	109
4703305626	-80.42	39.32	Harrison	124	119
4703303867	-80.43	39.28	Harrison	122	100
4703301581	-80.48	39.21	Harrison	129	99
4703303299	-80.50	39.16	Harrison	120	109
4703305236	-80.55	39.32	Harrison	115	88
4703302620	-80.47	39.33	Harrison	108	98
4703303690	-80.36	39.31	Harrison	140	118
4703303320	-80.32	39.31	Harrison	166	144
4703303028	-80.23	39.27	Harrison	92	86
4701703156	-80.57	39.39	Doddridge	93	65
4701704037	-80.65	39.36	Doddridge	100	71
4701702810	-80.71	39.28	Doddridge	104	74

4701703761	-80.73	39.25	Doddridge	109	82
4701706269	-80.69	39.32	Doddridge	110	77
4701703938	-80.75	39.21	Doddridge	114	73
4701702437	-80.81	39.32	Doddridge	108	72
4701703941	-80.79	39.28	Doddridge	109	76
4701702457	-80.78	39.30	Doddridge	114	69
4701703879	-80.72	39.30	Doddridge	128	80
4701704585	-80.64	39.29	Doddridge	119	83
4704102725	-80.47	39.11	Lewis	121	97
4704103684	-80.47	39.06	Lewis	140	105
4704100882	-80.52	38.97	Lewis	98	76
4704100777	-80.52	38.95	Lewis	80	72
4704103781	-80.55	38.96	Lewis	58	49
4704103741	-80.41	38.87	Lewis	55	55
4704101873	-80.69	39.01	Lewis	48	37
4704103997	-80.62	39.02	Lewis	34	25
4704103703	-80.56	39.02	Lewis	77	61
4704103680	-80.50	39.05	Lewis	134	96
4704101880	-80.39	39.07	Lewis	130	98
4704103201	-80.32	39.04	Lewis	119	85
4702104340	-80.81	39.09	Gilmer	74	39
4702104399	-80.82	39.07	Gilmer	79	33
4702104868	-80.86	38.98	Gilmer	78	27
4702105348	-80.89	38.90	Gilmer	84	26
4702104780	-80.90	38.78	Gilmer	82	25
4702104388	-80.99	38.93	Gilmer	80	20
4702104700	-80.92	38.95	Gilmer	96	26
4702104171	-80.82	38.99	Gilmer	75	22
4702104015	-80.76	39.02	Gilmer	96	28
4704702533	-81.63	37.46	McDowell	49	19
4704701196	-81.65	37.38	McDowell	50	17
4704700890	-81.63	37.32	McDowell	54	15
4704702573	-81.64	37.25	McDowell	55	23
4704700935	-81.92	37.45	McDowell	37	13
4704702593	-81.52	37.36	McDowell	56	24
4704702647	-81.38	37.33	McDowell	60	18
4710902979	-81.56	37.75	Wyoming	36	18
4710901097	-81.54	37.71	Wyoming	48	31
4710901081	-81.52	37.63	Wyoming	50	48
4710902982	-81.46	37.57	Wyoming	60	33
4710902945	-81.45	37.51	Wyoming	74	43
4710903007	-81.79	37.53	Wyoming	48	0
4710903027	-81.73	37.54	Wyoming	42	0
4710901024	-81.42	37.71	Wyoming	56	34
4708100688	-81.16	37.87	Raleigh	40	24
4708100775	-81.19	37.71	Raleigh	35	13

4708101497	-81.29	37.55	Raleigh	29	17
4708100710	-81.47	37.95	Raleigh	18	16
4708100585	-81.38	37.95	Raleigh	28	22
4708100847	-81.52	37.84	Raleigh	30	28
4708100708	-81.48	37.81	Raleigh	33	31
4708100737	-81.44	37.78	Raleigh	41	38
4708100296	-80.98	37.73	Raleigh	28	9
4705900991	-82.33	37.92	Mingo	28	0
4705901772	-82.23	37.85	Mingo	23	2
4705901500	-82.22	37.77	Mingo	20	4
4705901144	-82.11	37.63	Mingo	40	3
4705902114	-82.00	37.56	Mingo	43	0
4705901863	-81.85	37.58	Mingo	43	1
4705901868	-82.34	37.81	Mingo	49	4
4705901427	-82.14	37.86	Mingo	30	0
4705902247	-82.11	37.58	Mingo	35	5
4704502023	-82.05	38.00	Logan	66	12
4704502002	-82.05	37.90	Logan	60	11
4704501230	-82.02	37.81	Logan	73	10
4704501125	-81.96	37.73	Logan	58	19
4704501232	-81.89	37.69	Logan	50	8
4704501085	-81.67	37.79	Logan	49	1
4704501177	-81.86	37.71	Logan	46	0
4704501193	-81.97	37.82	Logan	58	10
4704501130	-81.86	37.83	Logan	48	4
4704501214	-81.78	37.85	Logan	66	3
4700501520	-81.75	38.18	Boone	42	2
4700501349	-81.77	38.10	Boone	44	18
4700500730	-81.74	38.03	Boone	50	1
4700500885	-81.75	37.95	Boone	52	0
4700501625	-81.72	37.83	Boone	74	0
4700501397	-81.54	38.03	Boone	41	8
4700501420	-81.58	37.92	Boone	47	7
4700501501	-81.57	37.86	Boone	39	20
4700501492	-81.92	38.12	Boone	72	0
4700502319	-81.59	38.13	Boone	68	4
4700502218	-81.87	37.98	Boone	54	0
4703901093	-81.28	38.50	Kanawha	57	28
4703904172	-81.32	38.41	Kanawha	54	33
4703904545	-81.33	38.29	Kanawha	60	36
4703904478	-81.41	38.21	Kanawha	52	17
4703904267	-81.42	38.06	Kanawha	60	21
4703904499	-81.82	38.37	Kanawha	55	7
4703905503	-81.48	38.32	Kanawha	58	3
4703903825	-81.40	38.36	Kanawha	57	10
4703903767	-81.79	38.29	Kanawha	45	2

4703904321	-81.51	38.21	Kanawha	40	10
4703904066	-81.43	38.09	Kanawha	56	13
4706700835	-80.73	38.44	Nicholas	27	15
4706700736	-80.88	38.34	Nicholas	58	36
4706700656	-81.07	38.22	Nicholas	60	32
4706700910	-80.65	38.26	Nicholas	46	27
4700702049	-80.64	38.81	Braxton	56	18
4700702051	-80.63	38.79	Braxton	54	22
4700700927	-80.66	38.69	Braxton	49	16
4700700394	-80.67	38.54	Braxton	42	26
4700702589	-80.97	38.68	Braxton	30	2
4700702479	-80.82	38.71	Braxton	39	4
4700702045	-80.65	38.78	Braxton	28	26
4700700536	-80.52	38.78	Braxton	77	48
4701304583	-81.12	39.04	Calhoun	54	30
4701304684	-81.16	38.97	Calhoun	64	26
4701300743	-81.17	38.72	Calhoun	55	45
4701304157	-81.21	38.93	Calhoun	65	28
4701304619	-81.04	38.97	Calhoun	54	28
4708704134	-81.29	38.88	Roane	53	10
4708703760	-81.30	38.78	Roane	66	12
4708703715	-81.37	38.71	Roane	62	7
4708700440	-81.28	38.65	Roane	65	10
4701900530	-81.13	38.23	Fayette	40	26
4701900517	-81.32	38.05	Fayette	23	22
4701900510	-81.31	37.97	Fayette	29	21
4701900572	-81.09	38.07	Fayette	32	13
4701900515	-80.99	38.07	Fayette	25	21
4701502500	-81.14	38.53	Clay	61	20
4701502655	-81.19	38.50	Clay	55	27
4701502672	-81.20	38.40	Clay	61	23
4701502376	-81.22	38.30	Clay	66	28

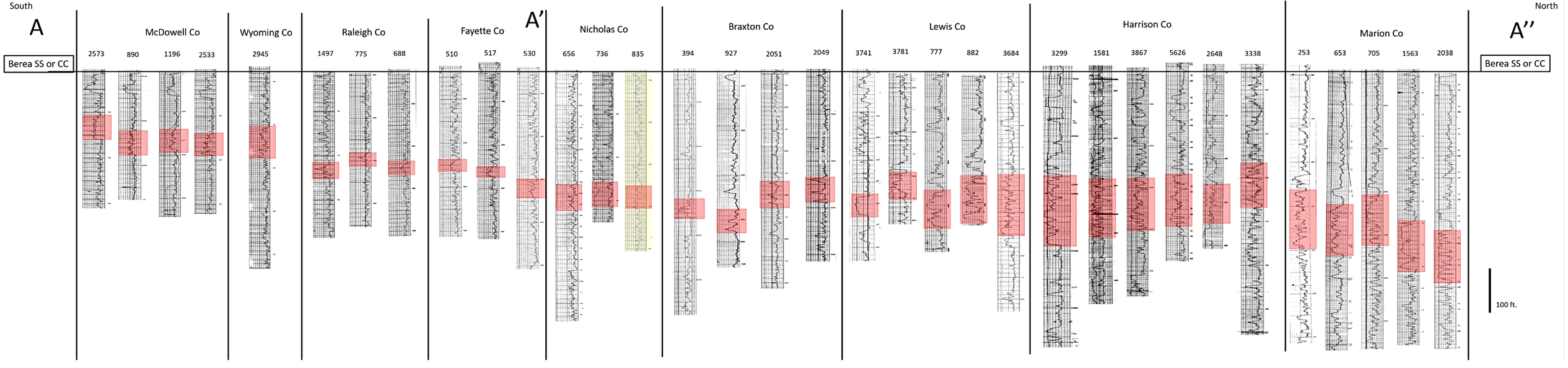

Cross-section: A-A’-A” shows the lateral continuity of the Gordon sandstone and correlative sediments across West Virginia. No horizontal scale. Well logs are shown spaced equidistantly. See Figure 4 for location of cross-sections.